

Title	熱パルスイオン源を用いた質量分析チップの開発
Author(s)	杉山, 清隆
Citation	
Issue Date	2015-03
Type	Thesis or Dissertation
Text version	ETD
URL	http://hdl.handle.net/10119/12769
Rights	
Description	Supervisor:高村 禪, マテリアルサイエンス研究科, 博士

**Development of on-chip mass spectrometer
with pulse-heating ionization source**

KIYOTAKA SUGIYAMA

Japan Advanced Institute of Science and Technology

Doctoral Dissertation

**Development of on-chip mass spectrometer
with pulse-heating ionization source**

Kiyotaka Sugiyama

Supervisor: Professor Dr. Yuzuru Takamura

School of Materials Science

Japan Advanced Institute of Science and Technology

March, 2015

PREFACE

Mass spectrometry (MS) is one of the highly sensitive and highly selective analytical methods for biochemical samples including DNA, peptides, and proteins. Fundamental technology of the MS relies on the controlling of charged particles such as electrons or ions in a vacuum. MS has been massively developed by the multiple contributions of the ion optics and highly sensitive optical detection in physics, ionization techniques of versatile analyte in chemistry, and high speed data processing in information science. Presently mass spectrometric analysis plays a key role in the health and life sciences research of drug discovery, biomarker analysis for medical diagnosis, genomics, and proteomics.

On the other hand, micro total analysis system (μ TAS) and lab-on-a-chip device also contribute to the progress of the life sciences research. The most advantage of the μ TAS is the miniaturization of the analytical systems into a desktop or handheld device to apply quick biochemical analysis on the site. Moreover, remarkable analytical devices which utilize the physical or chemical phenomena in micro to nanoscale were developed such as highly sensitive elemental analysis chip and the highly sensitive immunosensors in a cost effective way.

In this work, the key components for on-chip mass spectrometry including a vacuum pump, an ionization source, and an ion lens for time-of-flight mass analysis were miniaturized toward the highly sensitive detection of versatile

biomarkers. Conventionally, MS analysis system requires a high vacuum. However, the conceptual step to significantly miniaturize the mass spectrometer into a microchip is to operate it in a low vacuum using microfluidic channel. The pulse-heating ionization source developed herein enables the ionization of a peptide and a protein without laser, high voltage, or ambient gases. On-chip protein mass spectrometry was firstly performed with the integrated device of the ionization source and the ion lens. I hope that developed components for on-chip mass spectrometer in this research can be useful for next generation mass spectrometric devices for highly sensitive analysis of biological materials.

Kiyotaka Sugiyama

CONTENTS

PREFACE	-----	i
CONTENTS	-----	iii
LIST OF ABBREVIATIONS	-----	vii
CHAPTER 1 GENERAL INTRODUCTION	-----	1
Abstract	-----	1
1.1 Recent progress of analytical methods for medical diagnosis	-----	2
1.1.1 Biomarkers in biological samples	-----	2
1.1.2 Detection methods of biomarkers in biological samples	-----	5
1.1.3 Micro total analysis system	-----	9
1.1.4 Proteomic analysis	-----	10
1.2 Miniaturized mass spectrometer	-----	11
1.2.1 General principle of mass spectrometer	-----	11
1.2.2 Miniaturized mass spectrometer	-----	13
1.2.3 Microfabricated vacuum pumps	-----	15
1.2.4 Microfabricated ionization sources	-----	17
1.2.5 Microfabricated mass analyzers	-----	21
1.3 Strategy to miniaturize mass spectrometer on a microchip	-----	25
1.4 Research objectives	-----	28
1.5 Thesis organization	-----	29
References	-----	31
CHAPTER2 ON-CHIP VACUUM GENERATION METHOD	-----	37
Abstract	-----	37
2.1 Introduction	-----	38
2.2 Objective	-----	39
2.3 Principle	-----	39

2.3.1	Principle of vacuum generation on a chip	-----	39
2.3.2	Principle of pressure measurement on a chip	-----	41
2.3.3	Theoretical vacuum	-----	42
2.4	Experiment	-----	44
2.4.1	Design of the chip	-----	44
2.4.2	Chip fabrication	-----	45
2.4.3	Experimental setup for vacuum generation	-----	46
2.4.4	Experimental procedure for vacuum generation	-----	48
2.5	Results and discussion	-----	49
2.5.1	Vacuum measurement on a microchip	-----	49
2.5.2	Vacuum generation with gas-liquid phase transition	-----	51
2.6	Summary	-----	55
	References	-----	57

CHAPTER 3 ON-CHIP IONIZATION SOURCE FOR PEPTIDE AND PROTEIN ANALYTES

	Abstract	-----	59
3.1	Introduction	-----	60
3.2	Objective	-----	61
3.3	Principle	-----	62
3.4	Experiment	-----	63
3.4.1	Design of ionization chip	-----	63
3.4.2	Chip fabrication	-----	70
3.4.3	Experimental setup for pulse-heating ionization	-----	73
3.4.4	Sample preparation	-----	75
3.4.5	Experimental setup for TOF-MS with pulse-heating ionization	-----	76
3.5	Results and discussion	-----	79
3.5.1	Time-of-flight mass spectrometry of inorganic particles	-----	79
3.5.2	Pulse-heating ionization of proteins	-----	80
3.5.3	Time-of-flight mass spectrometry of proteins	-----	84
3.5.4	Time-of-flight mass spectrometry of peptides	-----	86

3.6 Summary	-----87
References	----- 88

CHAPTER 4 EFFECTS OF MATRIX AND SOLVENT FOR SAMPLE

FORMATION ON PULSE-HEATING IONIZATION	----- 90
Abstract	----- 90
4.1 Introduction	----- 92
4.2 Objective	----- 93
4.3 Principle	----- 94
4.4 Experiment	----- 95
4.4.1 Experimental setup	----- 95
4.4.2 Sample preparation	----- 96
4.5 Results and discussion	----- 98
4.5.1 Effect of the matrix on pulse-heating ionization	----- 98
4.5.2 Effect of the solvent for preparation of the sample layer	----- 104
4.5.3 TOF mass spectrometry with thin layer methods	----- 111
4.6 Summary	----- 116
References	----- 118

CHAPTER 5 MINIATURIZED ION LENS AND ON-CHIP MASS

SPECTROMETRY OF PROTEIN SAMPLE	----- 120
Abstract	----- 120
5.1 Introduction	----- 121
5.2 Objective	----- 122
5.3 Principle	----- 122
5.4 Numerical simulation	----- 123
5.4.1 Design of the chip	----- 123
5.4.2 Numerical simulation of ion optics in a micro channel	----- 124
5.5 Experiment	----- 130
5.5.1 Chip fabrication	----- 130
5.5.2 Experimental setup	----- 132

5.5.3	Sample preparation	-----	133
5.6	Results and discussion	-----	134
5.6.1	Ionization in a micro channel	-----	134
5.6.2	On-chip TOF mass spectrometry	-----	135
5.7	Summary	-----	139
	References	-----	140
 CHAPTER6 CONCLUSIONS			----- 141
 ACKNOWLEDGEMENTS			----- 143
ACHIEVEMENTS			----- 145

ABBREVIATIONS

AC	Alternating Current
BSA	Bovine Serum Albumin
CE	Capillary Electrophoresis
CHCA	α -Cyano-4-HydroxyCinnamic Acid
CNT	Carbon NanoTube
Da	Dalton
DC	Direct Current
DHAP	2,5-DiHydroxyAcetoPhenone
DHB	2,5-DiHyhydroxyBenzoic acid
DI	DeIonized
DNA	DeoxyriboNucleic Acid
EI	Electron Impact
ELISA	Enzyme-Linked ImmunoSorbent Assay
ESI	ElectroSpray Ionization
FET	Field Effect Transistor
GC	Gas Chromatography
LEP-AES	Liquid Electro Plasma - Atomic Emission Spectroscopy
M	Molar mol/L
<i>m/z</i>	Mass to charge ratio
MALDI	Matrix Assisted Laser Desorption/Ionization
MEMS	Micro Electro Mechanical Systems
min	Minute
MS	Mass Spectrometry
NEMS	Nano Electro Mechanical Systems
PDMS	Poly(DiMethylSiloxane)
PMMA	PolyMethyl MethAcrylate
QOL	Quality Of Life
RF	Radio Frequency

s	Second
S/N	Signal to Noise ratio
SA	Sinapic Acid or Sinapinic Acid
SPR	Surface Plasmon Resonance
TFA	TriFluoroacetic Acid
TOF	Time-Of-Flight
V	Volt
μTAS	micro Total Analysis System

CHAPTER 1

GENERAL INTRODUCTION

Abstract

In this chapter, recently discovered biomarkers in the biological samples and miniaturized analytical methods used for their analyses for the medical diagnosis are briefly introduced. Immunosorbent assay based analytical methods are widely used for biomarker detection because of highly specific binding affinity of the antibody and the antigen. However, detection of more versatile target molecules on a single analysis is required to utilize the latest research outcomes of the proteomics with mass spectrometry (MS). The preview of the mass spectrometry based miniaturized system such as the integrated devices of a micro vacuum pump, an ionization source, and a mass analyzer was introduced. The strategy to miniaturize the mass spectrometer on a chip with less bulky instruments was discussed. From the theoretical calculation of the mean free path, it was suggested that ion separation in a micro channel can be operated in a low vacuum at 1-10 Pa.

1.1 Recent progress of analytical methods for medical diagnosis

1.1.1 Biomarkers in biological samples

Biological molecules existing in human blood, saliva, urine, and sweat have considerable information for medical diagnosis because of the cause or consequence of many diseases in the body. To understand its nature related to life sciences, lots of analytical methods for biological samples have been developed. Specifically, many researchers are trying to analyze the functions of proteins which compose cells, organs, and whole human body by these analytical methods. Whole blood sample contains more than a half million proteins [1] with the different concentration. Figure 1.1 shows the reference intervals for 70 proteins in the plasma reported by Leigh et al [1]. From the literature, proteins seem to be divided into three major classes which are plasma proteins at the high abundance, tissue leakage proteins, and cytokines at the low abundance. Leigh et al [1] mentioned that *“Tissue leakage proteins are important because a serious pathology can be detected in a small volume of tissue by measuring release into plasma of a high abundance tissue protein”*. Especially in the low concentration region around ng/ml to pg/ml, significantly meaningful biomarkers for severe diseases such as cancers were discovered [2].

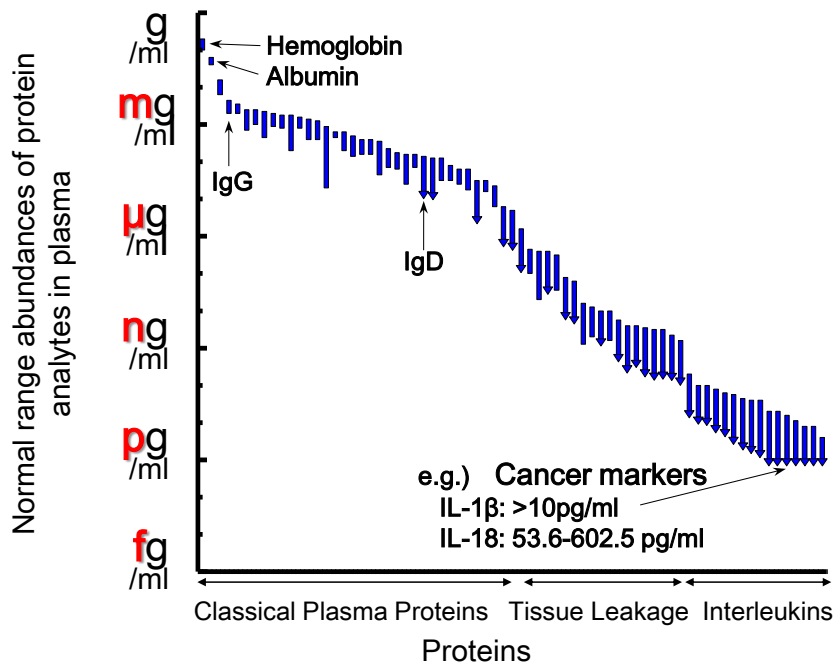


Figure 1.1 Normal range abundances of protein analytes in plasma [1] and biomarkers of cancers[2] discovered in blood sample.

Table 1.1 shows biomarkers of severe diseases found in human blood or saliva [3-8]. Some biomarkers of cancers (Interleukin-1 β [3], Interleukin-18 [4], and Cathapsin-D [5]) with the concentration in the range of ng/ml to pg/ml were detected from blood and saliva by Enzyme Linked Immunosorbent Assay (ELISA). ELISA is the most famous analytical method of biomarkers by using the highly specific binding of the proteins via the antigen-antibody interactions. Here, blood samples are more frequently used for the medical diagnosis than saliva or urine samples because the blood is directly related to the cellular activities like molecule transportation and biological defence. However, collection of enough blood samples for the analysis is accompanied with the pain and takes time. Saliva

and urine are expected to be the promising non-invasive sample for cancers diagnosis in the early stage. The issue of saliva in this purpose is that it is usually not enough to evaluate the pathology from a single biomarker due to its lower concentration than the biomarkers in blood [2]. Statistics analysis of peptides and proteins in saliva based on the MS with electrophoresis has been studied [6, 7]. Sugimoto et al reported that 57 principal metabolites [7] are found from saliva sample, which can be used to accurately predict the probability of being affected by oral, breast and pancreatic cancers. Biomarker analysis of volatile chemical compounds as well as proteins was also studied by GC-MS [8] for cancer diagnosis. The detection method of those gaseous biomarkers called “electronic nose” found that organic solvents such as 2-ethyl-1-hexanol and 3-methyl-1-butanol are related to the lung cancer.

If the prediction of the severe diseases is realized by screening of only saliva even in a small clinic, advanced diagnosis will be provided without a time-consuming thorough checkup in a hospital. Diagnosis in early stage of the diseases will be also realized to discover further biomarkers, leads improvement of Quality of Life (QOL) in the near future.

Table 1.1 *Lists of biomarkers for serious diseases found in blood or saliva sample, its concentration, and detection method of them.*

	Diseases	Sample	Concentration range	How to detect
IL-1 β [3]	Cardiovascular disease or Oral cancer	Blood/ saliva	>10pg/ml/ <10pg/ml	ELISA
IL-18 [4]	Cardiovascular disease or Oral cancer	Blood/ saliva	34.2-68.2pg/ml/ 53.6-602.5pg/ml	ELISA
Cathapsin-D [5]	Breast cancer	Blood	45.2pmol/mg	ELISA
Statistics analysis of 16 candidate proteins [6]	Lung cancer	Saliva	-	2-D difference gel electrophoresis and MS
Statistics analysis of 57 metabolites [7]	Oral, breast and pancreatic cancers	Saliva	-	CE-TOF-MS
2-ethyl-1-hexanol, 3-methyl -1-butanol [8]	Lung cancer	Saliva	29 ng/ml – 90 ng/ml, 3 ng/ml - 400ng/ml	GC-MS

1.1.2 Detection methods of biomarkers in biological samples

As mentioned in previous section, peptides and proteins in biological samples with low concentration have significant information for the medical diagnosis. To utilize the research outcomes to the clinical application, analytical systems should be considered. Important capabilities of the bio analytical systems are sensitivity, selectivity, target analytes, and cost. Table 1.2 shows the brief

summarization of developed bio analytical systems. ELISA [9] is the most famous bio analytical method with the specific binding of antigen and antibody. In ELISA, target analyte, usually an antigen is labelled by the antibody with enzyme conjugate, and then unattached antibodies and unfavourable substances in the sample are washed out for high S/N measurement. After that, added substrate and enzyme interaction create color change for the detection. Nie et al reported ELISA in the array of 888 microwells with microspheres [10] for higher S/N measurement than conventional ELISA. Highly sensitive analysis up to a few pg/ml [10] was accomplished to enhance the antigen-antibody interactions labelled with fluorescence by restricting the chamber volume and high surface-to-volume ratio of the microspheres. In those cases, colorimetric changes or fluorescent signal enhancement were used for the detection. In contrast to this, Field Effect Transistor (FET) [11] or Surface Plasmon Resonance (SPR) [12] was also used to detect the target antigen immobilized on the channel or the metal surface via the antibody. FET devices modified by nanomaterials such as silicon nanowires, carbon nanotubes, or graphene [11] were fabricated. These nanomaterials have significant advantage for highly sensitive biosensor with decreasing the non-specific binding of unfavorable substances on the nanomaterials of the channel as well as high electrical conductivity. Tawa et al reported highly sensitive biomarker detection using SPR based lab chip devices [12]. SPR is the collective oscillation of electrons in liquid or solid, usually gold substrate or gold nanoparticles by the specific incident light. They demonstrated that enhanced electric fields by SPR were utilized as the excitation field for

fluorescent biomolecules to realize high sensitive detection in the range up to 10^{-15} M.

Major miniaturized bio analytical devices use antigen–antibody interactions to selectively capture the specific biomolecules in biological samples. However, it is not easy to simultaneously detect several tens of multiple target analytes using immunochemical reactions because a series of antibodies having the specific binding affinity to each target analyte have to be preliminary equipped on the device. Mass spectrometric analysis like ESI-MS [13, 14] and MALDI-MS [15, 16] is frequently used for discovering biomarkers in life sciences research. The advantages of MS are high sensitivity and high selectivity, while the equipment is expensive because it is composed of high vacuum systems, high voltage source, and so on. An electrochemical biosensor [17, 18] is one of the applicants for the sensitive detection of multiple target analytes such as chemical compounds, proteins, and nucleic acids [18]. Reported performance of the electrochemical biosensor was not so sensitive in the range of μM for proteins [18]. Another highly sensitive miniaturized elemental analysis system called LEP-AES (Liquid Electrode Plasma Atomic Emission Spectroscopy) was reported by Kitano et al [19]. For the analysis of LEP, generated plasma with applying high voltage excites and atomizes injected samples in the microfluidic channel (width = $100\mu\text{m}$). Atomic emission spectrum is analyzed when the excited atoms return to the ground state. Tung et al reported that LEP-AES can apply to highly sensitive biomolecules analysis as the detection of hCG with the detection limit of 1.3 pg/ml [20]. These studies have been developed for fundamental studies of

molecular biology in the cell and biomarker discovering as well as analytical devices for clinical applications. For example, a commercially-available pregnancy test and a glucose sensor for patients of diabetes are widely used.

Table 1.2 *Lists of developed bio analytical systems and its characteristics.*

	Portability	Sensitivity	Selectivity	Target analyte	Materials and cost
ELISA [9]	Lab chip, pre-programmed and self-powered	10 ng/ml for CRP	Depends on antibody	Depends on antibody	PDMS
Microarrays ELISA [10]	Integrated desktop device	6-138pg/ml for Interleukins	Depends on antibody	Depends on antibody	PDMS/ Glass
FET based biosensor [11]	Lab chip	100pM forHER2	Depends on antibody	Depends on antibody	SiO ₂
SPR [12]	Lab chip	10nM to 700fM for sEGFR	Depends on antibody	Depends on antibody	PMMA
ESI-MS [13,14]	Poor	< 50nM for CE-ESI-MS/ 50ng/ml for paperspray ionization MS	m/Δm >11000 [13]	Chemicals, biological materials	Vacuum systems, Expensive
MALDI-MS [15, 16]	Poor	10fmol- 50amol for glycans [15]	m/Δm: 40000-60000 [16]	Chemicals, biological materials	Vacuum systems, Expensive
Electrochemical sensor [17, 18]	Lab chip	2.5μM for L-DOPA [17]	Available in undiluted human serum	Chemical compounds, proteins , DNA[18]	Scree - printing electrodes, cheap
Liquid Electrode Plasma [19,20]	Handheld device or Lab chip	0.52ng/ml for Cd [19]. 1.3 pg/ml for hCG [20]		Heavy metals or Labeled metal particle	Quartz or PMMA

1.1.3 Micro total analysis system

The ideas of micro total analysis system (μ TAS) and lab on a chip originated from the integration of chemical and biochemical experiments such as chemical handling, reactions, separations, and analyses into a chip to accelerate the research of efficient drug discovery, DNA sequencing, protein analysis, and cell analysis. In 1970s, miniaturized gas chromatography device fabricated on a silicon substrate [21] as a micro analysis system was firstly reported using photolithography and wet etching processes which have been used for semiconductor fabrication. In 1990s, high-throughput capillary electrophoresis in a microchip [22] was studied to accelerate the human genome project to analyze whole human genome. After that, the fabrication method based on inexpensive polymeric materials such as SU-8 [23] and poly (dimethylsiloxane) (PDMS) [24] were developed and microfluidic controlling elements including a pump and a check valve was also fabricated by soft-lithography techniques reported by Xie et al. The outstanding advantage of μ TAS and lab on chip is to fabricate the integrated miniature devices in the mass production, which can be available in the applications of environmental monitoring, food inspection, and medical diagnosis. Further development of lithography and dry etching process enabled the fabrication of nano structures on a chip having specific functions in nano-scale for the biological analysis of a single cell [25] and a single molecule [26], on the other hand, the development of stable microfluidic pumps and valves on a chip has been still big issue in this field. Integrated and automated systems of immune sensor and electrochemical sensor into desktop device for detection of insulin [27]

and cancer markers [10] were developed as successful studies of lab on chip. In near future, the chips for highly sensitive multiple target analysis of several tens of biomarkers, non-invasive diagnosis for cancers with saliva, urine, or sweat, and the diagnosis in very early stage of severe diseases are expected to be developed.

1.1.4 Proteomic analysis

Proteomics is a challenging study of analysis of proteins related to metabolism in the cells to understand its structures and functions. Human genome encodes series of amino acids, and the amino acids compose series of proteins in the body. A human body may contain more than one million different proteins [28], which are having different functions in cells. Understanding the functions of proteins is interesting research for future medical diagnosis and health care. However, study of the functions of every single protein in cells is difficult because huge proteins existing in the cell interact differently with each other. Proteomics has potential to discover new biomarkers for cancers and the other diseases in very early stage from non-invasive samples such as saliva and urine [7, 29, 30]. In proteomics, cyclopaedic protein expression analysis is required. To accomplish this requirement, massively-developed mass spectrometric analysis of peptides and proteins is one of the desired methods. Characteristics of high sensitivity and high selectivity of the MS supports the analysis of mixtures of peptides and proteins over 10,000 species in proteomic research. As mentioned above, MS is an effective analytical method having key roles in the understanding of the nature of

the biological system and in the future diagnosis system. To utilize the analytical methods and findings based on MS more effectively, some works of miniaturization of MS into a desktop device or a chip have been studied for a decade, which are overviewed in the later section.

1.2 Miniaturized mass spectrometer

1.2.1 General principle of mass spectrometer

MS is one of the most powerful and versatile analytical tools to measure gases, metals, chemical compounds and biological substances such as nucleic acids, peptides, and proteins. MS was initially used for precise measurements of atomic weight and isotopes by 1960s. After 1980s, soft ionization methods for biochemical compounds such as ESI [31] and MALDI [32, 33] were developed by Fenn et al, Tanaka et al, and Hillenkamp et al, respectively. These methods become the basis of analytical methods for massively progressed life sciences research.

Figure 1.2 illustrates the typical components of MS. MS is composed of an ionization source, a mass separation filter, and an ion detector in a vacuum chamber. In the initial step of MS, introduced samples are ionized by electron impact, plasma, laser, or high voltage source. The ionization is crucial phase for MS because analyzable substances are restricted by the ionization techniques. After ionization, generated ions are introduced to the mass analyzer, in which

motion of ions is controlled by external electric force and magnetic force. Two major mass analyzers are quadru-pole mass analyzer and a TOF mass analyzer. For quadru-pole mass analyzer, ions with specific mass-to-charge ratio are filtered to stably pass through the gap of four parallel metal rods applied radio frequency (RF) voltages. For TOF mass analyzer, mass-to-charge ratio is measured via flight time measurement of accelerated ions having the same kinetic energy as any other ion that has the same charge in an electric field. Finally, separated ions are captured and amplified by an electron multiplier. Ions are initially converted to electrons by collisions at the secondary electron emissive surface with high velocity, and then electrons are amplified by consecutive secondary electron emission with collisions to the reactive surface in a vacuum or by electron bombardment in a semiconductor. These components are aligned in a big vacuum chamber evacuated to high vacuum ($\sim 10^{-4}$ Pa), therefore MS has been expensive and cumbersome in an operation.

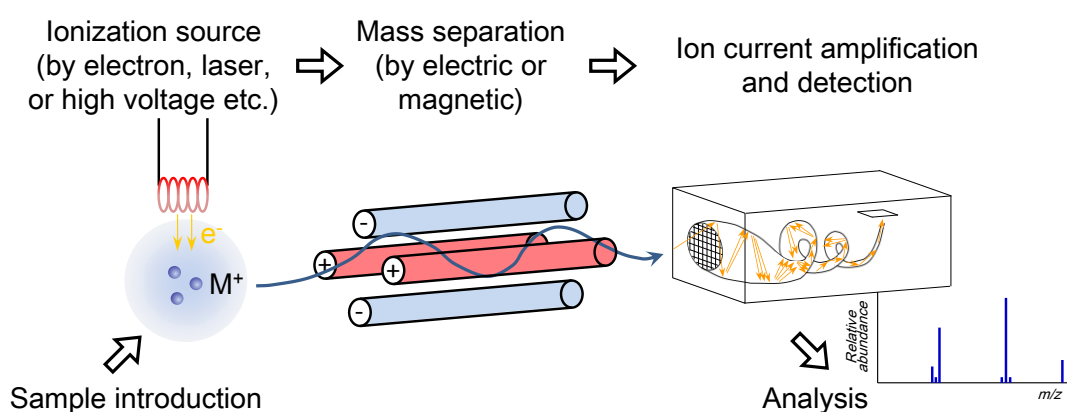


Figure 1.2 Schematic of the components of typical mass spectrometer.

1.2.2 Miniaturized mass spectrometer

Miniaturization of MS has been studied for the realization of highly sensitive and highly selective analysis on the site, not so much the lab as clinic, field, and environment. For example, miniaturized mass spectrometers were developed in use of real-time in-vivo analysis of the tissues [34] as a surgical tool [35] and on-site detection of chemical warfare agent, illicit drug, and explosives as backpack equipment [36]. Table 1.3 shows the previously reported miniaturized mass spectrometers. Two remarkable desktop mass spectrometers have been developed. Palm portable mass spectrometer developed by Yang et al [37] can analyze organic solvent in the air like dimethyl-methylphosphonate. The important progress in their research is that they created and maintained high vacuum (10^{-6} Torr $\sim 1.3 \times 10^{-4}$ Pa) in a portable device by miniaturized titanium ion getter pump. Mini 12 developed by Li et al [38] can analyze whole blood samples for POCT application. They developed the disposable sample cartridge with the disposable paper ionization source for the miniaturized paper spray ionization source [14]. The method can ionize sample solution containing the analytes under ambient conditions. On the other hand, further challenging studies to miniaturize the MS into microchip have been developed using μ TAS techniques. MEMS or NEMS techniques were used to fabricate a vacuum pump, an ionization source, and a mass analyzer on a chip. Unlike miniaturization of MS to desktop devices, on-chip MS have the significant advantage to be able to separate ions in a low vacuum [39] as well as the miniaturization. Integrated mass spectrometers on a chip [39-41] have been reported by Wapelhorst et al, Chaudhary et al, and

Wright et al. They fabricated EI or ESI ionization sources and the mass analyzers for the integration of MS into the chip and succeeded to analyze gaseous compounds [39, 40] and solution containing chemicals [41]. However analysis of peptides and proteins has not been realized by those on-chip MS because of the difficulty to ionize proteins without decomposition. Moreover, the on-chip MS currently works in a chamber maintaining at high vacuum with a conventional ion detector, therefore mass spectrometric analysis in a low vacuum have not been performed.

Table 1.3 *Lists of developed miniaturized mass spectrometer into a desktop device, a handheld device, or a chip. Details of its components, ionization source, mass analyzer, and vacuuming method were shown.*

	Size	Ionization	Mass analyzer	Vacuuming
Palm portable mass spectrometer [37]	Hand held (1.48kg)	Electron impact	Four-parallel-disk ion trap	Ion getter pump + Roughing pump
Mini 12 [38]	Desktop (4kg)	Paper spray ESI [14]	Rectilinear ion traps	Small turbo pump (1mTorr for MS scan)
A fully integrated TOF micro mass spectrometer [39]	Lab chip	Electron impact	TOF + Energy filter	–
Ion trap mass spectrometer arrays [40]	Lab chip	Electron impact	25 Cylindrical ion trap arrays	In a vacuum chamer (7.4×10^{-7} Torr)
MEMS-based nanospray-ionization mass spectrometer [41]	Lab chip	MEMS-based Nano-ESI	Quadru-pole	In a vacuum chamber (1m Torr in and analysis chamber)

1.2.3 Microfabricated vacuum pumps

A vacuum pump is an essential component for MS because the ions are separated in a vacuum with avoiding collisions to any other ions or neutral molecules existing in the chamber. Nowadays, many kinds of vacuum pumps are commercially-available such as a rotary pump, a diaphragm pump, a diffusion pump, a sorption pump, and a turbo-molecular pump. However, there are a few researches of miniaturization of vacuum pump into a microchip [42-44] despite some equipment for handling solution and surface analytical systems like scanning electron microscope (SEM) are utilized by a vacuum. One of the reasons is the difficulty to generate mechanical force in a microfluidic device to evacuate gas molecules from a microchip.

Figure 1.3 shows the fabricated miniaturized vacuum pumps without any moving parts. McNamara et al developed micro-machined Knudsen pump [42] using MEMS process as shown in Fig 1.3 (a). The Knudsen pump relies on the principle of thermal transpiration which is a net gas flow from the colder chamber to the hotter chamber through the narrow channel. Pressure difference between the two chambers is created through a narrow channel in which the gas is in the free molecular flow regime. They fabricated thermally-isolated chambers connected with micro channels and maintained a vacuum at 46 kPa in a cold chamber on a chip. Doms et al reported a micro-machined vapor jet pump [43] inspired by diffusion pump as shown in the Fig 1.4 (b). Diffusion pump is a vacuum pump to evacuate molecules from a chamber by boiling of the fluid with the high speed jet.

Basically, diffusion pump needs roughing vacuum pump and cooling system for capturing boiling fluid. They demonstrated the principle on a chip using the miniaturized device fabricated by MEMS. A vacuum at 87 kPa with the combination of nitrogen gas supply and roughing vacuum pump and a vacuum at 96 kPa with external water vapor and cooling water supply were maintained on a chip. Miniaturized MEMS-type glow-discharge micro pump [44] was reported by Grzebyk et al as shown in Fig 1.3(c). They used gettering of Ti in a miniaturized vacuum chamber where chemically-active gases such as hydrogen, oxygen, nitrogen, and so on are adsorbed on the surface accompanying with sputtered Ti ions. The ion gettering vacuum pump created minimum pressure of 3 Pa while a roughing vacuum pump must be required. High vacuum creation on a chip has not been realized without any roughing vacuum pump. Totally miniaturized vacuum pump can be useful for microfluidic handling and analytical systems if the issues of creating high vacuum, of maintaining a vacuum on a chip, and minimizing the dead volume are solved.

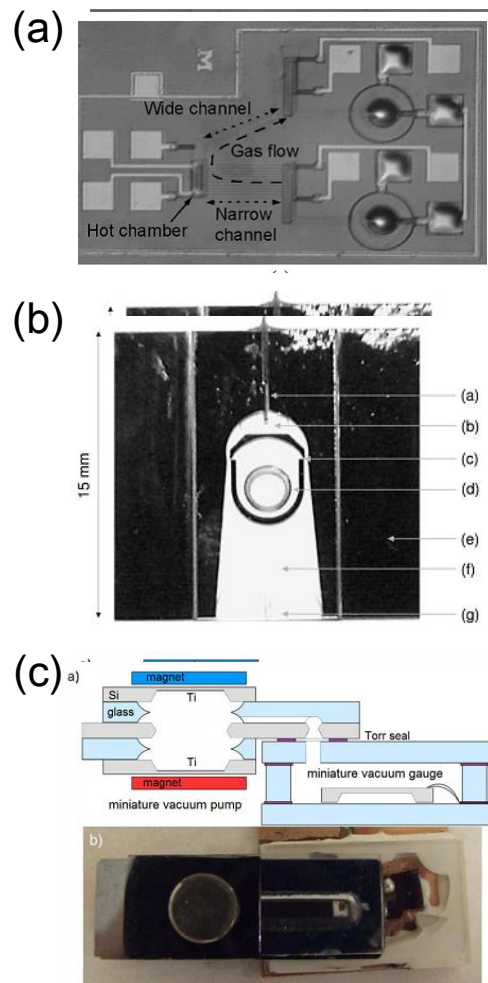


Figure 1.3 Images of the miniaturized vacuum pumps. (a) Knudsen pump [42]. (b) Microfabricated vapor jet pump [43]. (c) Titanium ion getter vacuum pump [44].

1.2.4 Microfabricated ionization sources

Ionization is one of significant processes in the mass spectrometric analysis. Biomolecules such as peptides, proteins, and nucleic acids have not been analyzed by MS until 1980s because it was difficult to evaporate without thermal decomposition before the ionization [45]. Fenn et al [31] and Tanaka et al [33]

developed the novel ionization methods of ESI and MALDI to ionize biomolecules without decomposition and denaturation via different soft ionization techniques. Such kind of the soft ionization techniques are required to apply biomolecules detection in a miniaturized mass spectrometer.

Figure 1.4 shows the miniaturized ionization sources for gases and solution fabricated by MEMS or NEMS techniques. Microfabricated EI ionization sources with micro tungsten filament [46] and with carbon nano particles [47] were reported by Yoon et al as shown in Fig. 1.4(a). The electron impact ionization is well-known as a typical ionization method for gases or organic volatile samples. Basically, the analytes are limited to gases to ionize the gaseous molecule with the impact of electron normally accelerated to 70 eV. They demonstrated thermal electron emission from the heated micro filaments fabricated on a chip. Positive ions of organic solvent as acetone were measured by an integrated TOF mass analyzer; however the fabricated miniaturized ionization sources were not used in MS on a chip because of low thermo ionization energy. Cold cathode electron emitting source using carbon nanotube (CNT) [48] was fabricated by Velasquez-Garcia et al as shown in the Fig. 1.4 (b). Electrons can be generated not only by heated filament (a few thousand K) but also by high electric field ($\sim 10^9$ V/m) to remove an electron from metal surface by the tunnelling effect. CNT is a suitable nano material for electron emissions because of the tiny tip (\sim a few dozen nm [48]) in which the electric potential is concentrated. Perpendicularly-grown CNT forests with its typical diameter of 33 nm were fabricated on the microfabricated structures for the ionization of argon gases.

Disadvantage of the both EI sources is that suitable samples are only gases or volatile solvents. Many studies have been studied to evaporate non-volatile samples such as peptides with little fragmentation by rapid heating technique (10 °C/s) and use of Teflon emitter [49] before the EI ionization, but the analysis of the mass spectrum was difficult.

In contrast to the EI ionizations on a chip, nano-ESI was fabricated for the ionization of non-volatile chemical compounds in the solution [50]. Figure 1.4 (c) shows the microfabricated nano-ESI source integrated with miniaturized quadru-pole mass analyzer. ESI is known as a soft ionization method to be able to ionize non-volatile analytes including biomolecules from liquid phase without decomposition of target analytes. Detailed principle of ESI has been still discussed, while aerosol is created at the outlet of nano-capillary in which high voltage (~kV) is applied to sample solution. Initially, positively charged droplets (diameter of μm) were produced after spraying of aerosol if the positive high voltage is applied to the capillary. The charge comes from the ambient excess ions (H^+ , NH_4^+ , Na^+ , and K^+), mainly protons in acidic solution [51]. The charged droplets undergo rapid solvent evaporation by vacuuming and heating through ambient gases. Finally, nano-size droplets containing the analyte of the interest with multiple charges are analyzed by the mass analyzer. Wright et al reported miniaturized vacuum interfaces to control three different vacuum stages, atmospheric pressure for sample injection, low vacuum for ionization, and high vacuum for MS analysis, as well as nano-capillary for ESI source on a chip. A 150 $\mu\text{g/ml}$ of tetrabutylammonium hydroxide solution was measured by the

microfabricated ionization with quadru-pole mass analyzer and the singly-charged target ion was successfully obtained [50]. Drawbacks of the ESIs are that high voltage source (700-850 V for microfabricated nano-ESI) and ambient heated gases are required for the ionization. Moreover, multiply-charged ions are more frequently produced than singly-charged ion, thus deconvolution processing is required for analysis of complicated mass spectrum. On the other hand, MALDI source is also well-known as a soft ionization method. In MALDI, samples containing target analytes and organic matrix having efficient absorption at the specific wavelength are irradiated by a laser, and then are desorbed by rapid thermal desorption. In the plume of desorbed sample gases, the charge transfers to the analyte from the charged matrix. Sometimes MALDI is superior to ESI for protein analysis as following reasons; (i) basically, singly-charged ions are more frequently produced than multiply-charged ions, which give relatively comprehensible mass spectrum. (ii) Integration with TOF mass analyzer provides highly sensitive and highly selective protein analysis up to m/z of 100,000 Da [33]. Currently, miniaturized MALDI source on a chip has not been reported due to the complexity of laser optical components with microfluidic systems.

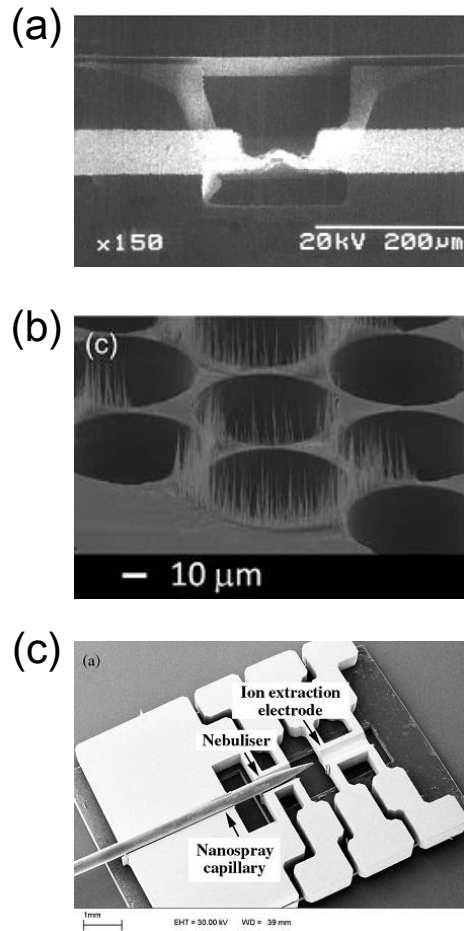


Figure 1.4 SEM images of the miniaturized ionization sources. (a) Electron impact ionization source fabricated by tungsten filament [46]. (b) Carbon nanotube cold emitter [48]. (c) Nano electrospray ionization source [50].

1.2.5 Microfabricated mass analyzers

First ion trapping techniques studied in 1950s such as Penning trap [52] and Paul trap (Quadru-pole trap) [53] developed by Dehmelt et al and by Paul et al, respectively. An electron or an ion trap is realized by the combination of electric and magnetic fields in a vacuum. For penning trap, charged particles are

trapped in a homogeneous static magnetic field and a spatially inhomogeneous static electric field. In contrast to this, charged particles are trapped in oscillating AC electric fields for quadru-pole trap. The quadruple trap system is normally used for MS due to the high scan rate for mass analysis by changing only electric potential. Specific ions circularly travel along the stable trajectory in the both of the trapping systems.

Figure 1.5 shows the fabricated miniaturized mass analyzers using MEMS or NEMS techniques [39-41]. Wapelhorst et al reported on-chip mass analyzer integrated with TOF separation and energy filter [39]. TOF mass analyzer is basically a kind of energy filtering of the ions. Same kinetic energy was applied by the electric potential difference to all the ions with same charge. After that, ions flight at the different velocity in the free flight region applied no electric and no magnetic fields. Mass to charge ratio m/z of the molecules is analyzed by measuring time of the free flight in a vacuum. Additionally, energy filter placed after TOF region was used to separate the ion having lower or higher initial energy for the highly selective analysis. One of the advantages of TOF mass analyzer is no limitation in the analytical range of m/z in theory if measurement time will be sufficiently long.

Miniaturized ion trap filters, quadru-pole mass analyzer [41] and cylindrical ion trap analyzer [40], were fabricated by Wright et al and Chaundhary et al, respectively. To fabricate miniaturized quadru-pole mass analyzer, electrode rods with a diameter of 650 μm were precisely aligned on the microfabricated

devices. Perfluorotributylamine was analyzed by miniaturized quadru-pole mass analyzer with the best resolution of $m/\Delta m \approx 140$ [41]. Cylindrical ion trap chip with 5×5 ion trap arrays [40] were fabricated using MEMS process. Such integrated array of MS components on a chip is challenging issues. Here, theoretical stability of the ions in quadru-pole electrode is discussed to estimate the capability of it in micro systems. The of motion of a charged particle in the x-y cross section of the quadru-pole electrodes applied the superimposed RF and DC voltages ($\pm(U+V\cos\omega t)$) is governed by the following Mathieu equation. [54]

$$\frac{d^2x}{d\tau^2} + (a_x + 2q_x \cos 2\tau)x = 0 \quad (1.1)$$

$$\frac{d^2y}{d\tau^2} + (a_y + 2q_y \cos 2\tau)y = 0 \quad (1.2)$$

where,

$$a_x = -a_y = \frac{4eU}{mr_0^2 \omega^2}, \quad q_x = -q_y = \frac{2eV}{mr_0^2 \omega^2}, \quad \tau = \frac{\omega t}{2} \quad (1.3)$$

U is the amplitude of DC voltage, and V is the amplitude of RF voltage applied in the quadru-pole, e is charge of the ion, m is mass of the ion, r_0 is the distance to the rod electrode from the center, and $\omega=2\pi f$ is angular frequency. Ions having the specific mass-to-charge ratio pass through the quadru-pole with stable oscillation in the x-y plane. Basically, amplitude of RF voltage is scanning for mass separation with holding a constant value of $2U/V$, thus the trapped ions satisfy the following equation.

$$\frac{m}{e} = K \frac{V}{r_0^2 \omega^2} \quad (1.4)$$

where, K is a constant depending on the geometry of quadru-pole electrodes. From the relation, high voltage is required to stabilize heavier ions such as proteins with the constant RF frequency. For the miniaturized quadru-pole, relatively high voltage $V = 770\text{V}$ and $f \approx 6.5\text{MHz}$ were used to trap the ion with m/z of 1,200 [41] despite the value of r_0 decreases.

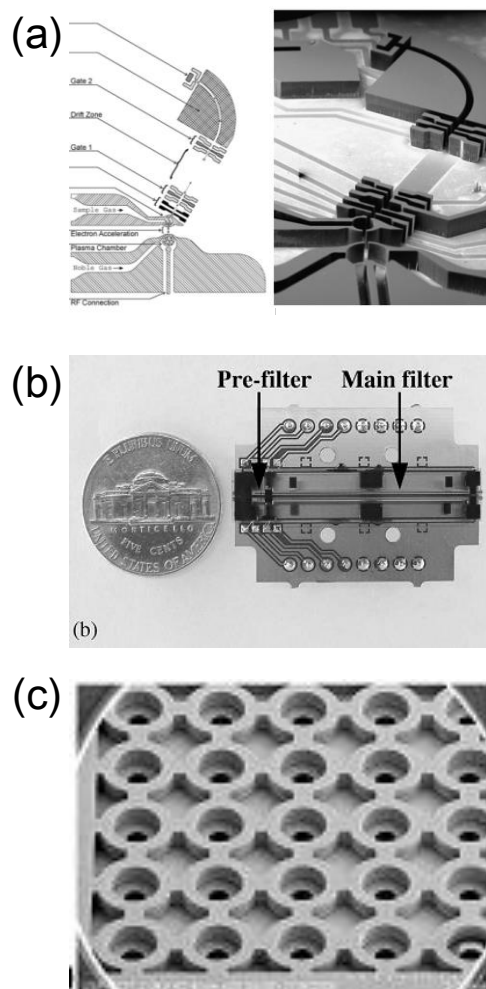


Figure 1.5 Images of the miniaturized mass analyzers. (a) TOF mass analyzer with an energy filter [39]. (b) Quadrupole mass analyzer [41]. (c) Cylindrical ion trap mass analyzer [40].

1.3 Strategy to miniaturize mass spectrometer on a microchip

Miniaturized mass spectrometers composed of various MS components were developed using the fabrication process, MEMS and NEMS due to its high sensitivity and high selectivity for multiple target analysis. Interestingly, Siebert et

al pointed that mass separation in microsystems can be employed at the pressure of 1-10 Pa [55] and calculated ion trajectory in the microstructure by numerical simulation. To discuss the ion separation, mean free path, the average distance travelled by gas molecules between collisions, is estimated by the following equation [56].

$$\text{mean free path} = \frac{7 \times 10^{-3}}{p [\text{Pa}]} [m] \quad (1.5)$$

where, p is the ambient pressure. The relation of mean free path versus pressure was shown in the Figure 1.6 (a). In conventional high vacuum system at the pressure of 10^{-3} Pa, mean free path of the remaining gases is about 7 m which is greater than the dimension of usual laboratory vacuum chamber. Figure 1.6 (b) shows the illustration of the concept of MS in the microsystem. Presently available mass spectrometer is used in a high vacuum (below 10^{-3} Pa) to prevent ion disruption and disturbance by collisions with the other ions or molecules as well as in a large chamber (~ 1 m) for highly selective analysis. If the ion generation and handling in the miniaturized chamber with the size of mm or μm are realized, required mean free path for MS to prevent the ion interactions in the miniaturized chamber will decrease to mm or μm scale. From the calculated mean free path, mass separation in a microchip can be operated even in a low vacuum approximately 10 Pa. Thus, bulky high vacuum system like a turbo-molecular pump will be not employed, if the required vacuum is down to 1-10 Pa. These

concepts have not been realized on a chip even the miniaturized ionization sources and mass analyzers were developed. The reasons of this are follows; (i) Development of the miniaturized vacuum pump having enough performance for the on-chip MS (1-10 Pa) without any external vacuum pump has not been realized. (ii) Currently developed miniaturized ionization source for biological samples i.e. on-chip nano-ESI was employed with high vacuum system at high exhaust velocity and with high voltage (~ 0.85 kV) which may cause problems of discharge in a low vacuum. (iii) Integration of whole components of MS, an ionization source, the interface for sample introduction, a mass analyzer, and a detector into a single device have not been realized.

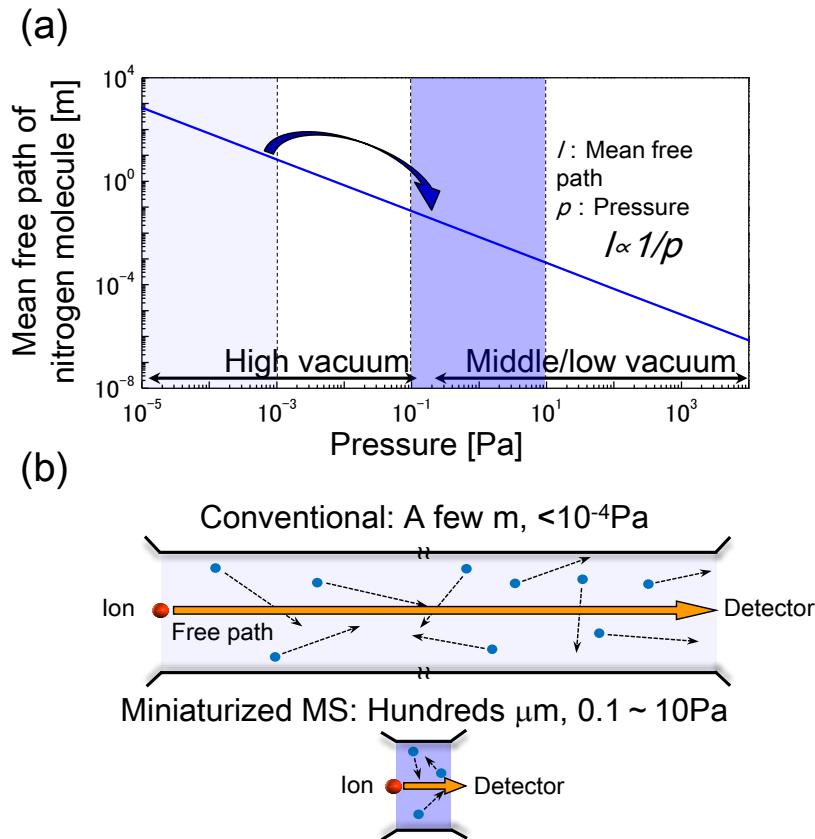


Figure 1.6 Schematic of the advantage of miniaturized mass spectrometry on a chip. (a) Dependence of mean free path on ambient pressure. (b) Comparison between conventional MS and on-chip MS.

1.4 Research objectives

In this thesis, the components of MS, the vacuum pump, the ionization source, and the TOF mass analyzer, are miniaturized using MEMS fabrication techniques for the development of on-chip mass spectrometer toward highly sensitive analysis of biological samples. A vacuum generation method on a chip with gas-liquid phase transition is studied for realization of a low vacuum toward

MS analysis without any external pumps. Second, an ionization source for biological samples such as peptides and proteins is developed on a chip without laser, high voltage, and ambient heated gases. The novel ionization source utilizes nano-second Joule heating from the micro heater to the solid-phase samples on a chip, which easily combines to relatively small homebuilt TOF mass analyzer for protein mass spectrometry. Finally, the developed ionization source is integrated with the miniaturized ion lens and TOF path fabricated on a chip to realize on-chip MS analysis. Protein MS is performed in the chip-based TOF mass analyzer.

1.5 Thesis organization

Chapter 1 explains recent progress of analytical methods for medical diagnosis including desktop or microfabricated lab on chip devices and miniaturized mass spectrometers and the strategy to effectively miniaturize the mass spectrometer on a chip. Finally research objectives are presented.

Chapter 2 shows the study of vacuum generation on a chip. Pressure measurement in a chamber and the vacuum generation method using gas-liquid phase transition on a chip are shown.

Chapter 3 presents pulse-heating ionization for peptides and proteins without laser, high voltage, and ambient gases. Numerical simulation, fabrication process of the chip, experimental setup for the ionization, and TOF mass analysis

are explained. And then protein mass spectrometry with the pulse-heating ionization chip and relatively small TOF mass analyzer is performed.

Chapter 4 discusses the effects of matrix and solvent for sample formation on the pulse-heating ionization. To minimize the generation of fragment ions in the ionization, effective matrix and sample preparation method are studied. Finally, the sensitivity of the pulse-heating ionization is estimated.

Chapter 5 explains the miniaturized ion lens and the TOF mass analyzer on a chip. Miniaturized TOF mass analyzer is studied by numerical simulation of the ion trajectory controlled by the electric fields with micro electrodes. On-chip mass spectrometry of protein sample is realized by the integration of the pulse-heating ionization source and the miniaturized TOF mass analyzer of 5 mm length.

Chapter 6 summarizes the works in this thesis.

References

- [1] Anderson, N. Leigh, and Norman G. Anderson. "The human plasma proteome history, character, and diagnostic prospects." *Molecular & cellular proteomics* 1.11 (2002): 845-867.
- [2] Pfaffe, Tina, et al. "Diagnostic potential of saliva: current state and future applications." *Clinical chemistry* 57.5 (2011): 675-687.
- [3] Morris, Andrew Conway, et al. "Diagnostic importance of pulmonary interleukin-1 β and interleukin-8 in ventilator-associated pneumonia." *Thorax* 65.3 (2010): 201-207.
- [4] Mallat, Z., et al. "Increased plasma concentrations of interleukin-18 in acute coronary syndromes." *Heart* 88.5 (2002): 467-469.
- [5] Foekens, J. A., et al. "Cathepsin-D in primary breast cancer: prognostic evaluation involving 2810 patients." *British journal of cancer* 79.2 (1999): 300.
- [6] Xiao, Hua, et al. "Proteomic analysis of human saliva from lung cancer patients using two-dimensional difference gel electrophoresis and mass spectrometry." *Molecular & Cellular Proteomics* 11.2 (2012): M111-012112.
- [7] Sugimoto, Masahiro, et al. "Capillary electrophoresis mass spectrometry-based saliva metabolomics identified oral, breast and pancreatic cancer-specific profiles." *Metabolomics* 6.1 (2010): 78-95.
- [8] del Noyal Sánchez, Miguel, et al. "Sensitivity Enhancement in the Determination of Volatile Biomarkers in Saliva Using a Mass Spectrometry-Based Electronic Nose with a Programmed Temperature Vaporizer." *Analytical chemistry* 86.15 (2014): 7890-7898.
- [9] Safavieh, Roozbeh, and David Juncker. "Capillaries: pre-programmed, self-powered microfluidic circuits built from capillary elements." *Lab on a Chip* 13.21 (2013): 4180-4189.
- [10] Nie, Shuai, et al. "An automated integrated platform for rapid and sensitive multiplexed protein profiling using human saliva samples." *Lab on a Chip* 14.6 (2014): 1087-1098.

- [11] Myung, Sung, et al. "Graphene-encapsulated nanoparticle-based biosensor for the selective detection of cancer biomarkers." *Advanced Materials* 23.19 (2011): 2221-2225.
- [12] Tawa, Keiko, et al. "Application of 300× Enhanced Fluorescence on a Plasmonic Chip Modified with a Bispecific Antibody to a Sensitive Immunosensor." *ACS applied materials & interfaces* 5.17 (2013): 8628-8632.
- [13] Lapainis, Theodore, Stanislav S. Rubakhin, and Jonathan V. Sweedler. "Capillary electrophoresis with electrospray ionization mass spectrometric detection for single-cell metabolomics." *Analytical chemistry* 81.14 (2009): 5858-5864.
- [14] Liu, Jiangjiang, et al. "Development, characterization, and application of paper spray ionization." *Analytical chemistry* 82.6 (2010): 2463-2471.
- [15] Kaneshiro, Kaoru, et al. "Highly sensitive MALDI analyses of glycans by a new aminoquinoline-labeling method using 3-aminoquinoline/ α -cyano-4-hydroxycinnamic acid liquid matrix." *Analytical chemistry* 83.10 (2011): 3663-3667.
- [16] Sato, Hiroaki, et al. "Application of high-resolution MALDI-TOFMS with a spiral ion trajectory for the structural characterization of free radical polymerized methacrylate ester copolymers." *Mass Spectrometry* 2.1 (2013).
- [17] Brunetti, Barbara, et al. "A disposable electrochemical biosensor for L-DOPA determination in undiluted human serum." *Electrochemistry Communications* (2014).
- [18] Vashist, Sandeep Kumar, et al. "Advances in carbon nanotube based electrochemical sensors for bioanalytical applications." *Biotechnology advances* 29.2 (2011): 169-188.
- [19] Kitano, Atsushi, et al. "Highly sensitive elemental analysis for Cd and Pb by liquid electrode plasma atomic emission spectrometry with quartz glass chip and sample flow." *Analytical chemistry* 83.24 (2011): 9424-9430.
- [20] Tung, Nguyen Hoang, et al. "Sensing technique of silver nanoparticles as labels for immunoassay using liquid electrode plasma atomic emission spectrometry." *Analytical chemistry* 84.3 (2012): 1210-1213.

- [21] Terry, Stephen C., John H. Jerman, and James B. Angell. "A gas chromatographic air analyzer fabricated on a silicon wafer." *Electron Devices, IEEE Transactions on* 26.12 (1979): 1880-1886.
- [22] Woolley, Adam T., and Richard A. Mathies. "Ultra-high-speed DNA sequencing using capillary electrophoresis chips." *Analytical chemistry* 67.20 (1995): 3676-3680.
- [23] Lorenz, Hubert, et al. "Fabrication of photoplastic high-aspect ratio microparts and micromolds using SU-8 UV resist." *Microsystem Technologies* 4.3 (1998): 143-146.
- [24] Anderson, Janelle R., et al. "Fabrication of microfluidic systems in poly (dimethylsiloxane)." *Electrophoresis* 21 (2000): 27-40.
- [25] Sims, Christopher E., and Nancy L. Allbritton. "Analysis of single mammalian cells on-chip." *Lab on a Chip* 7.4 (2007): 423-440.
- [26] Craighead, Harold. "Future lab-on-a-chip technologies for interrogating individual molecules." *Nature* 442.7101 (2006): 387-393.
- [27] Shiohara, Suguru, et al. "Development of the automated gold-linked electrochemical immunoassay system for blood monitoring." *Microsystem Technologies* 20.2 (2014): 273-279.
- [28] Lund, Ole, ed. *Immunological bioinformatics*. MIT press, 2005.
- [29] Soga, Tomoyoshi, et al. "Metabolomic profiling of anionic metabolites by capillary electrophoresis mass spectrometry." *Analytical chemistry* 81.15 (2009): 6165-6174.
- [30] Hirayama, Akiyoshi, et al. "Quantitative metabolome profiling of colon and stomach cancer microenvironment by capillary electrophoresis time-of-flight mass spectrometry." *Cancer Research* 69.11 (2009): 4918-4925.
- [31] Fenn, John B., et al. "Electrospray ionization for mass spectrometry of large biomolecules." *Science* 246.4926 (1989): 64-71.
- [32] Hillenkamp, Franz, et al. "Matrix-assisted laser desorption/ionization mass spectrometry of biopolymers." *Analytical chemistry* 63.24 (1991): 1193A-1203A.
- [33] Tanaka, Koichi, et al. "Protein and polymer analyses up to m/z 100 000 by

- laser ionization time of flight mass spectrometry." *Rapid communications in mass spectrometry* 2.8 (1988): 151-153.
- [34] Schäfer, Karl-Christian, et al. "Real time analysis of brain tissue by direct combination of ultrasonic surgical aspiration and sonic spray mass spectrometry." *Analytical chemistry* 83.20 (2011): 7729-7735.
- [35] Balog, Julia, et al. "Identification of biological tissues by rapid evaporative ionization mass spectrometry." *Analytical chemistry* 82.17 (2010): 7343-7350.
- [36] Hendricks, Paul I., et al. "Autonomous in Situ Analysis and Real-Time Chemical Detection Using a Backpack Miniature Mass Spectrometer: Concept, Instrumentation Development, and Performance." *Analytical chemistry* 86.6 (2014): 2900-2908.
- [37] Yang, Mo, et al. "Development of a palm portable mass spectrometer." *Journal of the American Society for Mass Spectrometry* 19.10 (2008): 1442-1448.
- [38] Li, Linfan, et al. "Mini 12, Miniature Mass Spectrometer for Clinical and Other Applications Introduction and Characterization." *Analytical chemistry* 86.6 (2014): 2909-2916.
- [39] Wapelhorst, Eric, Jan-Peter Hauschild, and Jörg Müller. "Complex MEMS: a fully integrated TOF micro mass spectrometer." *Sensors and Actuators A: Physical* 138.1 (2007): 22-27.
- [40] Chaudhary, Ashish, F. Van Amerom, and R. Timothy Short. "Development of microfabricated cylindrical ion trap mass spectrometer arrays." *Microelectromechanical Systems, Journal of* 18.2 (2009): 442-448.
- [41] Wright, Steven, et al. "Microfabricated quadrupole mass spectrometer with a Brubaker prefilter." *Microelectromechanical Systems, Journal of* 19.2 (2010): 325-337.
- [42] McNamara, Shamus, and Yogesh B. Gianchandani. "On-chip vacuum generated by a micromachined Knudsen pump." *Microelectromechanical Systems, Journal of* 14.4 (2005): 741-746.
- [43] Doms, Marco, and J. Mueller. "A micromachined vapor jet pump." *Sensors*

- and Actuators A: Physical* 119.2 (2005): 462-467.
- [44] Grzebyk, Tomasz, et al. "Integration of a MEMS-type vacuum pump with a MEMS-type Pirani pressure gauge." *Vacuum Nanoelectronics Conference (IVNC), 2014 27th International*. IEEE, 2014.
- [45] Cotter, Robert J. "Mass spectrometry of nonvolatile compounds by desorption from extended probes." *Analytical Chemistry* 52.14 (1980): 1589-1606.
- [46] Yoon, Hyeun Joong, et al. "Fabrication of a novel micro time-of-flight mass spectrometer." *Sensors and Actuators A: Physical* 97 (2002): 441-447.
- [47] Yoon, Hyeun Joong, et al. "Fabrication of two types of micro ion sources for a micro time-of-flight mass spectrometer." *Journal of Micromechanics and Microengineering* 17.8 (2007): 1542.
- [48] Velasquez-Garcia, Luis Fernando, Blaise Laurent Patrick Gassend, and Akintunde Ibitayo Akinwande. "CNT-based MEMS/NEMS gas ionizers for portable mass spectrometry applications." *Microelectromechanical Systems, Journal of* 19.3 (2010): 484-493.
- [49] Wright, Steven, et al. "MEMS-based nanospray-ionization mass spectrometer." *Microelectromechanical Systems, Journal of* 19.6 (2010): 1430-1443.
- [50] Beuhler, R. J., et al. "Proton transfer mass spectrometry of peptides. Rapid heating technique for underivatized peptides containing arginine." *Journal of the American Chemical Society* 96.12 (1974): 3990-3999.
- [51] Konermann, Lars, et al. "Unraveling the mechanism of electrospray ionization." *Analytical chemistry* 85.1 (2012): 2-9.
- [52] Dehmelt, H. G., and F. L. Walls. "" Bolometric" Technique for the rf Spectroscopy of Stored Ions." *Physical Review Letters* 21.3 (1968): 127.
- [53] Paul, Wolfgang. "Electromagnetic traps for charged and neutral particles." *Reviews of Modern Physics*, 62.3 (1990): 531-540.
- [54] Gross, Jürgen H. *Mass spectrometry* Springer, 2004.
- [55] Siebert, Peter, et al. "Surface microstructure/miniature mass spectrometer: processing and applications." *Applied Physics A: Materials Science & Processing* 67.2 (1998): 155-160.

[56] Chambers, Austin. *Basic vacuum technology 2nd edition*. IOP Publishing, 1998.

CHAPTER 2

ON-CHIP VACUUM GENERATION METHOD

Abstract

Development of an on-chip vacuum generation technique employing the gas-liquid phase transition was studied toward the use for miniaturized mass spectrometer on a chip. A vacuum-tight quartz chip was fabricated using conventional MEMS process. The fabricated chip was composed of a simple structural design of vacuum chamber and a diaphragm for pressure measurement with laser displacement meter. Efficient reduction of pressure in the chamber was realized by phase transition from the gas phase to liquid phase on a chip. The lowest pressure attained to 8.5 kPa from atmospheric pressure using degassed deionized (DI) water without any external vacuum pump. The highest performance was achieved among the previously reported on-chip vacuum pumps of Knudsen pump and micro vapor jet pump without any external vacuum pump.

The contents of this chapter were partially published in *Sensors and Actuators A: Physical* entitled “Development of on-chip vacuum generation by gas–liquid phase transition” [1].

2.1 Introduction

For microfluidic researches, pumping system [2, 3] has great potential to control air or liquid for handling chemical solution in microfluidic channel and to create a vacuum for analytical systems. Conventional bulky pumps such as rotary pumps, diaphragm pumps, and turbo-molecular pumps are composed of complex mechanical moving parts. Currently, desktop-size devices of ion getter vacuum pump [4] and turbo-molecular vacuum pump [5] were fabricated for the use of mass spectrometry. While the fundamental structures of the pumps were established, the miniaturization of a vacuum pump has not yet been realized in microfluidic systems. One of the reasons for this is the difficulty of generating strong mechanical force such as rotation and deformation on chip-based devices. Currently, a few previous experimental works have been studied about miniaturized vacuum pumps such as the miniaturized vapor jet pumps [6, 7], the micro Knudsen pumps [8], and the ion getter pumps [9]. Both of the vapor jet pump and Knudsen pump cannot create a vacuum down to 1-10 Pa which is adequate for miniaturized mass spectrometry from theoretical estimation discussed in the chapter 1 and the literature [10]. Titanium ion getter pump can

realize such the vacuum with the highest vacuum at 3Pa, while an external roughing vacuum pump must be employed.

2.2 Objective

In order to achieve the low vacuum (1-10 Pa) for miniaturized MS in the microchip, on-chip vacuum generation method using gas-liquid phase transition is studied. The method can evacuate a chamber from atmospheric pressure without any external pump using a temperature controller like a Peltier module. Larger volume of the connecting tubing than micro vacuum chamber in the chip having the volume lower than nL cause the massive dead volume. Therefore, on-chip pressure measurement is also integrated to reduce the dead volume.

2.3 Principle

2.3.1 Principle of vacuum generation on a chip

Effect of the condensation due to phase transition from gas-phase to liquid-phase was used to create vacuum on a chip. Figure 2.1 shows the conceptual diagram of the phase transition vacuum pump. Not only air initially occupied in the chamber but also additional solvent vapor due to liquid introduction can be removed from the working space of the chamber by this system with following steps: (i) The initial air is pushed out from the chamber by

introduction of the operation liquid; (ii) Then most of the operation liquid is removed from the chamber by the evaporation; (iii) The vapor of the operation liquid is removed from the working space in the chamber by adsorption and freezing onto the wall of the chamber in the cooling step. This system is a kind of conventional cryopump which have a vacuum chamber connected extremely cooled chamber to nearly absolute zero temperature. Here, atmospheric gas in the vacuum chamber is moved to the cooled chamber. Such separated system is not effective for micro system because of increasing of dead volume and difficulty of thermal insulation on a chip. Thus the combination of vacuum chamber and pump as described in this chapter is essentially effective design for such micro vacuum system. The advantages of the vacuum operation of the phase transition pump are listed as follows; (i) Pressure reduction is achieved by small temperature change around phase transition temperature; (ii) By using low boiling point liquid, the reduction of pressure is realized with small change of temperature around room temperature without extreme heating or cooling; (iii) No complicated structures or moving parts are required, thus, enabling more flexible configurations for chip designs and flow patterns; (iv) Vacuum operation from atmospheric pressure is possible without an external pump.

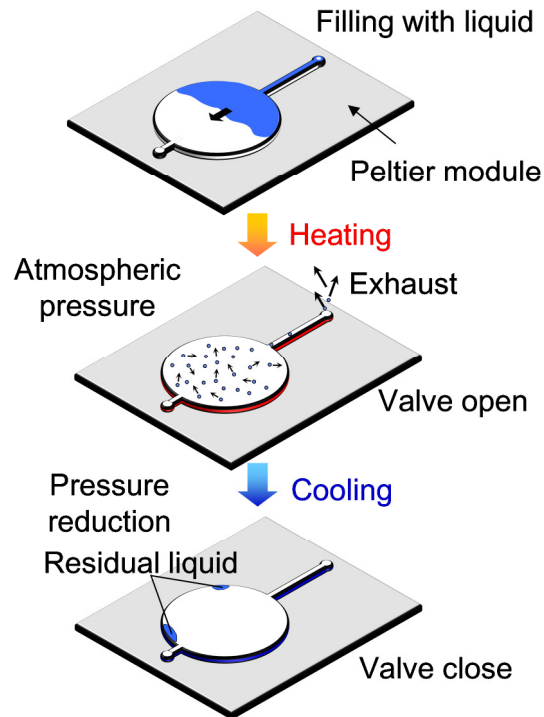


Figure 2.1 Schematic of vacuum generation with gas-liquid phase transition.

2.3.2 Principle of pressure measurement on a chip

Differential pressure in a chamber to atmosphere was calculated by measuring of the diaphragm displacement with a laser displacement meter. Diaphragm pressure sensor [11, 12] is the simplest and frequently used pressure sensing method in MEMS devices. A Pirani gauge and an ionization gauge are commonly used for high vacuum systems; however these gauges cannot be operative from atmospheric pressure [13]. Diaphragm type pressure sensor was adopted to integrate with the micro chamber.

2.3.3 Theoretical vacuum

Effect of the phase transition on the pressure reduction is theoretically estimated as shown in the Fig. 2.2. Pressure in the chamber filled with atmospheric gases follows to the ideal gas law, on the other hand, the pressure follows the vapor pressure if the chamber is fully occupied by the vapor of the liquid. Vapor pressure was calculated from the following Antoine equation [14].

$$P = \exp\left(A - \frac{B}{T+C}\right) \quad (2.1)$$

where, P is the vapor pressure, T is the temperature, and A , B , and C are Antoine constant depending of the liquid. Each Antoine constant is shown in the Table 2.1 [1]. Without any liquid in the chamber, pressure reduction from the atmospheric pressure at 100 °C was calculated. The pressure reduces linearly with decreasing of the ambient temperature. In contrast to this, the pressure reduces exponentially with decreasing of the temperature by gas-liquid phase transition. The lower pressure shows at the same temperature with phase transition of the liquid having higher evaporation temperature. However, the maximum temperature difference created by a conventional Peltier module is about 90 °C from the room temperature. Therefore DI water is employed for phase transition pump as one of suitable materials.

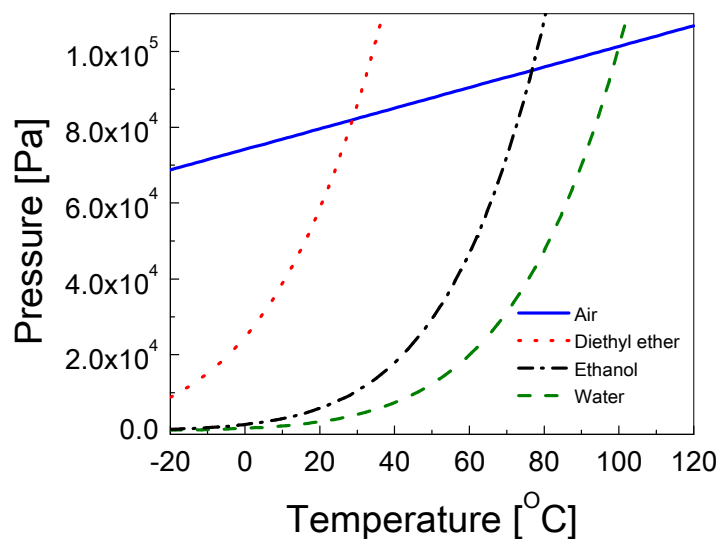


Figure 2.2 *Theoretical curves of vapor pressure calculated from Antoine equation*

Table 2.1 *Antoine constants used for the calculation of vapor pressure.*

	<i>A</i>	<i>B</i>	<i>C</i>
Diethyl ether	20.9756	2511.29	-41.95
Ethanol	23.8047	3803.98	-41.68
DI water	23.1964	3816.44	-46.13

Figure 2.3 shows the temperature dependence of logarithmic vapor pressure of the water in the range between -40 to 100 °C because cooling of the surface of the micro chamber down to -40 °C can be accomplished by a commercially available Peltier module. The minimum vapor pressure attains to about 10 Pa which corresponds to a low vacuum for on-chip MS as discussed in

the chapter 1. Using multi-layer Peltier modules and cooling media will achieve lower temperature down to $-40\text{ }^{\circ}\text{C}$ which realize higher vacuum than 10 Pa without any roughing pump.

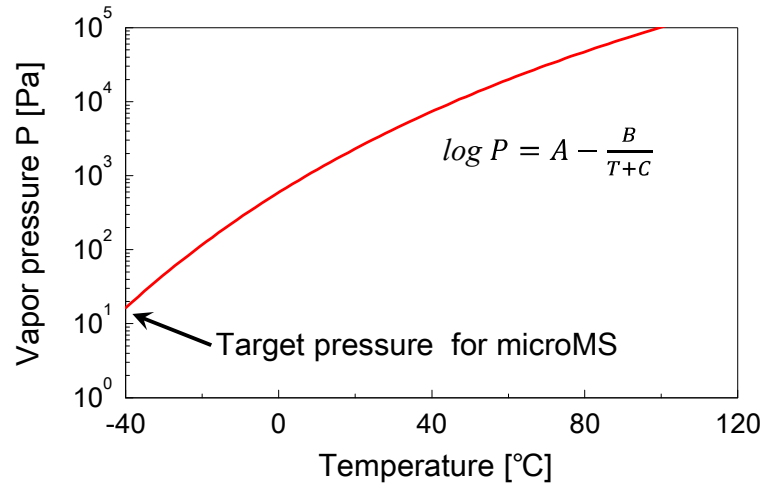


Figure 2.3 *Theoretical curves of vapor pressure. Antoine constants are $A=23.1964$, $B=3816.44$, and $C=-46.13$ for pure water.*

2.4 Experiment

2.4.1 Design of the chip

Figure 2.4 shows the schematic of the chip for the phase transition vacuum pump. The size of the main vacuum chamber was adjusted to 10 mm diameter to achieve large displacement of the membrane for the pressure measurement. The thickness of the upper membrane of the chamber was $220\text{ }\mu\text{m}$. The vacuum chamber was connected to both the inlet and the outlet through the micro channel (width = $100\text{ }\mu\text{m}$, height = $140\text{ }\mu\text{m}$) to introduce the liquid in the chamber.

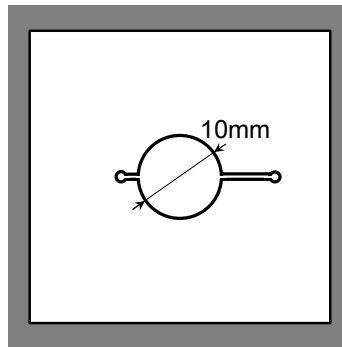


Figure 2.4 *Overhead view of the fabricated chip.*

2.4.2 Chip fabrication

The chip was made of quartz due to its low gas permeability. Circle shaped diaphragm was etched on the quartz substrate (35 mm × 35 mm × 0.5 mm) by wet etching for the pressure measurement. Fabrication process of the chip is illustrated in the Fig. 2.5. The Au/Cr (200/20 nm) layers were deposited by sputtering (MNS-2000, ULVAC, Japan) as metal masks for HF solution [15]. To pattern the metal film, photoresist OFPR-800 (TOKYO OHKA KOGYO, Japan) was spin-coated and patterned by standard photolithography techniques with the printed film mask. After the Au/Cr layers were patterned, the quartz substrate was etched about 140 μm on both sides with buffered HF solution, thus the thickness of the fabricated diaphragm was 220 μm. After that, through holes with the diameter of approximately 1 mm were made by ultrasonic drill to connect an external pump and a reference pressure gauge to the chamber. The etched quartz substrate and another flat quartz substrate were bonded with CYTOP (ASAHI GLASS, Japan) [16] after piranha washing. Both quartz wafers were dehydrated

at 90 °C for 20 min, and then the flat quartz substrate was spin-coated with CYTOP (1 μm). Then CYTOP coated quartz substrate was heated at 90 °C for 30 min. Finally, aligned both substrates were bonded at 160 °C for 3 h applying the pressure at approximately 0.5 MPa. After bonding the quartz substrates, Cr thin layer (100 nm) was sputtered on the membrane to increase reflection intensity of laser on the top of the chip in order to reduce errors in measuring the diaphragm displacement.

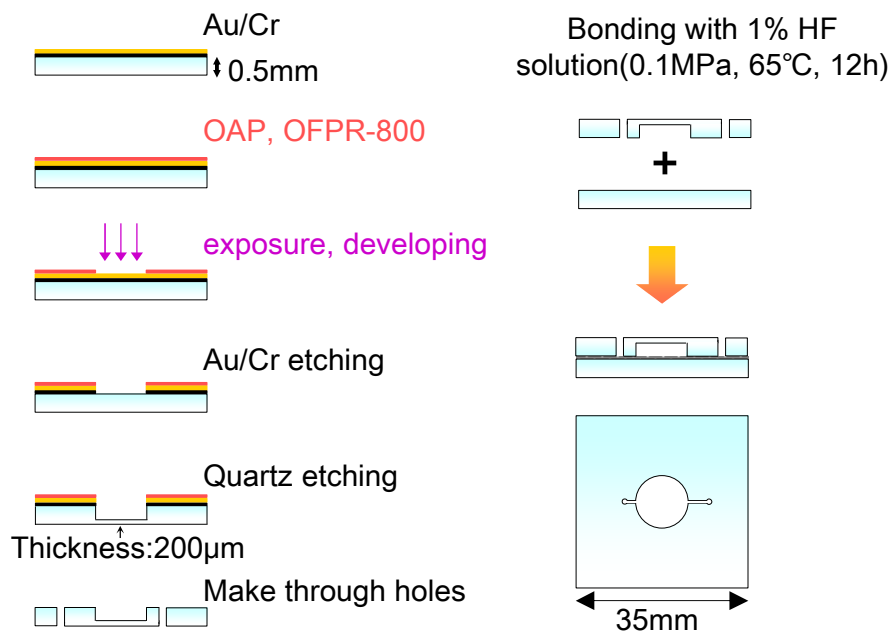


Figure 2.5 Schematic of the chip fabrication

2.4.3 Experimental setup for vacuum generation

Figure 2.6 shows the schematic view of the experimental setup for the pressure measurement and the vacuum generation. Photographs of the experimental setup are also shown in the Fig. 2.7. Handmade chip holder was

used to align a laser displacement meter and a Peltier module as well as to seal the inlet and outlet of the chip tightly. Gas tight sealing was realized with rubber O-ring and high vacuum grease. Dried nitrogen gas was continuously injected to reduce the error of this pressure measurement because dew condensation on the surface of the chip which affects the accuracy in the displacement measurement by laser reflection.

For the pressure measurement, calibration curve of the diaphragm displacement versus pressure was determined by preliminary experiment. The chamber was evacuated using external pumps (DA-20D, ALVAC, Japan, or GD-6EA, ENOMOTO MICRO PUMP, Japan) and a pressure gauge (ADP5100, Panasonic, Japan) for the calibration. Measurement position was placed at the center of the circle shaped diaphragm, in which maximum displacement was expected.

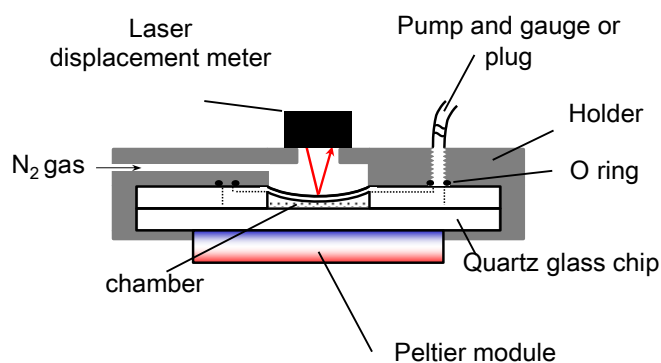


Figure 2.6 *Schematic view of experimental setup.*

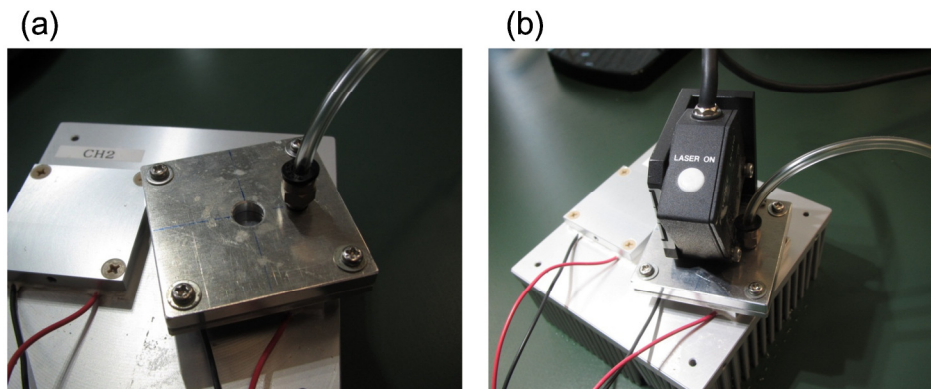


Figure 2.7 *Photographs of the experimental setup. (a) Image of the chip with the holder placed on a Peltier module. (b) Image of the setup after aligning a laser displacement meter on the chip.*

2.4.4 Experimental procedure for vacuum generation

Actual experimental procedure of the pumping is explained as below. In the first process, atmospheric gases in the chamber were replaced by the introducing liquid. The cavity was preheated at the evaporation temperature of the liquid for 5 min with a Peltier module to evaporate the liquid. The evacuation of the gas from the chamber was operated once in these processes. Then inlet of the chip was tightly sealed, and the chip was immediately cooled down below room temperature to liquefy the gases in the chamber. The pressure in the chamber decreases by transforming the fluids to liquid phase from gas phase. The vacuum in the chamber is maintained during the cooling.

2.5 Results and discussion

2.5.1 Vacuum measurement on a microchip

The measured relationship between the pressure in the chamber and the diaphragm displacement as well as numerical simulation results are shown in the Fig. 2.8. It was expected that the diaphragm more deforms at higher temperature due to thermal expansion. Hence, calibration of the measurement pressure was carried out at different temperature such as 1 °C, 21 °C (room temperature) and 101 °C. Figure 2.8 shows good linearity between the pressure and the diaphragm displacement in each temperature. Linear approximation formula was calculated by least squares approximation. For each temperature (1 °C, 21 °C, and 101 °C), the equations relating pressure: P [Pa] and displacement: x [μm] were obtained as $P = -4545.45x + 96363$, $P = -4672.90x + 94859$, and $P = -5208.33x + 96354$ with correlation coefficients of 0.995, 0.993, and 0.988, respectively. The minimum resolution of the laser displacement meter is 0.1 μm , therefore measurable pressure in this system are estimated to 454, 467, 521 Pa, respectively. From the finite elemental analysis at room temperature using COMSOL 4.2a, similar characteristics of the membrane deformation are shown in the Fig. 2.8. Typical image of the numerical simulation is shown in the Fig. 2.9. The simulation was calculated with the structural mechanics model at applying uniform pressure of 950 kPa on the membrane. The simulated vertical displacement corresponds to the experimental result.

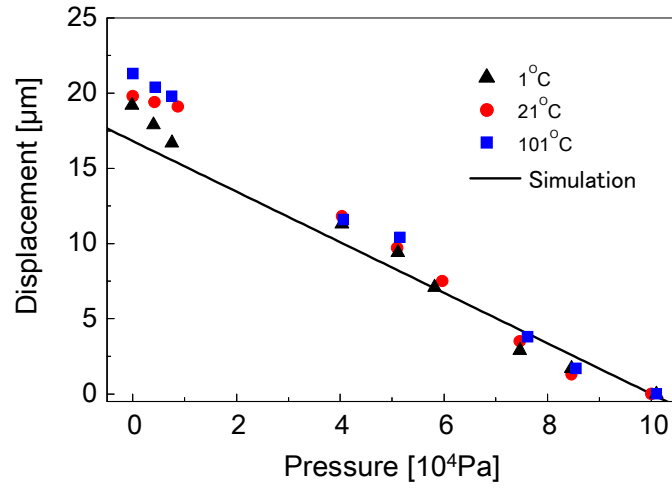


Figure 2.8 *The relationship between the membrane displacement and the pressure in the chamber. Dots show the experimental results in each temperature of the Peltier module and line shows the numerically calculated results at room temperature.*

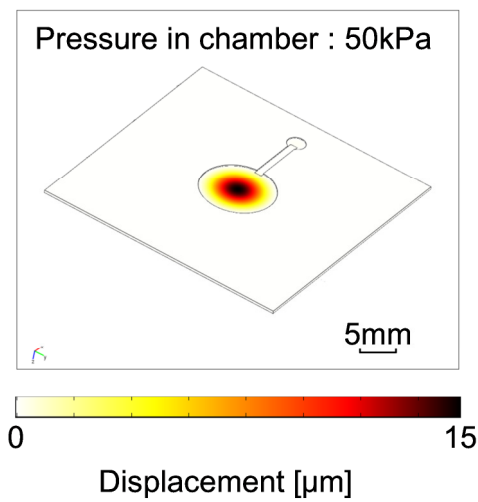


Figure 2.9 *Numerical simulation results of diaphragm displacement at applying uniform pressure of 950 kPa on the diaphragm.*

2.5.2 Vacuum generation with gas-liquid phase transition

Figure 2.10 shows the theoretical and experimental results of the vacuum generation with the phase transition on a chip. In the case without the replacement of the liquid to gases in the chamber, pressure reduces linearly with temperature decreasing. It agrees to the theoretically calculated pressure from the ideal gas law. In contrast to this, experimental results with the phase transition of diethyl ether indicates a clear inflection point on the pressure curve at the boiling temperature of the liquid. The result means that the pressure drastically reduces by the phase transition from gas-phase to liquid-phase. The measured pressure in a micro chamber agrees well with the theoretically-calculated vapor pressure below the boiling temperature of diethyl ether. Higher pressure reduction is observed if the DI water was used for the operation liquid. However, the experimental result of the pressure in the chamber does not attain to the theoretically-estimated vapor pressure of the liquid.

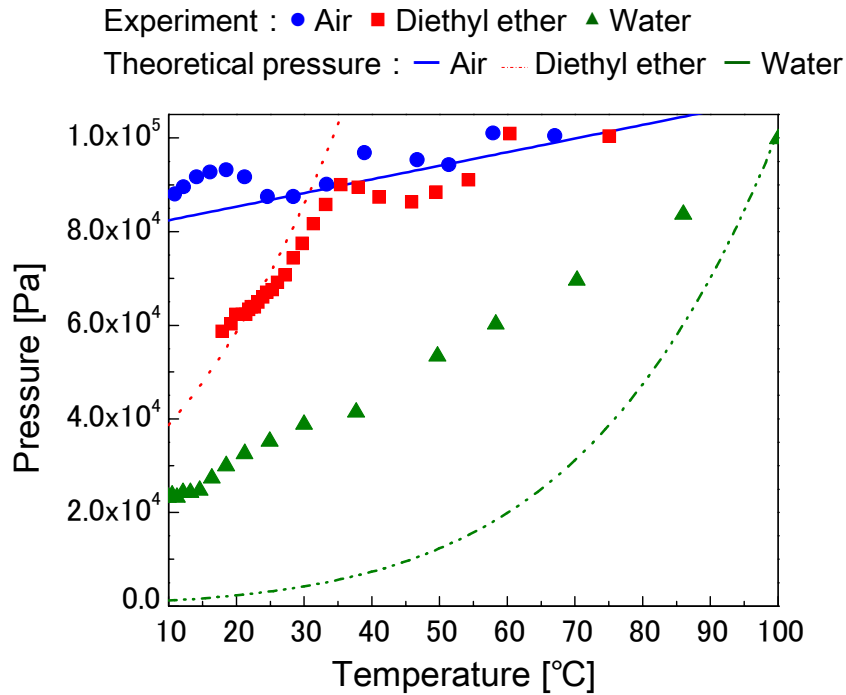


Figure 2.10 *On-chip vacuum generation with or without phase transition. Experimental results and theoretical vapor pressure are shown.*

To analyze this reason for the wide gap between the experiment and the theory, time dependence of temperature and pressure are evaluated as shown in the Fig. 2.11. Pressure in the chamber drastically decreases by cooling of the chamber within 4 min. The pressure remains nearly constant at approximately 25 kPa after 4 min despite the cooling still continues. On the other hand, the minimum pressure about 25 kPa maintains after 10 min to 20 min at the same temperature of 8 °C. This result implies that the chip is tightly sealed at the below the room temperature. From the results, it is expected that the chamber contains DI water vapor as well as atmospheric gases which was not completely replaced by the DI water in the initial heating step. Remaining atmospheric gases limit the

minimum pressure because the pressure of the gases follows the ideal gas law. Expected causes of remaining gases are due to dissolved gases in the DI water and absorbed bubbles on the micro chamber.

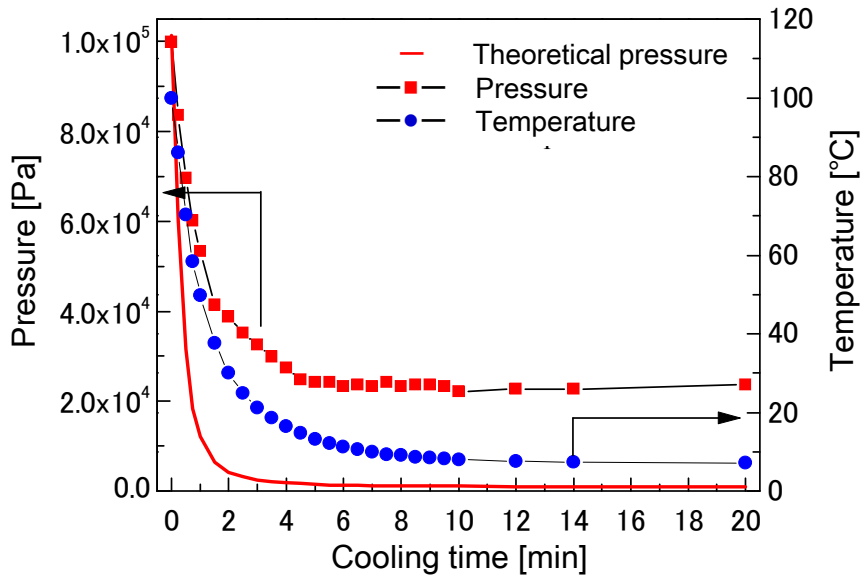


Figure 2.11 Time dependence of temperature and pressure for on-chip vacuum generation with phase transition of DI water.

To realize higher vacuum on a chip, degassing in the micro chamber was performed to fill the liquid completely in the micro chamber. For degassing, sonicated DI water was prepared and the chip filled with it was also sonicated about 10 minutes to remove the air bubble sticking on the wall surface in the channel. And then, the chip was placed in a vacuum chamber to remove atmospheric gas from the liquid. Figure 2.12 shows the comparison of pressure reduction by phase transition with or without degassing. Commercially available pressure sensor was used in the experiment because of the cooling down to -20°C .

Both pressure curves on the temperature shows the similar shape, despite pressure difference with or without degassing is nearly constant at 10 kPa in the range of 60 °C to -20°C. It suggests that the lower vacuum without degassing was caused by sticking air bubble and dissolved gas in the chamber. The lowest pressure reached at 8.5 kPa performing degassing of the liquid and the chamber. Theoretically, the pressure should be reduced to 0.6 kPa at 0 °C if the chamber is completely replaced with DI water. From these facts, it is expected that remaining gases occupies as volume of 10 % of the chamber. Attained pressure is still high relative to the theoretical vapor pressure. It may be caused by the gas which remains around the inlet and outlet valves with O-rings. In the developed micro vacuum system, mean free path of the gases in the vacuum chamber (8.5kPa) is estimated about 1 μm from kinetic theory of gases as shown in the Fig. 1.6 (a), while the distance is not enough for the on-chip mass spectrometry. The phase transition vacuum pump achieved higher vacuum (8.5 kPa) than previously-reported miniaturized vacuum pumps without any roughing pump, micro machined vapor jet pump (49.5 kPa [7]) and Knudsen pump (46.0 kPa [8]). To realize a low vacuum for the on-chip mass spectrometry, more tightly sealed valves with low dead volume on the chip as well as further cooling method with a multi-layer Peltier module and cooling media should be developed.

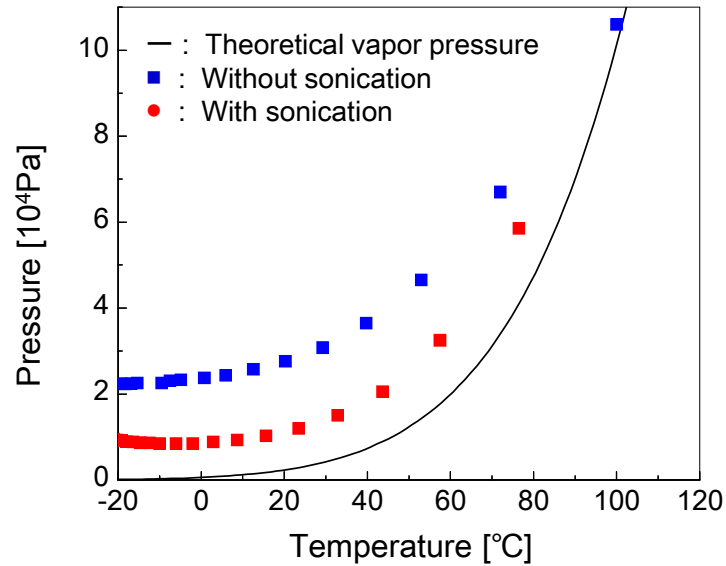


Figure 2.12 *Attained pressure in the micro chamber versus temperature with or without degassing by sonication.*

2.6 Summary

In this chapter, the on-chip vacuum generation technique using the gas-liquid phase transition with the on-chip diaphragm-type pressure measurement was developed. At first, the vacuum tight quartz chip with the micro chamber was fabricated by conventional MEMS process. Second, the vacuum sensing method on a chip was developed to measure the diaphragm deformation with a laser displacement meter. The method can be available in the range of 500 Pa to atmospheric pressure at the temperature of 1 to 100 °C. The effect of the phase transition on the vacuum generation on a chip was investigated using diethyl ether and DI water as an operation liquid. From the theoretical vapor pressure of DI water, a low vacuum about 10 Pa can be created at the temperature

of $-40\text{ }^{\circ}\text{C}$, which can be available for the on-chip mass spectrometry. Currently, a vacuum at 8.5 kPa was accomplished in a micro chamber on a chip using gas-liquid phase transition of DI water.

References

- [1] Sugiyama, Kiyotaka, et al. "Development of on-chip vacuum generation by gas-liquid phase transition." *Sensors and Actuators A: Physical* 176 (2012): 138-142.
- [2] Unger, Marc A., et al. "Monolithic microfabricated valves and pumps by multilayer soft lithography." *Science* 288.5463 (2000): 113-116.
- [3] Haeberle, Stefan, and Roland Zengerle. "Microfluidic platforms for lab-on-a-chip applications." *Lab on a Chip* 7.9 (2007): 1094-1110.
- [4] Yang, Mo, et al. "Development of a palm portable mass spectrometer." *Journal of the American Society for Mass Spectrometry* 19.10 (2008): 1442-1448.
- [5] Li, Linfan, et al. "Mini 12, Miniature Mass Spectrometer for Clinical and Other Applications Introduction and Characterization." *Analytical chemistry* 86.6 (2014): 2909-2916.
- [6] Doms, Marco, and J. Mueller. "A micromachined vapor jet pump." *Sensors and Actuators A: Physical* 119.2 (2005): 462-467.
- [7] Doms, M., and J. Muller. "A micromachined vapor-jet vacuum pump." *Solid-State Sensors, Actuators and Microsystems Conference, 2007. TRANSDUCERS 2007. International*. IEEE, 2007.
- [8] McNamara, Shamus, and Yogesh B. Gianchandani. "On-chip vacuum generated by a micromachined Knudsen pump." *Microelectromechanical Systems, Journal of* 14.4 (2005): 741-746.
- [9] Grzebyk, Tomasz, et al. "Integration of a MEMS-type vacuum pump with a MEMS-type Pirani pressure gauge." *Vacuum Nanoelectronics Conference (IVNC), 2014 27th International*. IEEE, 2014.
- [10] Siebert, Peter, et al. "Surface microstructure/miniature mass spectrometer: processing and applications." *Applied Physics A: Materials Science & Processing* 67.2 (1998): 155-160.
- [11] Tabata, Osamu, et al. "Mechanical property measurements of thin films using load-deflection of composite rectangular membrane." *Micro Electro Mechanical Systems, 1989, Proceedings, An Investigation of Micro*

Structures, Sensors, Actuators, Machines and Robots. IEEE. IEEE, 1989.

- [12]Ho, Chih-Ming, and Yu-Chong Tai. "Micro-electro-mechanical-systems (MEMS) and fluid flows." *Annual Review of Fluid Mechanics* 30.1 (1998): 579-612.
- [13]Chambers, Austin. *Basic vacuum technology 2nd edition*. IOP Publishing, 1998.
- [14]Thomson, George Wm. "The Antoine equation for vapor-pressure data." *Chemical reviews* 38.1 (1946): 1-39.
- [15]Nakanishi, H., et al. "Fabrication of electrophoresis devices on quartz and glass substrates using a bonding with HF solution." *Micro Electro Mechanical Systems, 1997. MEMS'97, Proceedings, IEEE., Tenth Annual International Workshop on*. IEEE, 1997.
- [16]Lu, Hang, Martin A. Schmidt, and Klavs F. Jensen. "Photochemical reactions and on-line UV detection in microfabricated reactors." *Lab on a Chip* 1.1 (2001): 22-28.

CHAPTER 3

ON-CHIP IONIZATION SOURCE FOR PEPTIDE AND PROTEIN ANALYTES

Abstract

An on-chip pulse-heating ionization source for peptide and protein samples was developed for the realization of the miniaturized mass spectrometry. A peptide and a protein analyte were ionized by applying only thermal energy to the solid phase sample without laser, high voltage, or heated ambient gases. A fabricated ionization source consisting of a Pt/Cr micro heater (width = 30 μm , length = 100 μm) on a silicon substrate was coupled with a relatively small time-of-flight mass analyzer (length = 80 mm) to detect target analytes of bovine serum albumin (BSA, $M = 66 \text{ kDa}$) and angiotensin I ($M = 1,296.48 \text{ Da}$). For the protein mass spectrometry with the pulse-heating ionization, a singly charged BSA ion and another multiply charged BSA ions were generated in the presence of 2,5-dihydroxybenzoic acid as a matrix. To detect the singly-charged BSA ion, relatively higher surface energy density of $1.65 \times 10^{-2} \mu\text{J}/\mu\text{m}^2$ than conventional matrix assisted laser desorption/ionization (MALDI) was required to the micro heater for 500 ns.

The contents of this chapter were partially published in *Analytical Chemistry* entitled “Pulse-Heating Ionization for Protein On-Chip Mass Spectrometry” [1].

3.1 Introduction

For the realization of the on-chip mass spectrometry (MS), development of the miniaturized ionization source for biological materials is particularly important component because the analyzable analyte and sample introduction method strongly depend on the ionization. For example, hot electron emitters [2] and field emission ionization sources [3] are typically used for the ionization of gaseous samples. Micro-fabricated electrospray ionization (ESI) [4], capillary electrophoresis coupled ESI [5], and paper-based ESI [6] have been developed for the analysis of the solution containing chemical compounds and peptides with a mass-to-charge ratio m/z ranging up to a few thousand. On the other hand, desorption method of non-volatile compounds from the extended probes [7] has been studied, before the development of the laser ionization [8] and the matrix assisted laser desorption/ionization (MALDI) [9]. In those methods, both techniques of rapid heating (10°C/s) and volatility enhancement [10] were used only for evaporation of the non-volatile compounds before the ionization. Electron impact (EI) ionization or chemical ionization such as proton transfer ionization with NH_4^+ [7] must be followed after the evaporation. These studies struggled to minimize the fragmentation of the target organic molecules like

amino acids in the mass spectrum. To solve this issue, photochemical ionization with laser sources and the matrix assistance was developed for the mass spectrometry of peptides and proteins in 1980s. While MALDI-MS has the advantage of analysis of proteins with m/z up to 100,000 [9] without the decomposition of the analyte, the currently miniaturized on-chip MS does not allow the analysis of proteins. The drawbacks of ESI and MALDI are that bulky equipment must be employed such as laser optics, a high voltage source with a high vacuum pump, or heated ambient gases.

Recently, novel ionization method was studied for the non-volatile compounds with the assistance of heated capillary inlet [11] or matrix evaporation in a vacuum [12]. In these reports, highly-charged protein ions up to M^{67+} were produced without the use of a high voltage source or a laser [13]. If the production of lowly-charged ions of peptide or protein occurs by applying pulse-heating to the sample instead of the heated inlet of the mass analyzer, significant miniaturization of the ionization source for the biological samples can be realized.

3.2 Objective

In this chapter, a method for the on-chip ionization of peptide and protein analyte with a simple device is discussed. I speculated that desorption and ionization occur due to thermal energy applied to the solid state sample by pulse-heating with a micro heater. Fabrication and demonstration of the miniaturized pulse-heating ionization source are studied. The miniaturized pulse

ionization source is coupled with the homebuilt TOF mass analyzer to detect protein and peptide analytes.

3.3 Principle

Details of ionization mechanisms in MALDI have been discussed for more than two decades [14], two-step gas-phase photochemical ionization [15] and cluster models [16] are commonly cited for now. For the mechanism of the two-step gas-phase photochemical ionization, it is explained that analyte molecules lift from the substrate by laser irradiation, and then proton transfers to the analyte from surrounding matrix molecules ionized by the photochemical reaction. In contrast to this, the cluster model explains that highly charged clusters are formed during disintegration of the matrix/analyte solid by laser irradiation. Here, McEwen et al reported new paradigm in ionization [12] that protein ions can be generated by only the assistances of the solid matrix, heat, and a vacuum. It means that miniaturization of the ionization source can be possible into a tiny heating source without laser or high voltage. However, thermal decomposition of analytes may arise from the knowledge of the rapid heating technique of peptides at a second rate [10] if thermal energy is more slowly applied to the samples than MALDI. To realize the ionization with little fragmentations, heating during nano seconds and the presence of materials for effective heat conduction to the analytes such as fine powders of cobalt or organic matrix are expected to be required as conventional MALDI.

3.4 Experiment

3.4.1 Design of ionization chip

In order to rapidly apply thermal energy to the sample on a chip, microfabricated heaters were used for the ionization. Kitano et al demonstrated rapid Joule heating of conductive solution in a locally-narrowed micro channel by applying pulse of high voltage to generate plasma [17]. Similarly geometric metal electrode was designed on a chip for the pulse-heating. At first, heating and cooling properties of the micro heater is discussed from the numerical simulation. Second, optimized shape of the micro heater to control the generated ions above the heater is also discussed from the numerical simulation of the ion trajectory.

- *Numerical simulation of heating and cooling properties*

Figure 3.1 (a) shows the 3D numerical simulation of electric potential and temperature distribution of Cr micro electrode (width=30 μm , length=100 μm , thickness=250 nm) applied pulse voltage of 30 V for 500 ns. Following equations were numerically calculated using COMSOL 4.2a.

$$\mathbf{E} = -\nabla V \quad (3.1)$$

$$\mathbf{J} = \sigma_e \mathbf{E} + \varepsilon_0 \varepsilon_r \frac{\partial \mathbf{E}}{\partial t} \quad (3.2)$$

$$\rho c_p \frac{\partial T}{\partial t} + \nabla \cdot (k \nabla T) = \nabla \cdot \mathbf{J} + Q \quad (3.3)$$

Each equation shows the relations of electric field E , current density J in the micro electrode, and heat conduction equation in solids carrying electric current.

where, V is electric potential, σ_e is conductivity of the electrode, ϵ_0 is the vacuum permittivity, ϵ_r is relative permittivity, ρ is density, c_p is specific heat at constant pressure, T is temperature, k is thermal conductivity, and Q is heat flux depends on the boundary conditions. The electrode will be heated in a vacuum for MS, thus major contributions of energy transfer are thermal radiation and thermal conduction between the electrode and the silicon substrate. The following equations show the conditions at the boundary between a vacuum and the heater and at the boundary between the heater and the silicon substrate, respectively

$$Q = -\sigma\epsilon(T_h^4 - T_{amb}^4) \quad (3.4)$$

$$-k_h \left(\frac{\partial T_h}{\partial n} \right)_B = -k_{si} \left(\frac{\partial T_{si}}{\partial n} \right)_B, \quad (T_h)_B = (T_{si})_B \quad (3.5)$$

where, σ is Stefan-Boltzmann constant, ϵ is the emissivity of the metal electrode, subscripts of h , amb , si mean the heater, ambient vacuum, and silicon substrate at the boundary, respectively. The other parameters used in the calculation are shown in the Table 3.1. To obtain high resolution results, electric potential was initially calculated with the model of the whole electrode ($2.5 \text{ mm} \times 12 \text{ mm}$). From the result, approximately 94% of applied electric potential concentrates in the calculated region (width =

220 μm , height = 200 μm) as shown in the Fig. 3.1 (a). After that, the potential and temperature distribution were calculated with finer mesh. Maximum temperature of the micro electrode reaches at 2,700 K with the pulse voltage of 30 V for 500 ns as shown in the Fig. 3.1 (a). Almost of narrowed region is selectively heated. Figure 3.1 (b) shows the applied voltage dependence on the maximum temperature of the heater. From the literature [18], it was experimentally estimated that the maximum temperature of the DHB matrix attained to 1,100 K after UV irradiation ($\lambda = 355 \text{ nm}$, width = 5 ns) for MALDI. To achieve similar heating property to the sample in the ionization, it is expected that 20-30 V for 500 ns pulse will be required to evaporate the samples without melting or evaporating the Cr layer.

Table 3.1 *Parameters of the materials for the numerical simulation.*

	Vacuum	Heater (Cr)	Substrate (Si)
Electric conductivity [S/m]	-	$1/3.4 \times 10^7$	1
Density [kg/m^3]	-	7150	2320
Thermal conductivity [$\text{W}/(\text{m} \cdot \text{K})$]	-	93.7	34
Relative permittivity	-	1	-
Heat capacity at constant pressure [$\text{J}/(\text{kg} \cdot \text{K})$]	-	448	678
Resistivity temperature coefficient [1/K]	-	5.84×10^{-10}	-
Ambient temperature [K]	293	-	293 (at bottom side)
Surface emissivity	-	0.4 (to vacuum)	-

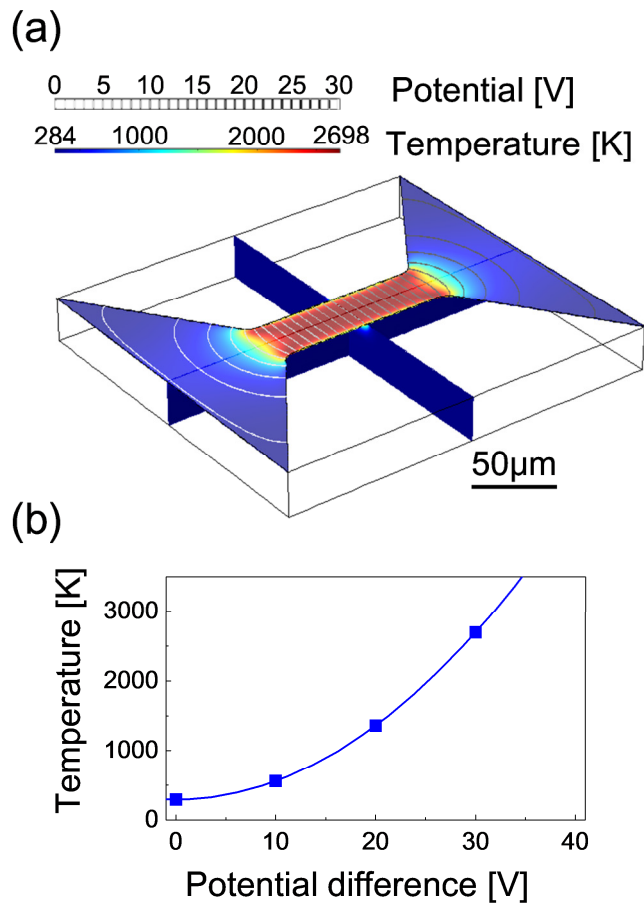


Figure 3.1 Numerical simulation of the Joule heating applying pulse voltage.
 (a) 3D simulation of potential and temperature after 500 ns pulse heating of 30 V.
 (b) Input voltage dependence of the temperature in center region of the micro heater.

Next, cooling characteristics of the micro heater was calculated. To realize the pulse ionization of the sample, temperature of the heat source should be quickly turn to near room temperature. The heat conduction equation in solids of eq. (3.3) was numerically calculated for

the condition of no electric current ($\nabla \cdot \mathbf{J} = 0$) by COMSOL 4.2a. Wider and deeper area ($400 \mu\text{m} \times 400 \mu\text{m}$, thickness = $25 \mu\text{m}$) than previous simulation was calculated to take into account of thermal diffusion in micro seconds. Thickness of the silicon substrate was adjusted a hundred times thicker than the thickness of the micro electrode due to vertical thermal conduction. For the boundary condition, temperature of the bottom surface of the silicon substrate was fixed to room temperature (293 K). Figure 3.2 shows the 3D temperature distribution of the micro heater after pulse heating of 30 V for 500 ns and time dependence of the maximum temperature of the micro heater. Temperature of the micro heater decreases to 424 K after $3 \mu\text{s}$ by heat radiation and thermal conduction into the bottom silicon substrate. Thermal energy mainly transfers to the bottom silicon substrate from the cross section image of the 3D numerical simulation. Figure 3.2 (b) shows the time-dependent cooling property of the micro heater. The temperature exponentially decreases below 300°C within $1 \mu\text{s}$. In actual case, thermal energy also transfers to the solid-phase sample, thus this result implies that the pulse-heating within $1 \mu\text{s}$ can be possible.

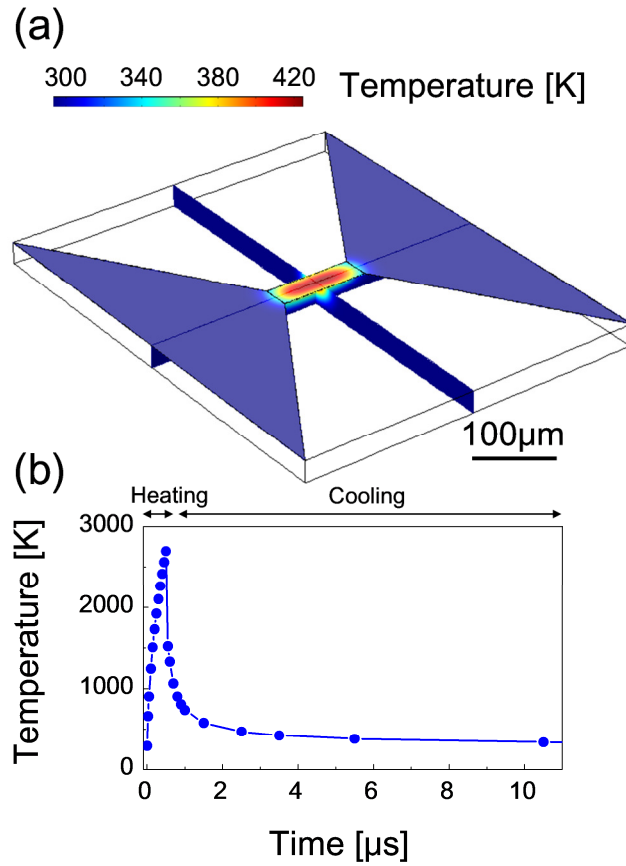


Figure 3.2 Numerical simulation of cooling after pulse voltage. (a) 3D simulation of temperature at 3 μs after pulse heating of 30 V. (b) Time dependence of the temperature in center region of the micro heater.

- **Numerical simulation of ion trajectory above the micro heater**

To analyze the ion convergence above the ionization source toward the ion control for MS, trajectory of the ions was numerically calculated by COMSOL 4.2a. The following equations of electric potential and of motion of a charged particle in an electric field were calculated.

$$\mathbf{E} = -\nabla V \quad (3.6)$$

$$\frac{d(m_p \mathbf{v})}{dt} = qz\mathbf{E} \quad (3.7)$$

where, m_p is mass of a charged particle, v is velocity of a charged particle, q is elementary charge, and z is valence of an ion. m_p value was fixed at $66,000 \times 1.602 \times 10^{-27}$ kg supposing protein molecule (BSA) with singly charged state. The calculated 3D geometries and the ion trajectories are shown in the Fig. 3.3. Major boundary conditions of electric potential are indicated in the figure. Figure 3.3 (a) shows the results of ion convergence above the locally-narrowed micro electrode. Inhomogeneous vertical electric field between the micro electrode and suppressor is shown in particular region indicated by dotted line, which results in poor convergence of the ions. To improve the uniformity of the vertical electric field for better ion convergence, side electrodes were fabricated on the adjacent area of the narrowed micro heater. The convergence of ions in the entrance of the TOF mass filter is improved due to the uniform vertical electric field.

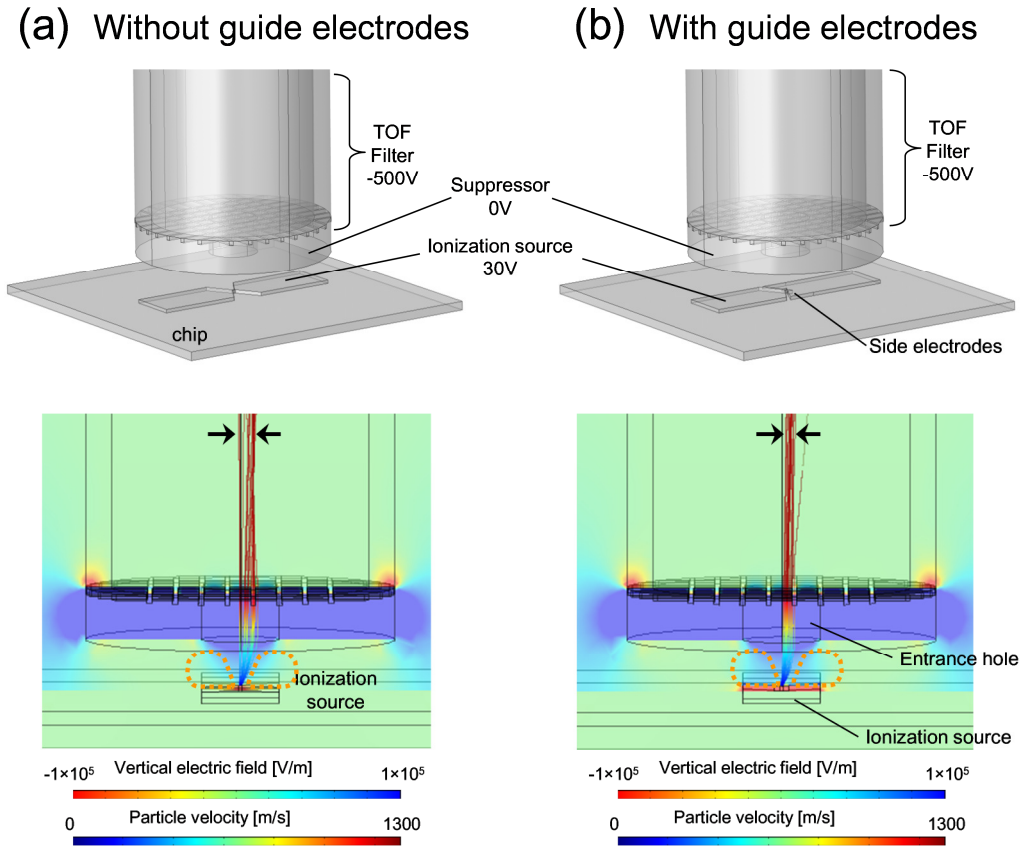


Figure 3.3 Numerical simulation of the electric potential and the ion convergence (a) without side electrodes or (b) with side electrodes. Initial velocity of particles was adjusted $v_0 = \sqrt{v_x^2 + v_y^2 + v_z^2} = 54.078 \text{ m/s}$ supposed the energy of 1 eV .

3.4.2 Chip fabrication

Figure 3.4 shows the fabrication process of the designed micro heater. The micro heaters fabricated by lift-off processing on a silicon substrate with a thermally grown 100-nm-thick SiO_2 . First of all, silicon substrate was cut into $20 \text{ mm} \times 20 \text{ mm}$ pieces and then was washed acetone and DI water with sonication.

The substrate was heated at 180 °C for 10 min to evaporate water molecules and then was cooled down to room temperature. Bilayer of LOR10-B (MicroChem, USA) and photoresist OFPR-800 (Tokyo ohka kogyo, Japan) were spin-coated (MIKASA, 1H-DX2, Japan) at 5000 rpm for 45 sec and at 3000 rpm for 20 sec, respectively. After that, UV light ($\lambda = 365\text{nm}$) was exposed during 3 sec (Union, Double-View Mask Aligner, PEM-800, Japan) via the film mask with micro patterns. The photoresist was developed by NMD-3 solution (Tokyo ohka kogyo, Japan) for 75 sec at room temperature. Pt/Cr metal layers (220 nm for Cr, 20 nm for Pt) were deposited by sputtering (ULVAC, MNS-2000, Japan). Pt layer was deposited for covering Cr layer for connecting the wires with soldering. Then, photoresist was removed by PG remover (MicroChem, USA). Finally, SiO₂ layer (thickness = 200 nm) was spin-coated at 5000 rpm using spin-on-glass solution after ashing of the remaining photoresist by oxygen plasma (Yamato, PDC210, Japan). Connection parts to the wires were covered by Teflon tape before spin-coating. This SiO₂ layer functions to form a uniform hydrophilic surface on the micro heater. Moreover, the insulation layer will prevent thermal electron emission from the Pt surface, which may affect the generated ions above the micro heater.

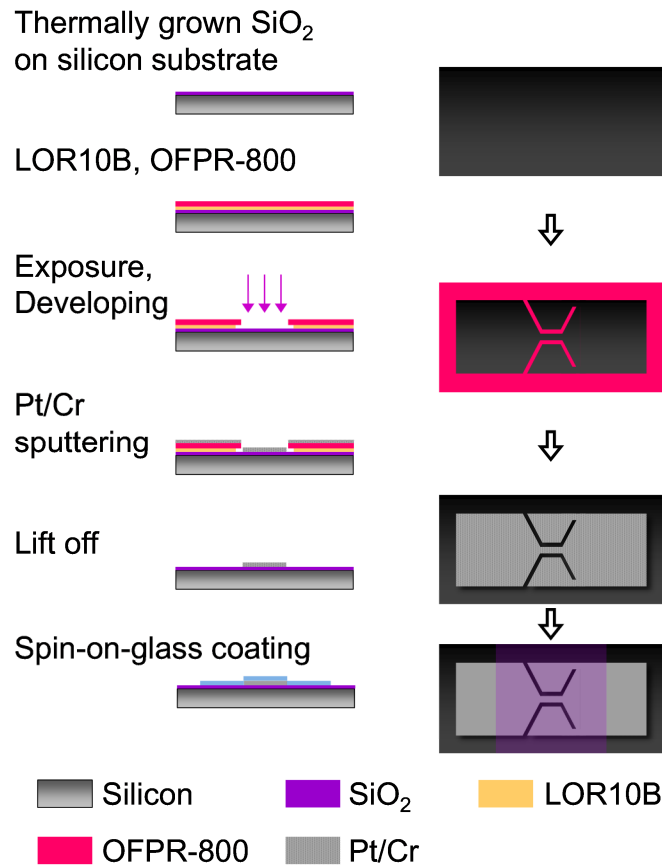


Figure 3.4 Schematic of fabrication process of the ionization chip.

Figure 3.5 shows the microscopic images and photograph of the ionization chip in the fabrication process. Figure 3.5 (a) shows that the brightest and the darkest regions indicate OFPR-800 on LOR-10B and exposed silicon surface, respectively. Bi-layer of the photoresists with undercut was fabricated. Same geometry of the electrode as the designed micro pattern was realized as shown in the Fig. 3.5 (b). After spin-coating of SiO_2 , color of the surface turned to purple as shown in the Fig. 3.5(c). Five ionization sources were fabricated on a chip, and each electrode was connected to wires with soldering.

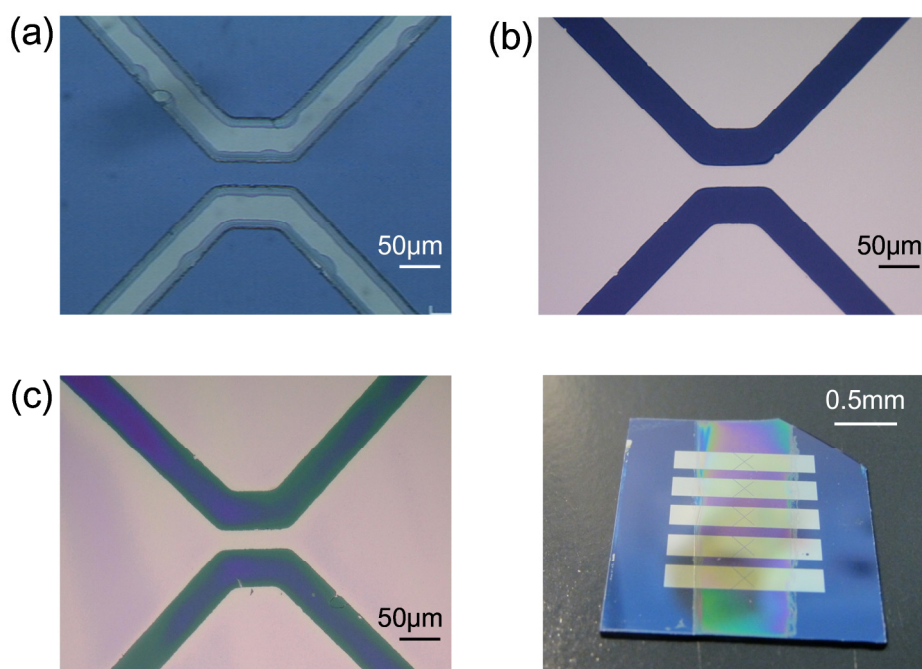


Figure 3.5 *Microscopic images of the chips (a) after photolithography and development (b) after Pt/Cr deposition (c) after coating of spin-on-glass. (d) Photograph of the chip.*

3.4.3 Experimental setup for pulse-heating ionization

Figure 3.6 shows the schematic of the miniaturized ionization source fabricated on a chip. Mixture solution of the analyte and matrix was dropped by pipetting onto the chip and then was dried. Applied voltage was controlled by a field effect transistor (FET). The voltage of right side electrode connected to side electrodes immediately drops to 0V once the FET turns on. The electrical circuit for the pulse generation is shown in the Fig. 3.7. The circuits were composed of a pulse generator (Figure 3.7(a)) and FET connected to the chip via a vacuum chamber (Figure 3.7(b)).

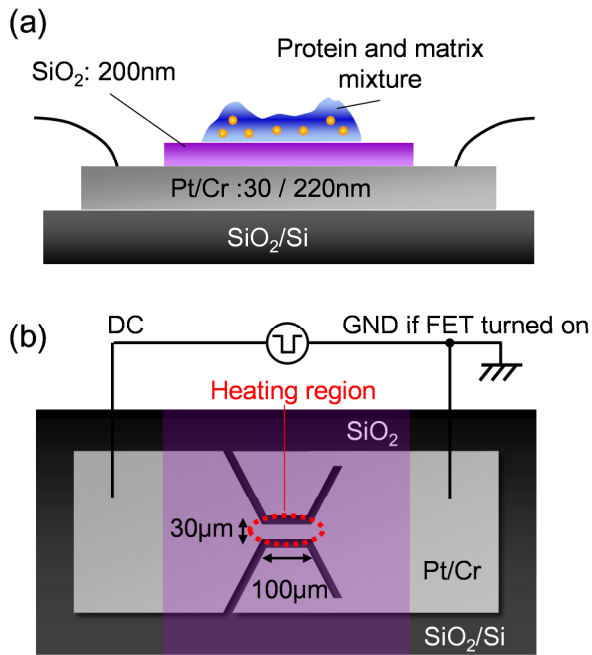


Figure 3.6 Structure of the miniaturized ionization source on a chip.

(a) Cross section view. (b) Overhead view.

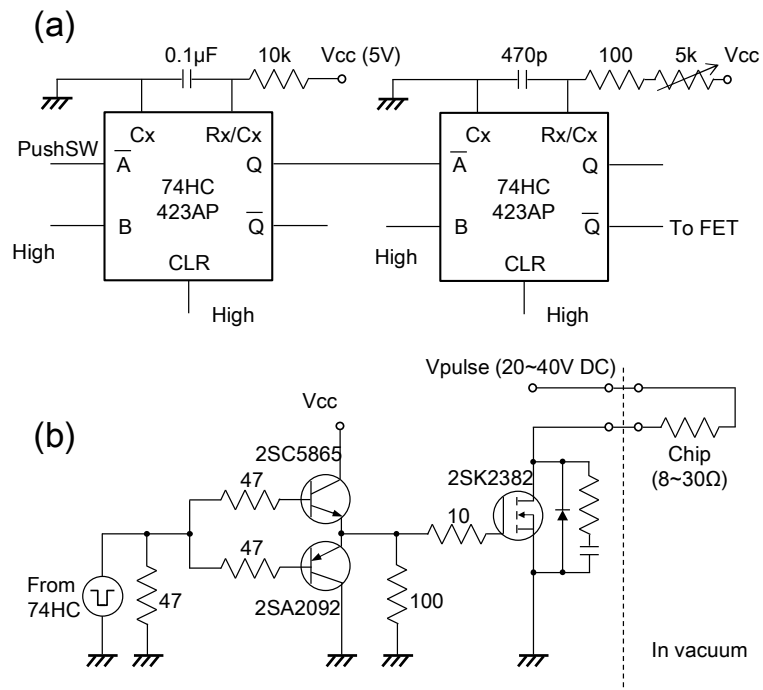


Figure 3.7 Electrical circuits for controlling single pulse heating. (a) Circuits for pulse generation. (b) Circuits of current amplification for pulse heating.

3.4.4 Sample preparation

For the calibration of the TOF mass spectrometer, inorganic copper particles ($M=63.546$, 99.85%) purchased from Kanto Chemical (Japan) were suspended in milliQ water (Nanopure Diamond, Barnstead, USA) and then were sonicated for 30 min. The solution containing the particles was dropped and dried in a vacuum. Similarly conventional MALDI [19], organic samples for the ionization and mass spectrometry were prepared by the following steps. BSA as a protein analyte purchased from Sigma (USA) was diluted in milliQ water at the concentration of 1 $\mu\text{g/ml}$ or 100 $\mu\text{g/ml}$. Angiotensin I as a peptide analyte purchased from Wako Chemicals (Japan) was diluted in milliQ water at the concentration of 100 $\mu\text{g/ml}$. 2,5-dihydroxybenzoic acid (DHB, $M=154.12$) purchased from Kanto Chemical (Japan) as a matrix was diluted in the mixture solution of milliQ water and acetonitrile (1:1, v/v) with 0.1% trifluoroacetic acid (TFA). Subsequently, 500 nl of pre-mixed solution of the protein or the peptide and matrix was applied onto the center part of the ionization source by pipetting, and then was dried in a vacuum chamber. Figure 3.8 shows typical microscopic images of the fabricated micro heater before sample dropping and after drying sample solution of BSA and DHB. Light yellow transparent film like layer is formed on the micro heater.

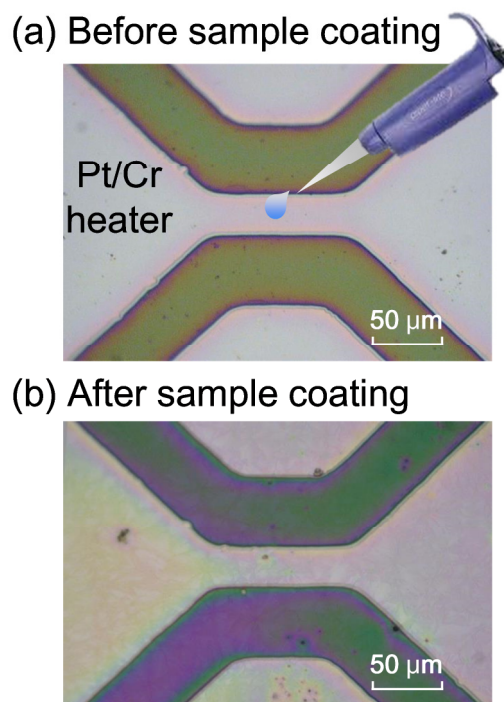


Figure 3.8 *Microscopic images (a) before sample dropping and (b) after matrix/protein solid formation.*

3.4.5 Experimental setup for TOF-MS with pulse-heating ionization

Figure 3.9 shows the experimental setup for the investigation of capability of the ionization and TOF mass spectrometry. The fabricated ionization chip was coupled with a homebuilt TOF mass analyzer and a commercially available channeltron electron multiplier (Detector Technology, Model 414, USA). Free flight region with no electric field was adjusted to 80mm long between the suppressor and the exit of the free flight region. Fabricated chip and the detector were aligned with a gap of 2 mm from the free flight region, respectively. These components were placed in a vacuum chamber with a turbo-molecular pump

(HiCube 300 Classic, Pfeiffer Vacuum, Germany). Pressure in the vacuum chamber was approximately 10^{-3} Pa in the experiments. To apply a single pulse voltage for pulse-heating, previously mentioned FET and electrical circuits were connected to the chip. The full width at half maximum of the pulse voltage was set at 500 ns for all experiments. The applied voltage was varied in the range of 22 V to 40 V for the pulse-heating ionization.

Figure 3.10 shows the time-series chart for TOF measurement. During the pulse-heating, electric field between the chip and TOF entrance turns almost zero. After pulse-heating, positive ions generated above the micro heater were extracted at the leading edge of the input pulse voltage. Accordingly, accelerated ions travelled within 80 mm long of the TOF region at a constant velocity. Mass-to-charge ratio m/z is calculated with the measured TOF using the following equation derived from the energy conservation law.

$$\frac{m}{z} = \frac{t^2}{l^2} \frac{2V_f e}{u} \quad (3.8)$$

where, m is relative molecular weight, t is the time-of-flight, $l = 80$ mm is distance of free flight, V_f is applied potential to the free flight region, e is elementary charge, and u is atomic unit mass. Positive ions are captured and amplified by a factor of approximately 10^4 by a negatively-biased channeltron electron multiplier. The electron multiplier was connected to an amplifier unit (C9663, Hamamatsu photonics, Japan), having a conversion factor of 4 mV/ μ A. TOF signals were

recorded by an oscilloscope (TDS2022C, Tektronics Inc., USA) for the analysis of the mass spectrum.

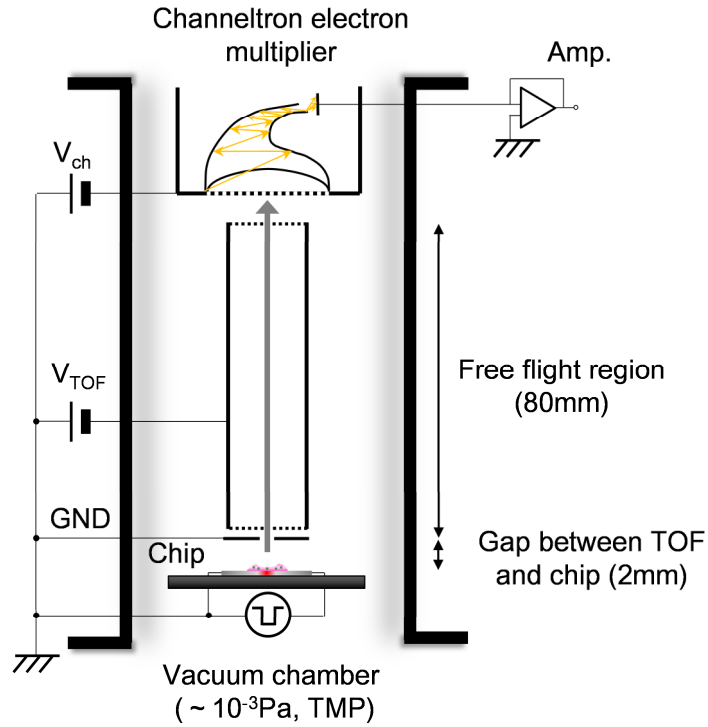


Figure 3.9 *Experimental setup for homebuilt TOF mass spectrometer with the fabricated ionization chip constructed in a vacuum chamber.*

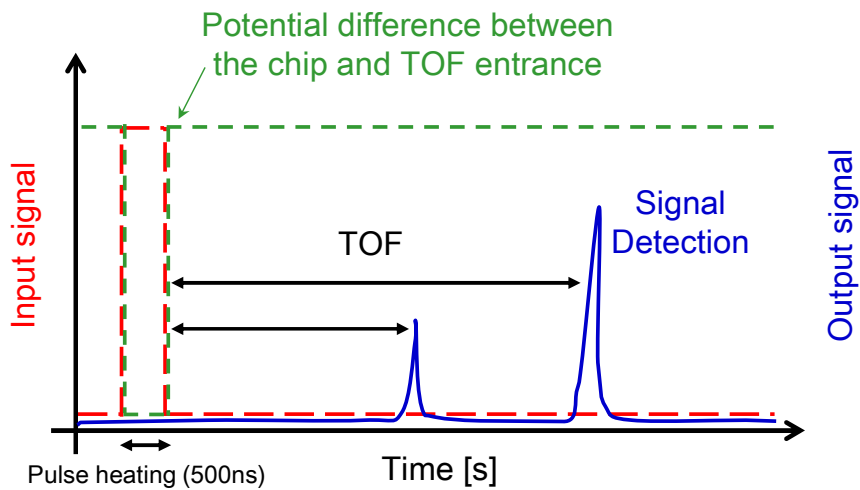


Figure 3.10 *Time series chart for the TOF measurements.*

3.5 Results and discussion

3.5.1 Time-of-flight mass spectrometry of inorganic particles

Before the ionization and mass spectrometry of organic molecules, inorganic metals were evaporated by pulse-heating and were analyzed because organic samples like peptides and proteins may easily cause organic reactions and decomposition in the ionization process. Copper particles with the diameter of a few microns were used for the calibration of TOF-MS. Figure 3.11 (a) shows the microscopic image after applying Cu particles on a chip without SiO₂ thin layer on the micro electrode. Six-times averaged mass spectrum is shown in the Fig. 3.11 (b). To obtain the mass spectrum, pulse-voltage was repeatedly applied to the micro heater at intervals more than 30 sec to wait the cooling of the micro heater. Cu positive ions are generated and are detected after pulse-heating with the TOF of approximately 2.6 μ s which correspond to m/z of 63.5. From the results, validity of the fabricated micro heater and the homebuilt TOF mass analyzer was confirmed.

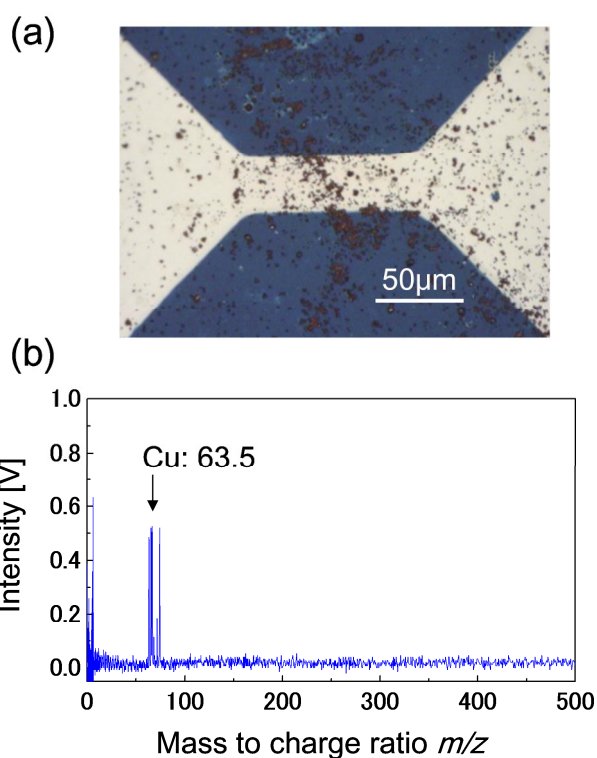


Figure 3.11 Calibration of mass spectrometry with evaporated copper particles.
 (a) Microscopic image of the ionization source after applying Cu particles. (b)
 Averaged mass spectrum of evaporated Cu particles.

3.5.2 Pulse-heating ionization of proteins

At first, desorption of the matrix/protein solid on a chip is investigated after a single pulse-heating. Figure 3.12 shows the microscopic images after sample applying and after a single pulse-heating. Thin film like layer of protein and matrix is formed on the micro heater. Samples are desorbed from the center part of the micro heater when a single pulse-voltage was applied. Almost of all samples on the narrowed region is desorbed with the pulse voltage of $1.45 \times 10^{-2} \mu\text{J}/\mu\text{m}^2$ as shown in Fig. 3.12(d). After pulse-heating, thickness of the sample

layer was evaluated measured by measuring of A-A' section. Averaged sample thickness of matrix/protein films was approximately 300 nm with three different samples on a chip.

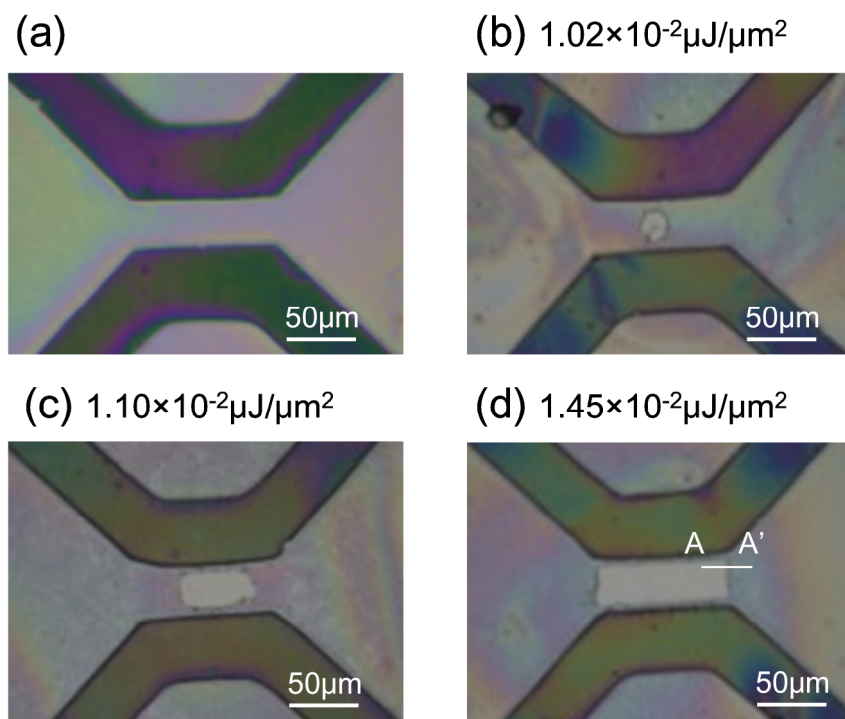


Figure 3.12 *Microscopic image of the ionization source (a) after applying DHB matrix with BSA analyte. Microscopic images after single pulse heating of (b) $1.02 \times 10^{-2} \mu\text{J}/\mu\text{m}^2$, (c) $1.10 \times 10^{-2} \mu\text{J}/\mu\text{m}^2$, and (d) $1.45 \times 10^{-2} \mu\text{J}/\mu\text{m}^2$*

Figure 3.13 shows the detected positively charged molecules after pulse-heating via TOF mass analyzer. Applying energy for these signals corresponds to the energy for microscopic images after sample desorption as shown in the Fig. 3.12. In case of $1.02 \times 10^{-2} \mu\text{J}/\mu\text{m}^2$ and $1.10 \times 10^{-2} \mu\text{J}/\mu\text{m}^2$, charged molecules are not observed despite some of the samples desorb from the micro

heater. In contrast to this, some peaks are detected when pulse-heating energy exceeding $1.45 \times 10^{-2} \mu\text{J}/\mu\text{m}^2$ is applied, indicating the generation of positive ion. Remarkably, the results show not only the occurrence of desorption but also the generation of ions by pulse-heating. The number of the peaks increases drastically when the pulse-heating energy greater than $1.61 \times 10^{-2} \mu\text{J}/\mu\text{m}^2$ was applied.

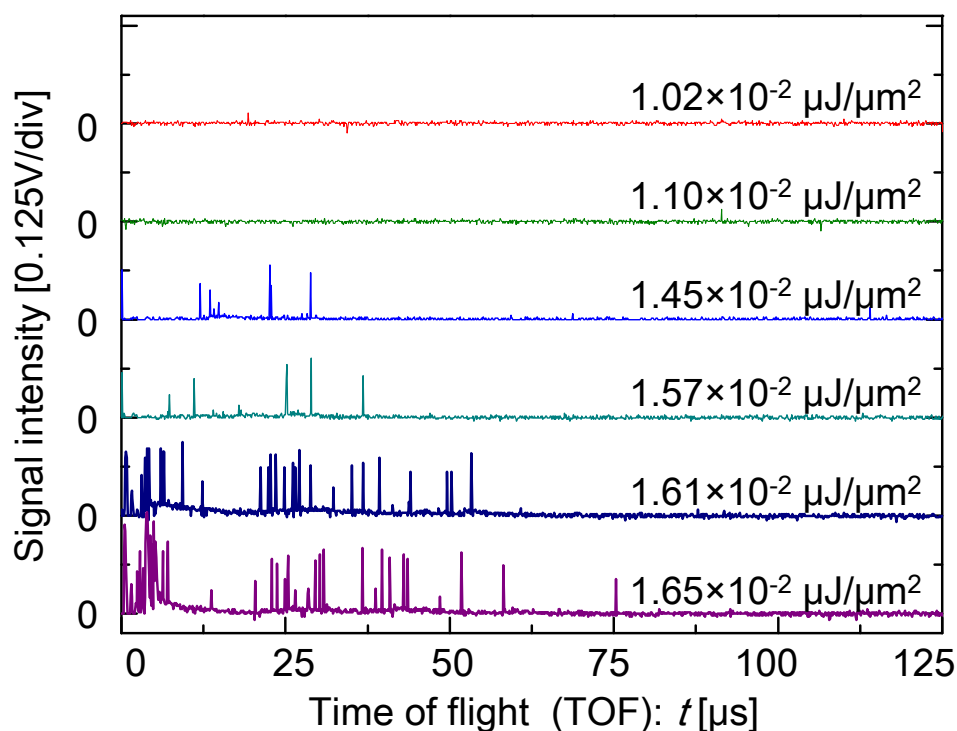


Figure 3.13 *Time-of-flight signals with applying single pulse heating to the mixture of DHB matrix and BSA analyte.*

The results in the Fig. 3.13 are quantitatively evaluated as shown in the Fig. 3.14. The ratio of the desorbed sample and peak count of the detected ions are plotted against the pulse heating energy. Ratio of the desorbed sample was calculated from the area of the desorbed sample region observed brightly in the

microscopic images such as Figures 3.12 (b-d) divided by the area of the micro heater ($30 \mu\text{m} \times 100 \mu\text{m}$). Desorption occurs at pulse heating energy larger than $1.02 \times 10^{-2} \mu\text{J}/\mu\text{m}^2$. In contrast to this, higher energy than $1.45 \times 10^{-2} \mu\text{J}/\mu\text{m}^2$ is required for the ionization. Figure 3.14 (b) shows the ratio of the desorbed sample and the maximum TOF of the detected ions are plotted against the pulse heating energy. In these experiments, TOF signals were recorded for 200 μs after pulse-heating. The longer TOF peaks, i.e. for those heavier ions or lowly-charged ions, are observed only at the higher energy of pulse-heating.

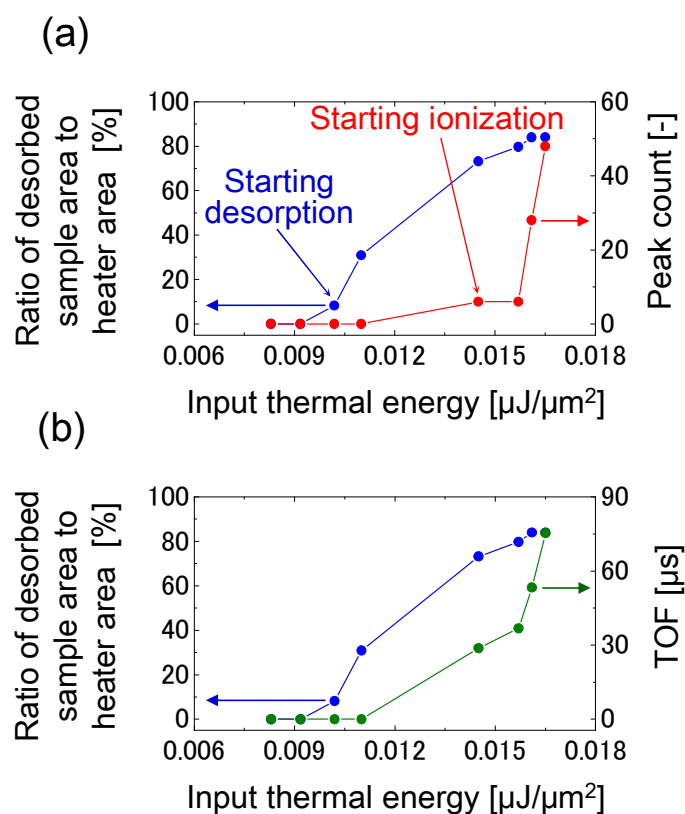


Figure 3.14 Characteristics of sample desorption and ionization. (a) Amount of the desorbed sample and peak count of ions are plotted against the input thermal energy. (b) Amount of the desorbed sample and maximum TOF of the detected ions are plotted against the input thermal energy.

Figure 3.15 shows acceleration voltage dependence of TOF signals of BSA/matrix mixture sample. The signals were obtained with different acceleration voltage of $V_f = -100, -300, -500$ V applied to the TOF mass analyzer. Applied pulse-voltage was fixed at $1.65 \times 10^{-2} \mu\text{J}/\mu\text{m}^2$ in the experiments. Maximum TOF of the detected signals decreases with increasing of acceleration voltage due to its higher velocity of molecules. This results support the TOF mass analyzer working properly. To minimize the variance of TOF due to the initial velocity distribution, the highest potential difference $V_f = -500$ V was used in further experiments.

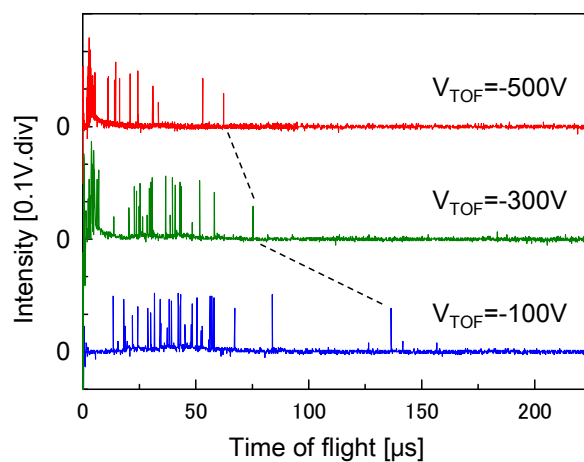


Figure 3.15 Acceleration voltage dependence of TOF signals. Pulse-heating of $1.65 \times 10^{-2} \mu\text{J}/\mu\text{m}^2$ was applied to the sample of BSA with DHB matrix.

3.5.3 Time-of-flight mass spectrometry of proteins

The mass spectrum was analyzed to convert the flight time of the obtained peaks into a mass-to-charge ratio m/z using the eq. (3.8). The aim of the mass spectrum analysis is to determine whether the detected charged molecules

originated in the BSA protein. Figure 3.16 shows the mass spectra of DHB, BSA, and BSA mixed with DHB matrix at the pulse-heating energy of $1.65 \times 10^{-2} \mu\text{J}/\mu\text{m}^2$ for 500 ns. An acceleration voltage of -500 V was used to minimize the velocity variation of the accelerated ions. The mass spectra were obtained by averaging three times pulse-heating experiments with different sample dropping and washing. The chip was washed with ethanol and plenty of deionized water, and then fresh sample was applied onto the chip between each experiment. The mass spectrum of DHB matrix shows that the peaks appeared in the range of m/z 0-1000. In the case of BSA without the presence of any matrix, ions are detected in the range of m/z 0-10,000. In contrast to this, mass spectra of BSA mixed with DHB matrix indicate signals over the m/z of 10,000 including M^{1+} , M^{2+} , M^{3+} , M^{4+} , M^{5+} , and M^{6+} BSA ions. The clear difference in the presence or absence of the matrix suggests that the matrix assistance plays significant role in the pulse-heating ionization. Unlike ESI, singly-charged protein ion is obtained as similar to the conventional MALDI-MS of BSA [20] while fragment like peaks are also detected. For conventional MALDI, applied energy during a laser pulse is typically 3 to 30 μJ with the laser spot of 0.1 mm diameter [19], which corresponds to 3.8×10^{-4} to $3.8 \times 10^{-3} \mu\text{J}/\mu\text{m}^2$. It means that relatively higher thermal energy is required for pulse-heating ionization than MALDI to ionize protein. The possible cause of this is loss of thermal energy through the insulation layer and sample layer.

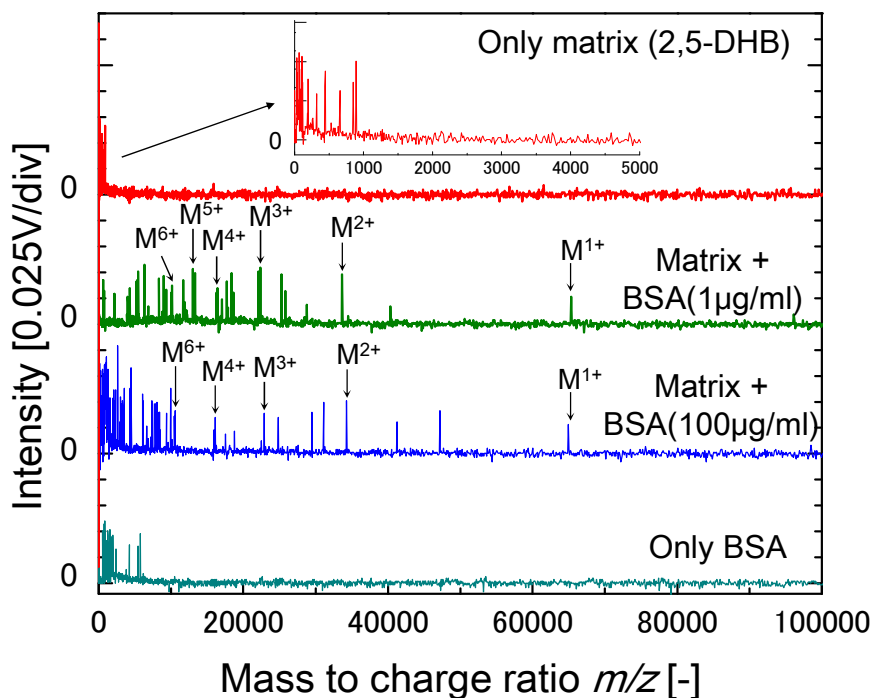


Figure 3.16 Mass spectra of only DHB matrix, BSA mixed with DHB matrix, and only BSA analyte with the pulse-heating energy of $1.65 \times 10^{-2} \mu\text{J}/\mu\text{m}^2$. 100 $\mu\text{g}/\text{ml}$ or 1 $\mu\text{g}/\text{ml}$ BSA samples were mixed with 10 mg/ml matrix at a ratio of 1:1. 0.5 μl of the sample solution was applied to the ionization source and was analyzed by TOF mass analyzer with the acceleration voltage of -500 V.

3.5.4 Time-of-flight mass spectrometry of peptides

Figure 3.17 shows the TOF mass spectrum of Angiotensin I as a peptide sample mixed with the DHB matrix. Pulse voltage at the energy of $0.902 \times 10^{-2} \mu\text{J}/\mu\text{m}^2$ was applied to the ionization chip without SiO_2 layer for 500 ns. Closely distributed many peaks observe around m/z of 1,300, which correspond to the singly-charged positive ion of the Angiotensin I. However, fragment ions and the

cluster ions accompanying with the other molecules such as matrix are also detected in the m/z of 1,144 and in higher m/z than 1,300. The results indicate that peptides as well as proteins can be analyzed by pulse-heating ionization on a chip.

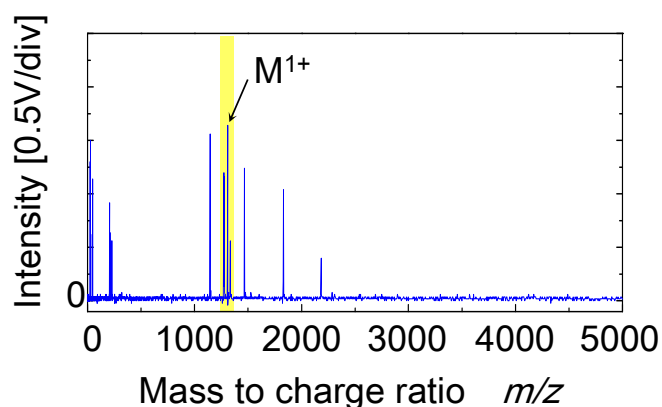


Figure 3.17 TOF mass spectrum of Angiotensin I ($M=1296.48$, Asp - Arg - Val - Tyr - Ile - His - Pro - Phe - His - Leu - OH) as a peptide sample mixed with DHB matrix.

3.6 Summary

On-chip pulse-heating ionization technique was developed with the fabricated micro heaters on a silicon substrate. Protein and peptide samples are ionized by applying Joule heating from the micro heater for 500 ns without laser, high voltage, and heated ambient gases. The fabricated on-chip ionization source is easily integrated with a relatively small homebuilt TOF mass analyzer which enables analysis of peptides and proteins. Inorganic copper particle is also analyzed via the small TOF mass analyzer. DHB matrix plays a key role to the ionization of protein analyte.

References

- [1] Sugiyama, Kiyotaka, et al. "Pulse-heating ionization for protein on-chip mass spectrometry." *Analytical chemistry* 86.15 (2014): 7593-7597.
- [2] Yoon, Hyeun Joong, et al. "Fabrication of two types of micro ion sources for a micro time-of-flight mass spectrometer." *Journal of Micromechanics and Microengineering* 17.8 (2007): 1542.
- [3] Velasquez-Garcia, Luis Fernando, Blaise Laurent Patrick Gassend, and Akintunde Ibitayo Akinwande. "CNT-based MEMS/NEMS gas ionizers for portable mass spectrometry applications." *Microelectromechanical Systems, Journal of* 19.3 (2010): 484-493.
- [4] Licklider, Larry, et al. "A micromachined chip-based electrospray source for mass spectrometry." *Analytical Chemistry* 72.2 (2000): 367-375.
- [5] Mellors, J. S., et al. "Fully integrated glass microfluidic device for performing high-efficiency capillary electrophoresis and electrospray ionization mass spectrometry." *Analytical chemistry* 80.18 (2008): 6881-6887.
- [6] Wang, He, et al. "Paper spray for direct analysis of complex mixtures using mass spectrometry." *Angewandte Chemie* 122.5 (2010): 889-892.
- [7] Cotter, Robert J. "Mass spectrometry of nonvolatile compounds by desorption from extended probes." *Analytical Chemistry* 52.14 (1980): 1589-1606.
- [8] Karas, Michael, et al. "Matrix-assisted ultraviolet laser desorption of non-volatile compounds." *International journal of mass spectrometry and ion processes* 78 (1987): 53-68.
- [9] Tanaka, Koichi, et al. "Protein and polymer analyses up to m/z 100 000 by laser ionization time of flight mass spectrometry." *Rapid communications in mass spectrometry* 2.8 (1988): 151-153.
- [10] Beuhler, R. J., et al. "Proton transfer mass spectrometry of peptides. Rapid heating technique for underivatized peptides containing arginine." *Journal of the American Chemical Society* 96.12 (1974): 3990-3999.
- [11] McEwen, Charles N., et al. "New paradigm in ionization: multiply charged ion formation from a solid matrix without a laser or voltage." *Analytical chemistry* 82.22 (2010): 9164-9168.

- [12] Pagnotti, Vincent S., Nicholas D. Chubaty, and Charles N. McEwen. "Solvent assisted inlet ionization: an ultrasensitive new liquid introduction ionization method for mass spectrometry." *Analytical chemistry* 83.11 (2011): 3981-3985.
- [13] Lietz, Christopher B., et al. "Inlet ionization: protein analyses from the solid state without the use of a voltage or a laser producing up to 67 charges on the 66 kDa BSA protein." *Rapid Communications in Mass Spectrometry* 25.22 (2011): 3453-3456.
- [14] Knochenmuss, Richard. "MALDI ionization mechanisms: the coupled photophysical and chemical dynamics model correctly predicts 'temperature'-selected spectra." *Journal of Mass Spectrometry* 48.9 (2013): 998-1004.
- [15] Knochenmuss, Richard. "Ion formation mechanisms in UV-MALDI." *Analyst* 131.9 (2006): 966-986.
- [16] Karas, Michael, Matthias Glückmann, and Jürgen Schäfer. "Ionization in matrix - assisted laser desorption/ionization: singly charged molecular ions are the lucky survivors." *Journal of Mass Spectrometry* 35.1 (2000): 1-12.
- [17] Kitano, Atsushi, et al. "Highly sensitive elemental analysis for Cd and Pb by liquid electrode plasma atomic emission spectrometry with quartz glass chip and sample flow." *Analytical chemistry* 83.24 (2011): 9424-9430.
- [18] Koubenakis, Antonis, et al. "Time-resolved surface temperature measurement of MALDI matrices under pulsed UV laser irradiation." *The Journal of Physical Chemistry A* 108.13 (2004): 2405-2410.
- [19] Gross, Jürgen H. *Mass spectrometry*, Springer, 2004.
- [20] Amado, Francisco ML, et al. "Analysis of peptide and protein samples containing surfactants by MALDI-MS." *Analytical Chemistry* 69.6 (1997): 1102-1106.

CHAPTER 4

EFFECTS OF MATRIX AND SOLVENT FOR SAMPLE FORMATION ON PULSE-HEATING IONIZATION

Abstract

The pulse-heating ionization source was able to apply the mass spectrometric analysis of proteins and peptides. However, the ionization produced ions of target analyte as well as a number of fragment ions. To minimize the fragmentation in the ionization, effects of the matrix and solvent for sample formation on the ionization were studied. 2,5-dihydroxyacetophenon (DHAP) matrix was found as one of the suitable matrices for the pulse-heating ionization of bovine serum albumin (BSA) protein. Mass spectrum including the singly-charged BSA ion with little fragment ions was obtained to apply thin-layer method using fast drying of DHAP matrix dissolved in acetone as highly volatile solvent. Both making thin-film like layer consisting of microcrystals of the matrix/analyte and use of volatile matrix in a vacuum were required for the pulse-heating ionization to generate the singly-charged ion on a chip. Mass spectra of BSA with DHAP matrix required by the pulse-heating ionization source and by

conventional MALDI were compared. Fragment signals drastically reduced to use the thin-layer method using acetone as compared to MALDI mass spectrum. Estimated sensitivity of the pulse-heating ionization showed 750 attomole as low as conventional MALDI-MS.

The contents of this chapter were partially published in *Analytical Chemistry* entitled “Pulse-Heating Ionization for Protein On-Chip Mass Spectrometry” [1].

4.1 Introduction

Miniaturized pulse-heating ionization of peptides and proteins was studied toward the on-chip mass spectrometry. In the chapter 3, ionization of protein and peptide analytes was demonstrated applying pulse-heating for 500 ns to the mixture of the matrix and target analyte. 2,5-dihydroxybenzoic acid (DHB) was used for the pulse-heating ionization as a matrix. However, the suitable matrix should be used for the specific target analyte [2] in matrix assisted laser desorption/ionization (MALDI), for example, sinapic acid (SA) is normally used for protein analysis [3], α -cyano-4-hydroxycinnamic acid (CHCA) is used for peptide analysis [3, 4], DHB is used for oligosaccharide analysis [5] and so on. Lots of matrices and deposition methods of the samples have been studied for highly sensitive MS detection of the target analytes. This reason is that signal from MALDI is very sensitive to crystallization of the matrix and analyte in solid phase. The technique to make thin-film like layer consisting of fine crystals has been studied. In fact, multiply-charged ions and fragment-like ions of proteins were frequently produced by pulse-heating ionization [1]

with the DHB matrix as shown in the chapter 3. These signals may cause improper analysis for the real samples containing lots of substances. Therefore, effects of the matrices and solvents for sample formation on the pulse-heating ionization have to be evaluated for highly sensitive and highly selective analysis.

4.2 Objective

To obtain the mass spectrum with little fragment peaks and multiply charge ions, the effects of the matrix and sample preparation techniques are studied. For the matrix, the effects of DHB, SA, and CHCA are investigated as matrix normally used in MALDI. 2,5-dihydroxyacetophenon (DHAP) utilized for the inlet ionization without laser or high voltage [6] is used for pulse-heating ionization. To analyze the ionization mechanism, MALDI-TOF-MS spectra analyzed by commercially available system and the pulse-heating ionization TOF-MS spectra are compared. Moreover, six solvents are used to control the speed of matrix crystallization by its evaporation. Finally, sensitivity of the pulse-heating ionization with homebuilt TOF mass spectrometry is briefly estimated.

4.3 Principle

For MALDI, the matrix has a number of functions [2] such as intermediate material to effectively transfer thermal energy with its high surface areas [7] or with its strong optical absorption in UV range [8], protonation, deprotonation, electron transfer, and dispersion of the analyte in the matrix. The DHB matrix used in the pulse-heating ionization has no property to selectively transfer energy to the matrix from laser due to its optical absorption and to efficiently transfer thermal energy to the analyte. Moreover, thermal energy transfers through the samples itself on the micro heater without laser irradiation. Sometimes proper thermal energy does not transfer to the surface of the samples if the sample layer becomes locally aggregated or much thicker than the micro electrode.

Here, McEwen et al [6] found that “*DHAP as the matrix has a significantly lower optimum ion transfer capillary temperature than DHB.*” From the finding, they demonstrated the ionization of peptides [6] and proteins [9] mixed in DHAP matrix without use of laser or high voltage. As reported by Inutan et al [10], it is required for ionization that “*molecules are transferred from solid-phase to gas-phase ions through the simple exposure of a material of interest in a suitable matrix to vacuum without laser or high voltage*”. Vorm et al [11] reported the technique to improve the resolution

and sensitivity as called thin-layer method. Fast evaporation of matrix solution based on acetone produces a thin layer consisting of microcrystals. They reported following advantages; (i) An improvement in sensitivity, peptides can routinely be analyzed in the attomole range. (ii) Sample surfaces become much more homogeneous, allowing very fast data acquisition. (iii) Spectra show a more linear mass scale and higher resolution.

4.4 Experiment

4.4.1 Experimental setup

For the TOF mass spectrometry with the pulse-heating ionization, same ionization chip and same experimental setup as shown in the chapter 3 were used. The micro heater without surficial SiO₂ layer was used as an ionization source to obtain the hydrophobic surface on a chip for fast spreading and evaporation of the matrix solution. For the MAIDI-TOF-MS analysis, ultrafleXtreme (BRUKER, USA) was used as linear mode. 2,000×5 times averaged mass spectra were obtained applying the laser pulse ($\lambda = 355$ nm) at a frequency of 1,000 Hz, and the applied voltage to the detector was adjusted to 3000V. Same laser intensity was used in all MALDI-TOF-MS analysis.

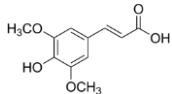
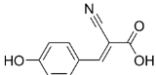
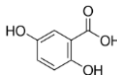
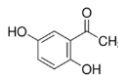
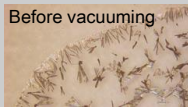
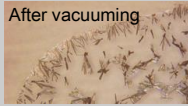




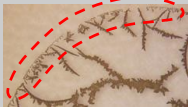

4.4.2 Sample preparation

Table 4.1 shows the summarization of the characteristics of matrices used in the experiments. SA, CHCA, and DHB are frequently used for conventional MALDI-MS. DHAP was used for the inlet ionization [6] without laser. Each matrix was dissolved in the mixture solution of milliQ water and acetonitrile (1:1, v/v) containing 0.1% TFA at the concentration of 10 mg/ml. BSA as a protein analyte was prepared in milliQ water at the concentration of 0.1mg/ml as same manner in the chapter 3. A 500 nl of mixture solution of the both protein and matrix solution was dropped onto the ionization source, and then was dried in a vacuum. For MALDI-TOF-MS analysis, the samples were applied onto 384-well stainless steel target plate (BRUKER, USA). At the beginning, 500 nl of matrix solution was dropped, subsequently 500 nl of protein solution was added before drying of the matrix solution for acquiring 2,000×5 times averaged mass spectra. After that, the solution was dried in atmosphere.

To investigate the effect of the solvent and thin-layer method, each matrix was dissolved in different milliQ/acetonitrile solution (5:5 or 2:8, v/v), tetrahydrofuran, ethanol, methanol, or acetone at the concentration of 10 mg/ml. BSA was prepared in milliQ water containing 0.1% TFA at the concentration of 0.1 mg/ml. In the first step, 250 nl of matrix solution was dropped onto center region of the ionization source. The

matrix solution containing water was dried in a vacuum, i.e. tetrahydrofuran, ethanol, and acetone easily vaped in atmosphere within a few seconds. After that, 250 nl of pre-mixed solution of the sample and matrix was dropped onto the solid matrix layer on the ionization source, and then was dried in a vacuum. Microscopic images of the sample surface with difference size of area were taken by VHX-5000 (KEYENCE, Japan).

Table 4.1 Summarization of the characteristics of matrices used in the experiments.

	Sinapinic acid (SA) 	α -cyano-4-hydroxycinnamic acid (CHCA) 	2,5-dihydroxybenzoic acid (DHB) 	2,5-dihydroxyacetophenone (DHAP) 
Target for MALDI	Protein	Peptide	Protein, Oligosaccharide	Protein, Peptide
Mass [Da]	224.21	189.17	154.12	152.15
Isoelectric point	6.2	4.08	3.76	-
Hydrophilicity	Hydrophobic	Hydrophobic	Hydrophilic	Hydrophobic
Volatility in a vacuum (5×10^{-4} Pa)	Non-volatile	Non-volatile	Slightly-volatile	Volatile
	Before vacuuming  After vacuuming 	 	 	 

4.5 Results and discussion

4.5.1 Effect of the matrix on pulse-heating ionization

To investigate the effect of the matrix, TOF mass spectrum with the pulse-heating ionization, surface morphology of applied sample on a chip, and MALDI-TOF mass spectrum are shown in use of each matrix. Figure 4.1 shows the results of DHB as a matrix. As discussed in the chapter 3, singly- and multiply-charged ions are detected. Moreover, fragment like peaks are also detected including at m/z of 48,000, 42,000, 24,000, and 18,000. Sample surface shows the thin-film like morphology without any special treatment. Thin-layer of the matrix and the protein was desorbed and was ionized as shown in the Fig. 3.11(d). MALDI-TOF mass spectrum of BSA mixed with DHB matrix is shown in the Fig. 4.1 (c). Singly- and doubly-charged ions of BSA are detected despite its low signal intensity due to relatively low concentration of BSA (0.1mg/ml, 1.5 μ M). From the literature [13, 14], sharper peaks were obtained by the analysis of BSA with ten times higher concentration (40 μ M or 1 mg/ml). Fragment ions are generated at the m/z of 48,000, 39,000, 37,000, 35,000, 18,000, 17,000, and 15,500, some of them are also detected in the pulse-heating ionization.

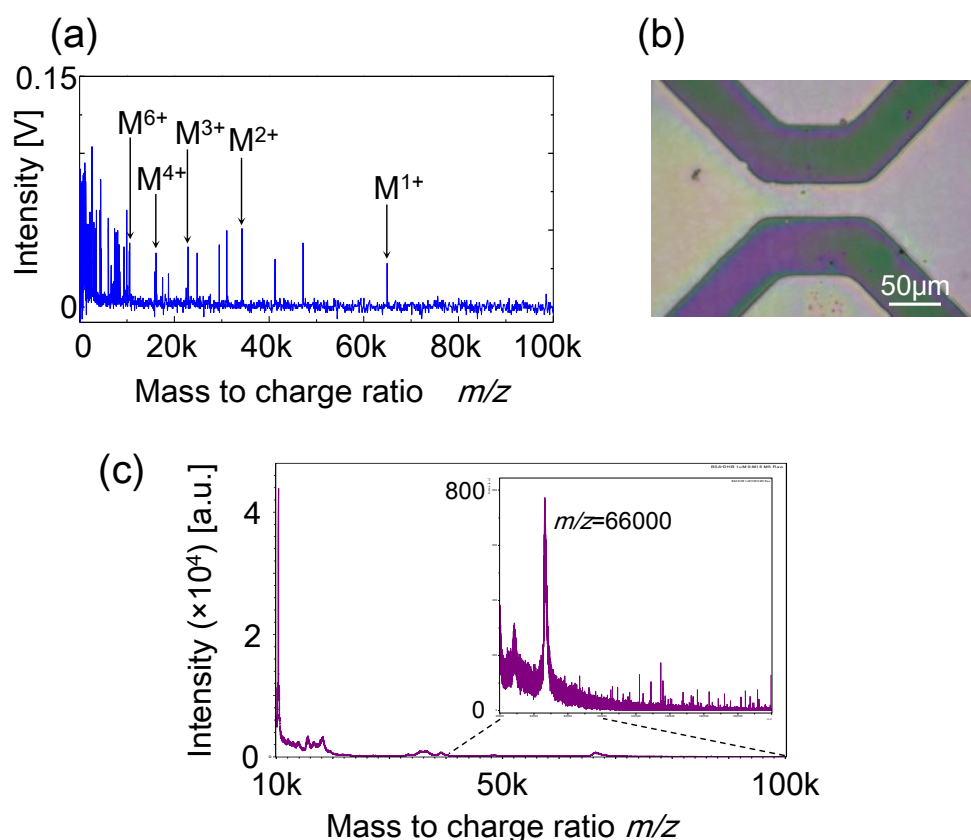


Figure 4.1 *The results of DHB as a matrix (a) Averaged mass spectrum of BSA with DHB matrix. (b) Typical microscopic image after sample applying. (c) MALDI-TOF mass spectrum.*

Figure 4.2 shows the results of SA which is normally used for MALDI of the protein analyte as a matrix. The mass spectrum shows that the singly-charged ion is not detected, while multiply-charged ions including M^{2+} and M^{3+} ions are observed. Many peaks closely distribute in the range of m/z 0-10,000 cause the difficulty for further analysis of the mass spectrum. From the microscopic image, grain like morphology of

the matrix with the size of approximately 50 μm is shown on the chip. Thin-film like morphology as shown in the Fig. 4.1 (b) is not formed in the both cases of drying in a vacuum and atmosphere. In contrast to this, MALDI-TOF-MS shows that clearer peaks of singly- and doubly-charged BSA ions are detected than the use of DHB as a matrix because generation of ions in the range lower m/z of 10,000 is suppressed. It suggests that SA is the suitable matrix for analysis of protein in MALDI.

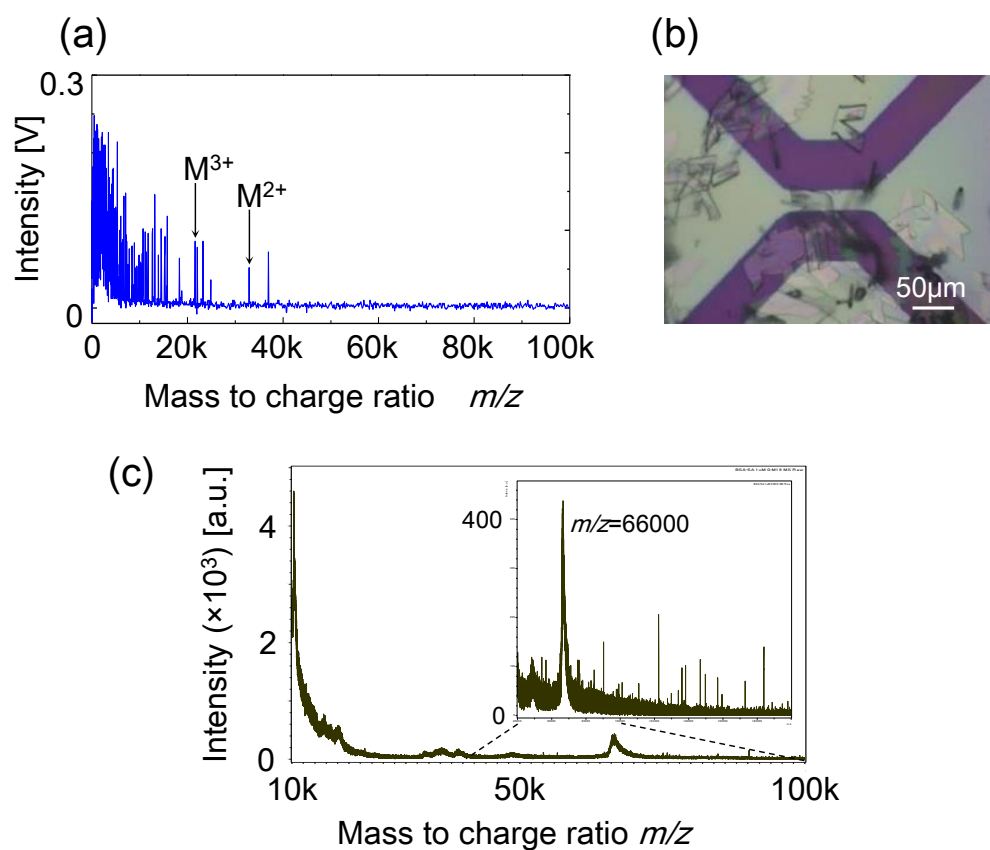


Figure 4.2 The results of SA as a matrix (a) Averaged mass spectrum of BSA with SA matrix. (b) Typical microscopic image after sample applying. (c) MALDI-TOF mass spectrum.

Figure 4.3 shows the results of CHCA as a matrix. CHCA matrix is sometimes used for BSA analysis from the literature [13, 14]. The mass spectrum shows closely distributed peaks in the range of m/z 0-10,000, while singly- and multiply-charged ions are detected. The microscopic image shows the grain like morphology as similar as the use of SA matrix. The size of the matrix/analyte particles is approximately 5 to 10 μm which is smaller than the case of SA matrix. Figure 4.3 (c) shows the MALDI-TOF mass spectrum of BSA mixed with CHCA. Very weak signal of the singly-charged BSA is observed.

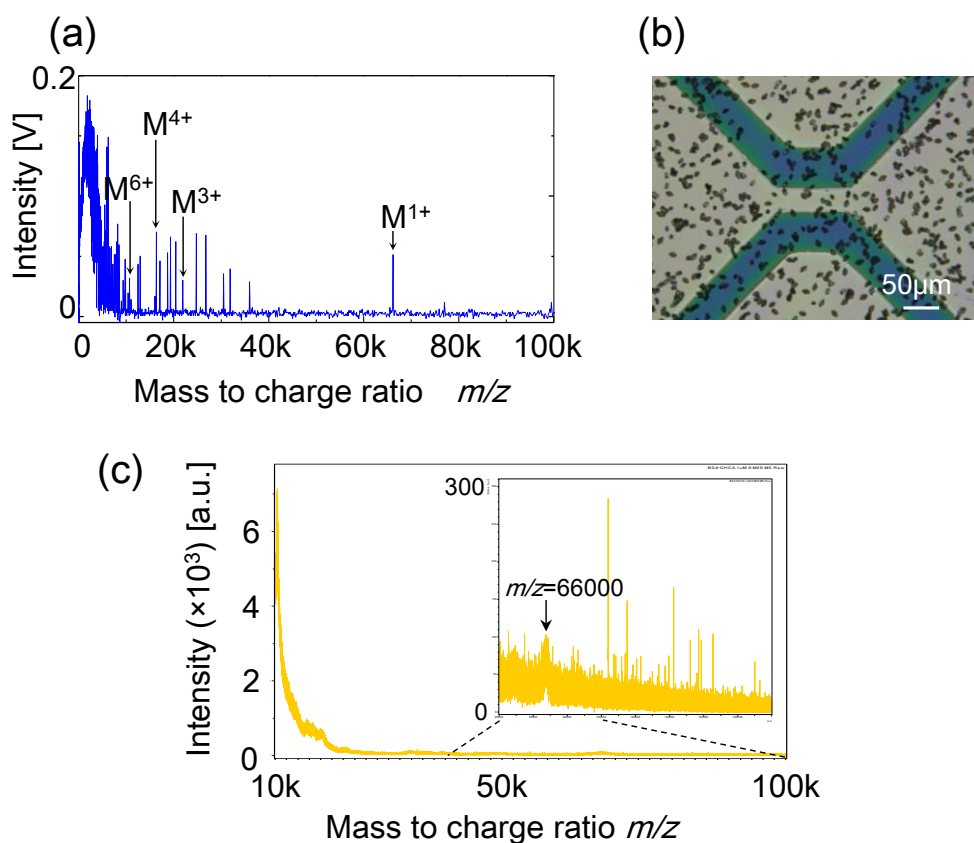


Figure 4.3 *The results of CHCA as a matrix (a) Averaged mass spectrum of BSA with CHCA matrix. (b) Typical microscopic image after sample applying. (c) MALDI-TOF mass spectrum.*

Figure 4.4 shows the results of DHAP as a matrix. DHAP is used for inlet ionization because of its lower thermal requirements for desolvation of the matrix/analyte clusters [6]. It suggests that DHAP is highly volatile than DHB in a vacuum. In the mass spectrum, multiply-charged ions of M^{2+} , M^{3+} , M^{4+} , M^{5+} , and M^{6+} ions are clearly detected. Interestingly, the fragment-like peaks at $m/z=18,000$, $24,000$,

42,000, and 48,000 found in the Fig. 4.1 (a) for DHB matrix are not observed. Figure 4.4 (b) shows the grain like morphology of the matrix with the size of approximately 10 μm . From the mass spectrum obtained by MALDI-TOF-MS, any meaningful peaks derived from BSA protein are not detected.

For the pulse-heating ionization, DHAP matrix indicates the favorable mass spectrum without fragment-like peaks while singly-charged ion is not detected. The singly-charged ion is detected with DHB or CHCA as a matrix. In both cases, the matrix/analyte forms thin-film structure or fine grain structure. On the other hand, SA matrix indicates sharp peak of singly-charged ion with little fragment signal from MALDI-TOF-MS as same as discussed in the conventional MALDI. From above summarization of the results, proper matrix for pulse-heating ionization is estimated as follows; (i) Matrix/analyte mixture must be formed thin-film like morphology consisting of microcrystals for the detection of the singly-charged ion to effectively transfer thermal energy to the whole sample on the micro heater. In case of laser ionization, energy is applied from the upper side of the sample, thick sample layer does not cause significant problem for the ionization. (ii) Highly volatile matrix in a vacuum may be proper for the pulse-heating ionization because of the lack of selective heating for the matrix due to its specific optical absorption by laser irradiation.

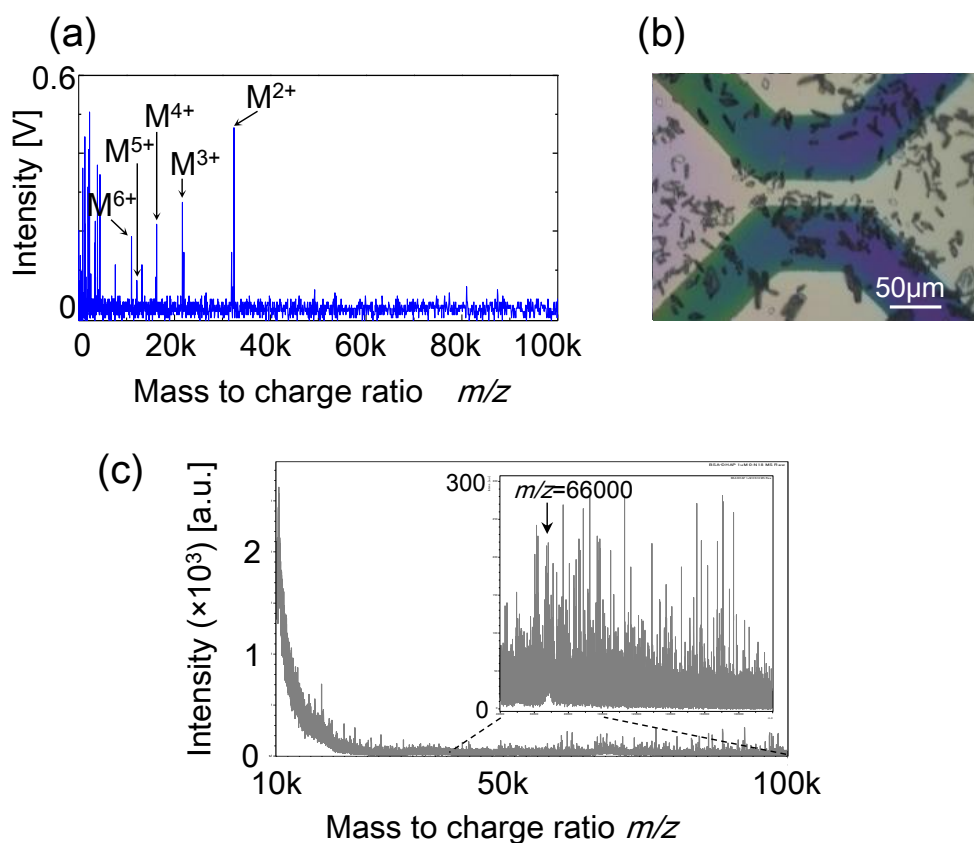


Figure 4.4 *The results of DHAP as a matrix (a) Averaged mass spectrum of BSA with DHAP matrix. (b) Typical microscopic image after sample applying. (c) MALDI-TOF mass spectrum.*

4.5.2 Effect of the solvent for preparation of the sample layer

From the comparison among the matrices, it is suggested that surface morphology affects the pulse-heating ionization. To control the surface morphology of the mixture sample of the matrix and the analyte deposited on the micro heater, solvents

dissolved with the matrix and preparation methods are studied. Here, combinations of six different solvents usually used in MS and two preparation methods, pre-mixing and thin-layer method, are systematically investigated for three matrices, DHB, DHAP, and SA.

Table 4.2 show the summarization of surface morphology of DHB as a matrix. By using every six solvents with pre-mixing method, thin-film like layers of matrix/analyte are formed on the micro heater. In the case of highly volatile solvents, ethanol, methanol, and acetone with thin-layer method, sometimes the sample is not covered on the narrowed heating region. It suggests that slow evaporation of the solvent provides uniform thin-layer in the case of DHB matrix. Figure 4.5 show the characteristic microscopic images with different size of the area. Large crystals of DHB matrix with the size of approximately 100 μm appears along with the outer circumference of applied solution in both cases of pre-mixing and thin-layer method. In these cases, thin-layer with the thickness of a few hundreds nm is formed on the ionization source.

Table 4.2 Summarization of surface morphology of DHB as a matrix.

2,5-Dihydroxybenzoic acid (DHB) as a matrix

Solvent	Water/ acetonitrile (5:5)	Water/ acetonitrile (2:8)	Tetrahydro -furan	Ethanol	Methanol	Acetone
Pre-mixing	Film	Film	Film	Film	Film	Film
Thin-layer	Film	Film	Film	Partially film	Non- uniform film	Non- uniform film

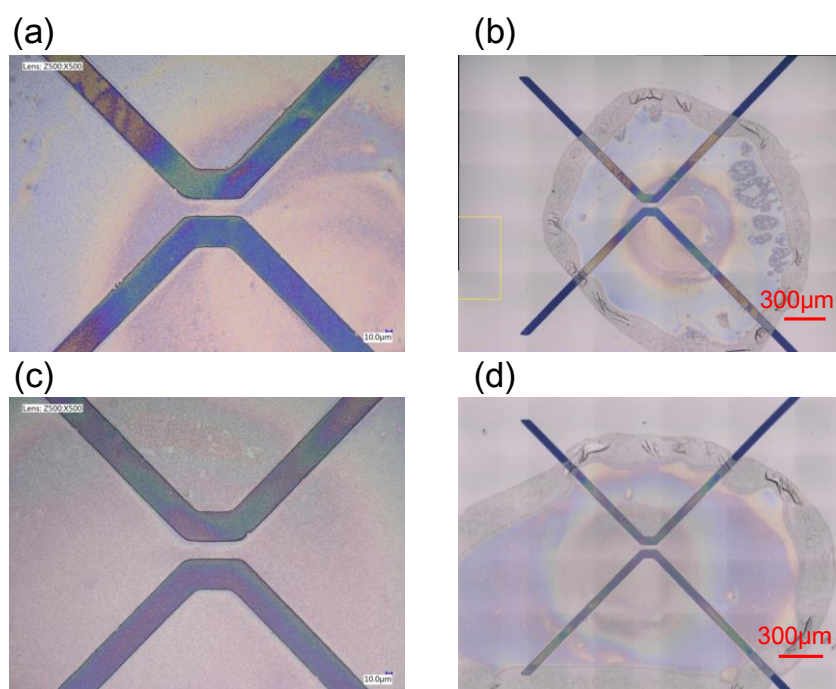


Figure 4.5 Microscopic images of surface morphology of the DHB matrix dissolved in mixture solution of milliQ water and acetonitrile (1:1,v/v). (a,b) Applying pre-mixed sample. (c,d) Thin-layer method.

Table 4.3 shows the summarization of surface morphology of DHAP as a matrix. Grain like sample surface is observed for every six solvents with pre-mixing method as shown in the Fig. 4.4 (b). In contrast to this, surface morphology is drastically changed to apply thin-layer method. Thin-layer method enables making smaller matrix crystals on the ionization source than pre-mixing method. Figure 4.6 shows the most drastic change in the microscopic images. For pre-mixing method, the matrix particles are locally dispersed with different sizes (10 to hundreds μm) due to slow evaporation of the solvent. On the other hand, figure 4.6 (c) shows thin-film of matrix/analyte formed by thin-layer method. Figure 4.6 (d) shows the bilayer structures of bottom matrix layer and upper matrix/analyte layer. Yellow dash line and orange dash line illustrate the edge of both layers, respectively. Matrix solution rapidly spreads near the edge of the micro heater (Pt/Cr layer), and then rapidly evaporates within a second. After that, dropped matrix/analyte solution creates thin-film like structure consisting of microcrystals on the thin-matrix layer.

Table 4.3 Summarization of surface morphology of DHAP as a matrix.

2,5-Dihydroxyacetophenone (DHAP) as a matrix

Solvent	Water/ acetonitrile (5:5)	Water/ acetonitrile (2:8)	Tetrahydro -furan	Ethanol	Methanol	Acetone
Method						
Pre-mixing	Grain	Grain	Grain	Grain	Film+Grain	Grain
Thin-layer	Grain	Fine grain	Film+Grain	Grain	Film+Grain	Film

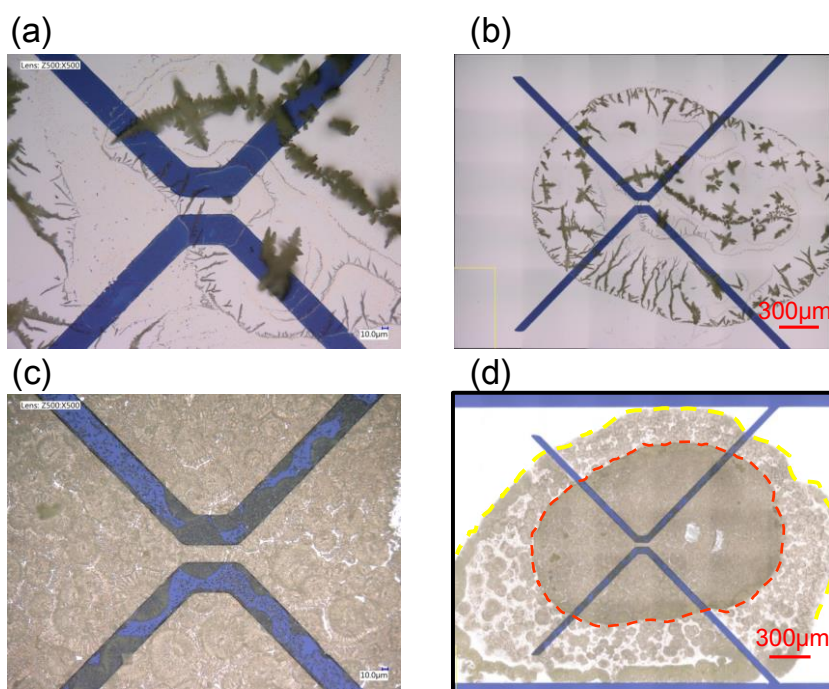


Figure 4.6 Microscopic images of surface morphology of the DHAP matrix dissolved in acetone. (a,b) Applying pre-mixed sample. (c,d) Thin-layer method.

Table 4.4 show the summarization of surface morphology of SA as a matrix. Grain like sample surface is observed for every six solvents with pre-mixing method. Matrix crystals with the size of 30 to 100 μm are dispersed on the whole surface of the micro heater as shown in the Fig. 4.7 (a). A few matrix crystals are placed on the narrowed region of the micro heater. In contrast to this, fine grains are created on the chip by thin-layer method with highly volatile solvents such as ethanol, methanol, and acetone. Thin-layer method shows the highly concentrated smaller matrix crystal with the size of 5 to 10 μm than pre-mixing as shown in the Fig. 4.7 (c). Bottom matrix layer forms transparent thin layer by fast evaporation of the acetone. However, upper matrix/analyte layers are not formed like thin-film unlike DHAP matrix with thin-layer method as shown in the Fig. 4.6 (d).

Table 4.4 Summarization of surface morphology of SA as a matrix.

Sinapinic acid (SA) as a matrix

Solvent	Water/ acetonitrile (5:5)	Water/ acetonitrile (2:8)	Tetrahydro- furan	Ethanol	Methanol	Acetone
Method						
Pre-mixing	Film+Grain	Film+Grain	Grain	Grain	Grain	Film+Grain
Thin-layer	Grain	Grain	Grain	Fine grain	Fine grain	Fine grain

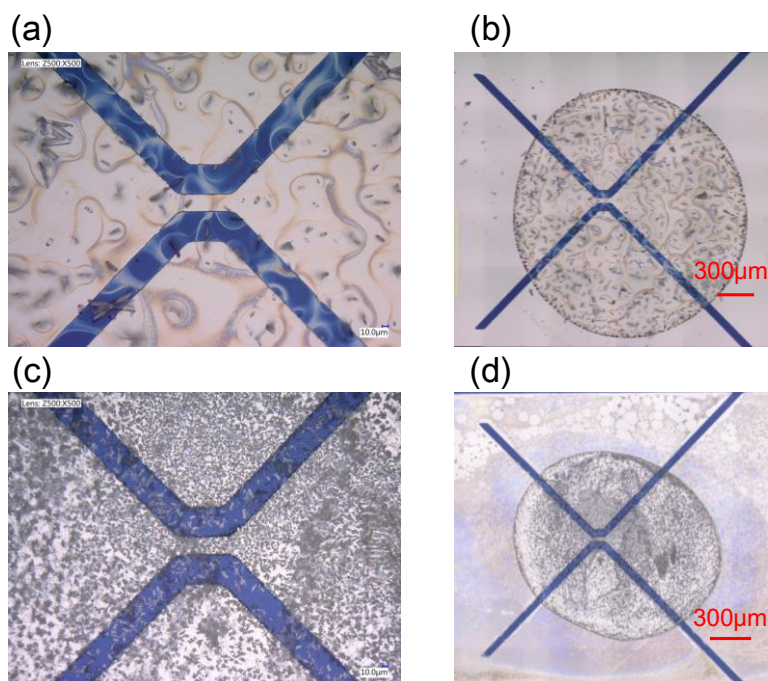


Figure 4.7 Microscopic images of surface morphology of the SA matrix dissolved in acetone. (a,b) Applying pre-mixed sample. (c,d) Thin-layer method.

4.5.3 TOF mass spectrometry with thin layer methods

To investigate the effect of making thin-layer consisting of microcrystals on the pulse-heating ionization, TOF mass spectra of BSA mixed with SA or DHAP matrices are analyzed using the thin-layer method. Figure 4.8 shows the results of TOF mass spectrometry of BSA with SA matrix. Microscopic image before pulse-heating shows the fine grains of matrix/analyte on the ionization source. In the mass spectrum, no signal derived from molecular weight of the protein is detected. On the other hand, continuous spectrum observed in the range of m/z 0-10,000 with pre-mixing sample (Fig. 4.2 (a)) disappears from the mass spectrum. The result implies that making thin-layer of the sample on the ionization source affects producing fragment ions in lower range of m/z . It is thought that SA matrix is the best matrix for MALDI mass spectrometry of proteins such as BSA. SA matrix, however, is not suitable for the pulse-heating ionization because of the lack of photoexcitation by laser irradiation for the ionization. The result suggests that another property different from optical absorption of the matrix is required for pulse-heating ionization to effectively transform the thermal energy to the sample from the micro heater.

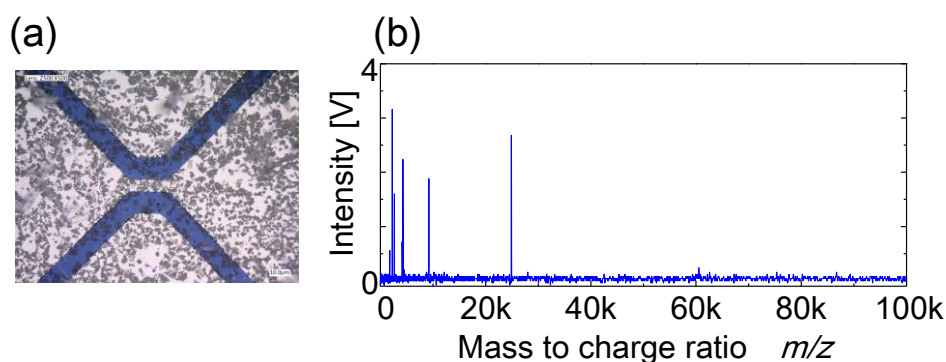


Figure 4.8 *TOF mass spectrometry with pulse-heating ionization and thin-layer method using acetone. (a) Microscopic image of the ionization source after sample applying of BSA with SA matrix. (b) TOF mass spectrum of BSA with SA matrix.*

TOF mass spectra of BSA with DHAP matrix with thin-layer method are shown in the Fig. 4.9. Sample morphology was controlled by changing the solvents to dissolve the matrix at the same concentration. Acetone, tetrahydrofuran, and acetonitrile/milliQ solution (8:2, v/v) was used as a solvent. Thickness of the sample layer was estimated from confocal scanning laser microscopy (VK-9710, KEYENCE, Japan) after the pulse-heating. Uniform thin-film with the thickness within 1 μm is formed by acetone as a solvent. Thin-film and grains with the thickness of approximately 1 to 3 μm is formed by tetrahydrofuran as a solvent. Relatively thick layer with the thickness of approximately 3 to 5 μm is formed by acetonitrile/milliQ solution (8:2, v/v). TOF mass spectra were obtained with applying same pulse-heating energy of

$1.07 \times 10^{-2} \mu\text{J}/\mu\text{m}^2$ for 500 ns to each sample. Sharp peak of the singly-charged BSA ion is produced to apply the pulse-heating to the thin-film of DHAP matrix/analyte as shown in the Fig. 4.9 (a). Interestingly, multiply-charged ions observed in the pulse-heating ionization with pre-mixing sample (Fig. 4.4 (a)) are not produced. Figure 4.9 (b) shows the doubly-charged ion as well as singly-charged ion when the sample forms partially thin-film and grain structures to apply the sample with thin-layer method using tetrahydrofuran as lower volatile solvent than acetone. Figure 4.9 (c) shows no signal derived from the protein to apply the pulse-heating to the thick sample layer formed by slow evaporation of the solvent with its low volatility. From the results, making thin-film layer of the matrix/analyte is effective to produce the singly-charged protein ion. The matrix of DHAP used in the inlet ionization due to its lower thermal requirements for desolvation of the matrix/analyte is one of the suitable materials for the pulse-heating ionization without laser or high voltage.

Figure 4.10 shows the comparison of the mass spectra of BSA using the thin-layer method with acetone and DHAP as a matrix. Generated fragment ions are drastically suppressed as compared to conventional MALDI-MS. For the case of protein MS, it is reported that little fragmentations occur for IR-MALDI as compared to UV-MALDI [16]. Berkenkamp *et al* reported that metastable decay of protein analyte is

prevented for IR-MALDI [17]. This result also implies that the ionization without photo excitation is effective to prevent the generation of fragment ions.

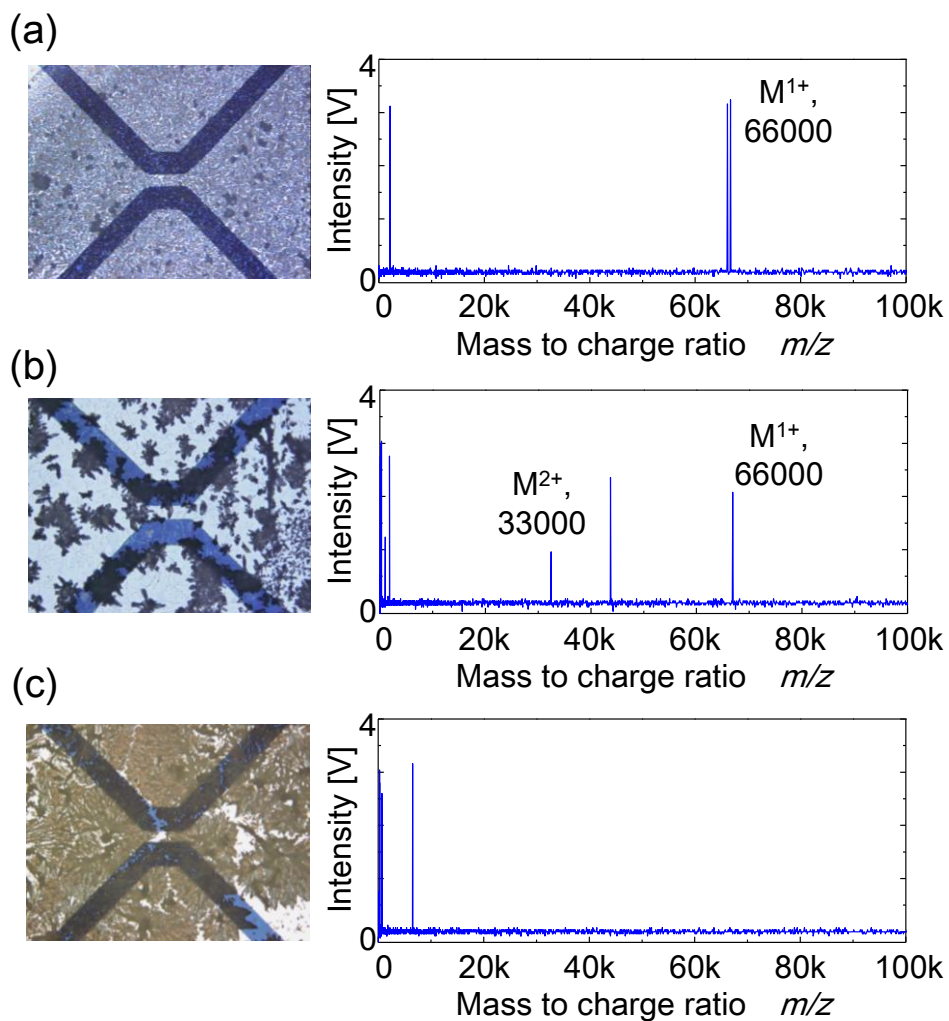


Figure 4.9 Microscopic image and TOF mass spectra of BSA with the matrix by using thin-layer method and controlled sample film. (a) Thin-film formed with acetone. (b) Partial thin-film and grain structure formed with tetrahydrofuran. (c) Thick-film formed with acetonitrile and milliQ water (8:2, v/v).

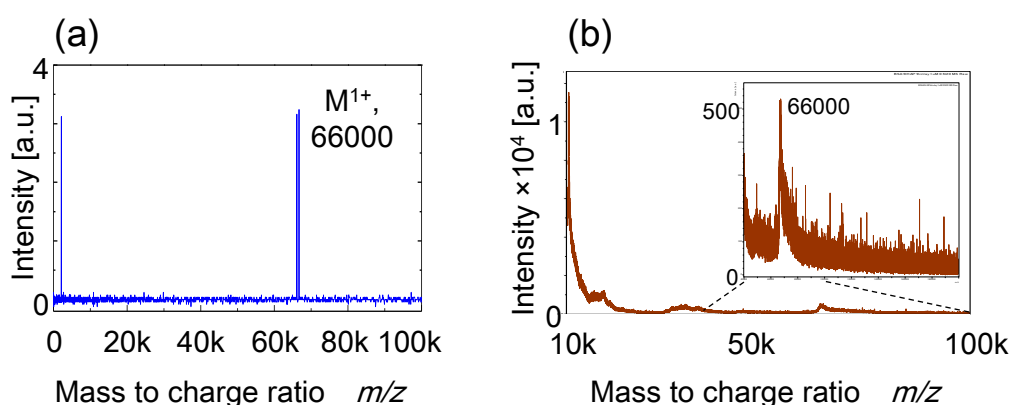


Figure 4.10 Comparison of mass spectrum of BSA mixed with DHAP matrix. (a) Single pulse-heating ionization. (b) 10,000 averaged MALDI mass spectrum.

Finally, sensitivity of the pulse-heating ionization with thin-layer method is estimated from the mass spectrum and microscopic image. The concentration of BSA analyte was 0.1 mg/ml i.e. $\approx 1.5 \mu\text{M}$. 250 nl of the mixture of same volume of matrix and protein solution was dropped onto the ionization chip, thus 125 nl of 1.5 μM BSA analyte was introduced. From typical microscopic image in the Fig. 4.6 (d), dropped solution mostly forms uniform solid film with the diameter of approximately 1 mm. In the pulse-heating ionization, limited samples placed on the only narrowed region ($30 \mu\text{m} \times 100 \mu\text{m}$) of the micro heater are desorbed and ionized. It means that 0.4 % of applied proteins can only be ionized if the protein disperses uniformly in the sample layer. Therefore, the amount of ionized and detected molecules with the pulse-heating ionization is estimated from the following equation.

$$1.5 [\mu M] \times 125 [nl] \times 0.004 = 750 [attomole] \quad (4.1)$$

One of the issues is not good reproducibility of formation of the solid-phase sample from the sample solution. To precisely evaluate the sensitivity of the pulse-heating ionization, integrated tens or hundreds of ionization sources on a chip or continuous sample introduction system will be required to accomplish a number of the ionization from the same sample like thousands of laser irradiation in MALDI. The briefly estimated sensitivity shows as low as conventional MALDI [15], indicating the potential of highly sensitive analysis of biomarkers on a chip mass spectrometer.

4.6 Summary

In this chapter, the effects of the matrix and the solvent for sample formation on the pulse-heating ionization were studied. Mass spectra with the pulse-heating ionization, MALDI-MS, and microscopic images of the surface morphology of dried sample were compared with different matrices used in conventional MALDI and the inlet ionization. While the pulse-heating ionization with SA matrix produces little signals of proteins with abundant fragment ions, the matrix shows the MALDI mass spectrum including singly-charged BSA ion with little fragments. Use of DHB matrix

shows the similar mass spectrum including singly-charged ion and specific fragment ions in both cases of the pulse-heating ionization and MALDI. DHAP matrix shows the better mass spectrum including multiply-charged BSA ions with little fragment ions than above matrices. To apply thin-layer method using acetone as a highly volatile solvent to the pulse-heating ionization, singly-charged protein ion is produced on a chip. The estimated sensitivity of the pulse-heating ionization of BSA analyte with thin-layer method is to approximately 750 attomole as low as conventional MALDI-MS.

References

- [1] Sugiyama, Kiyotaka, et al. "Pulse-heating ionization for protein on-chip mass spectrometry." *Analytical chemistry* 86.15 (2014): 7593-7597.
- [2] Gross, Jürgen H. *Mass spectrometry*, Springer, 2004.
- [3] Kussmann, Martin, et al. "Matrix - assisted laser desorption/ionization mass spectrometry sample preparation techniques designed for various peptide and protein analytes." *Journal of Mass Spectrometry* 32.6 (1997): 593-601.
- [4] Landry, France, Christian R. Lombardo, and Jeffrey W. Smith. "A method for application of samples to matrix-assisted laser desorption ionization time-of-flight targets that enhances peptide detection." *Analytical biochemistry* 279.1 (2000): 1-8.
- [5] Stahl, Bernd, et al. "Oligosaccharides from human milk as revealed by matrix-assisted laser desorption/ionization mass spectrometry." *Analytical biochemistry* 223.2 (1994): 218-226.
- [6] McEwen, Charles N., et al. "New paradigm in ionization: multiply charged ion formation from a solid matrix without a laser or voltage." *Analytical chemistry* 82.22 (2010): 9164-9168.
- [7] Tanaka, Koichi, et al. "Protein and polymer analyses up to m/z 100 000 by laser ionization time of flight mass spectrometry." *Rapid communications in mass spectrometry* 2.8 (1988): 151-153.
- [8] Allwood, D. A., et al. "UV Optical Absorption of Matrices Used for Matrix - assisted Laser Desorption/Ionization." *Rapid communications in mass spectrometry* 10.13 (1996): 1575-1578.
- [9] Lietz, Christopher B., et al. "Inlet ionization: protein analyses from the solid state without the use of a voltage or a laser producing up to 67 charges on the 66 kDa

- BSA protein." *Rapid Communications in Mass Spectrometry* 25.22 (2011): 3453-3456.
- [10] Inutan, Ellen D., and Sarah Trimpin. "Matrix assisted ionization vacuum (MAIV), a new ionization method for biological materials analysis using mass spectrometry." *Molecular & Cellular Proteomics* 12.3 (2013): 792-796.
- [11] Vorm, Ole, Peter Roepstorff, and Matthias Mann. "Improved resolution and very high sensitivity in MALDI TOF of matrix surfaces made by fast evaporation." *Analytical Chemistry* 66.19 (1994): 3281-3287.
- [12] Wenzel, Thomas, et al. "2, 5-Dihydroxyacetophenone: a matrix for highly sensitive matrix - assisted laser desorption/ionization time - of - flight mass spectrometric analysis of proteins using manual and automated preparation techniques." *Rapid communications in mass spectrometry* 20.5 (2006): 785-789.
- [13] Amado, Francisco ML, et al. "Analysis of peptide and protein samples containing surfactants by MALDI-MS." *Analytical Chemistry* 69.6 (1997): 1102-1106.
- [14] Mank, Marko, Bernd Stahl, and Günther Boehm. "2, 5-Dihydroxybenzoic acid butylamine and other ionic liquid matrixes for enhanced MALDI-MS analysis of biomolecules." *Analytical chemistry* 76.10 (2004): 2938-2950.
- [15] Valaskovic, Gary A., Neil L. Kelleher, and Fred W. McLafferty. "Attomole protein characterization by capillary electrophoresis-mass spectrometry." *Science* 273.5279 (1996): 1199-1202.
- [16] Hoffmann, Edmond. *Mass spectrometry*. John Wiley & Sons, Inc., 2007.
- [17] Berkenkamp, Stefan, et al. "Performance of Infrared Matrix - assisted Laser Desorption/Ionization Mass Spectrometry with Lasers Emitting in the 3 μm Wavelength Range." *Rapid communications in mass spectrometry* 11.13 (1997): 1399-1406.

CHAPTER 5

MINIATURIZED ION LENS AND ON-CHIP MASS SPECTROMETRY OF PROTEIN SAMPLE

Abstract

To realize on-chip mass spectrometry, the miniaturized electrostatic ion lens and the time-of-flight (TOF) path were developed and integrated with the pulse-heating ionization source on a chip. Characteristics of the ion focusing with the electrostatic ion lens fabricated in a micro channel were numerically calculated. The simulated results showed that the position of the micro electrodes for the ion extraction and the electrode shape were important to control the ions in a micro channel. Finally, on-chip TOF mass spectrometry of bovine serum albumin (BSA) as a protein analyte was firstly reported using the pulse-heating ionization and the 5 mm length of TOF mass analyzer with the electrostatic ion lens. The separated peaks of ions were shown at 7.8 and 10.5 μ s of TOF which approximately corresponded to numerically calculated TOF of the singly-charged ion and the doubly-charged ion of BSA protein sample, respectively.

5.1 Introduction

Mass separation of ions in a micro structure is an interesting study toward the mass spectrometry in a low vacuum which enables significant miniaturization of the mass spectrometer without use of the high vacuum system like a bulky turbo-molecular pump. Some previous works developed miniaturized mass analyzers on a chip, the surface microstructure/miniature mass separator [1], the miniaturized TOF mass filter [2], the combination of TOF mass filter with energy filter [3], the quadru-pole mass filter with Brubaker prefilters [4, 5], and the cylindrical ion trap filter [6]. Currently fabricated mass analyzers are able to measure gases (N^+ , Ne^+ , N_2^+ , and Ar^+ [3]) or small molecule chemical compounds of acetone [2], perfluorotributylamine [4, 6], and reserpine [5]. Mass separation and detection of protein molecules on a chip have not been realized because of the following reasons; (i) The quadru-pole ion filter and the cylindrical ion trap filter are very effective to analyze the ions having m/z up to a few thousands while high RF voltage is required to stabilize the ions having higher m/z such as a protein by those filters as discussed in the chapter 1. (ii) Currently developed miniaturized ionization sources are not able to apply protein mass spectrometry. The developed pulse-heating ionization source can be used for protein mass spectrometry to integrate with a miniaturized TOF mass analyzer on a chip.

5.2 Objective

To analyze the biological sample including peptides and proteins on a chip, the miniaturized pulse-heating ionization is integrated with the on-chip ion lens for TOF mass spectrometry. First, ion optics in a micro channel is studied using numerical simulation by COMSOL 4.2a. To control the ions in an electric field formed by micro electrodes, some effective parameters, electrode geometry, and applied voltage are evaluated. Second, the chip composed of the pulse-heating ionization source and the ion lens is fabricated using photolithography. Finally, on-chip mass spectrometry of protein sample is performed.

5.3 Principle

Trapping of charged particles such as ions or electrons based on its mass has been studied for decades. An electric field and a magnetic field are normally used for controlling the charged particles. A magnetic field is normally used for the separation of charged particles a few decades ago whereas use of a magnetic field is no longer majority in the mass spectrometry except very highly selective mass spectrometry like a Fourier transform mass spectrometer [7]. Similarly to the currently miniaturized mass analyzer such as quadru-pole mass filter, only an electric field is used to control the ion trajectory in a micro structure. To control the electric field, fabricated micro electrodes are utilized in this study. Photolithography technique enables the fabrication of the ionization source as

well as the micro electrodes which can precisely control the electric field in the micro structure.

5.4 Numerical simulation

5.4.1 Design of the chip

Figure 5.1 shows the calculation model for the numerical simulation of the ion trajectory in a micro channel. The equations of the electric potential and the motion of the charged particles were numerically calculated by COMSOL 4.2a as discussed in the chapter 3. Red color indicates the bottom substrate with the ionization source and blue color indicates the upper substrate. A series of micro electrodes with the width of 150 μm were uniformly arranged in the length of 5 mm between the on-chip ionization source and an off-chip channeltron electron multiplier. Repeller electrode was placed above the ionization source to focus the ion beam inward to the center of the micro channel. Both upper and bottom substrates were bonded with electrically conductive double-sided tape (0.02 Ω/cm^2 , thickness: 95 μm) (No.792, TERAOKA, Japan) to acquire electrical connection between the upper and bottom micro electrodes. The gap of two substrates was adjusted using two tapes to 190 μm i.e. the height of the micro channel. To control the ions in a micro channel, distance L between the ionization source and the first micro electrode and applied voltages to the micro electrodes, V_r , V_1 , V_2 , and V_3 were adjusted. Moreover, electrode shapes were also considered.

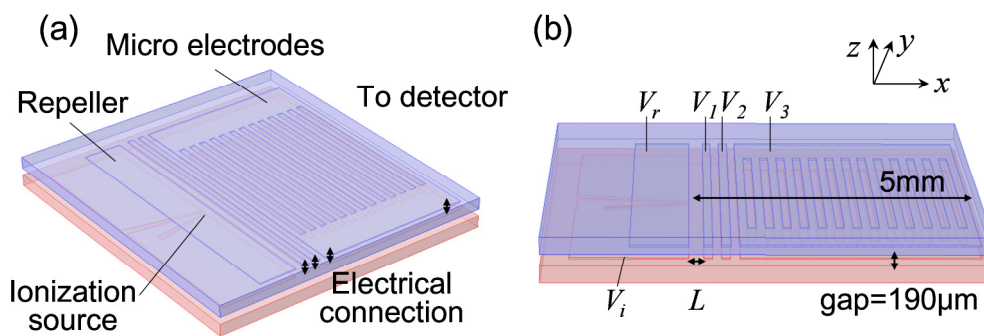


Figure 5.1 Schematic view of the model for numerical simulation of on-chip ion control. Red color indicates the bottom substrate with the ionization source and blue color indicates the upper substrate with the repeller. (a) Over view. (b) Side view.

5.4.2 Numerical simulation of ion optics in a micro channel

It was found that the electrode shape and the five parameters as shown in the Fig. 5.1 (b) are important to control the ions in a micro channel. Vertical ion focusing and horizontal ion focusing in a micro channel were studied by changing these parameters of the electrode shape, the position of the micro electrode for ion extraction, and the applied voltage. For the every simulation in this chapter, electrical potential difference ($V_3 - V_i$) for accelerating positive ions and particle mass were adjusted 100 V and 66 kDa (BSA), respectively. At first, the applied voltage to the micro electrodes was fixed at following value; $V_i = 30\text{V}$, $V_r = 60\text{V}$, $V_1 = V_2 = V_3 = -70\text{V}$. Figure 5.2 shows the images of numerically calculated ion trajectory with the different length between the ionization source and the micro electrode. The simulation shows that the position of the micro electrode affects the

vertical focusing of the ion beam. The ion trajectory is sensitive to x-axis initial position due to the width of the ionization source (30 μm). Figure 5.2 (c) shows the most converged trajectory of the ions which is generated at the center part of the ionization source.

Figure 5.3 shows brief summarization of the ion convergence rate at the end of the micro channel. For the numerical simulation, the position of the micro electrode and voltage V_r applied to the repeller were varied. It was assumed that 100 particles were uniformly distributed on the ionization source (20 \times 95 μm) at intervals of 5 μm at a start time of the simulation. To focus the ions in a micro channel with shorter distance, higher voltage is required to apply the repeller. The ion convergence ratio is less than 20 % in this condition. Presently, the distance between the ionization source and the extraction electrode was adjusted to approximately 300 μm for further optimization.

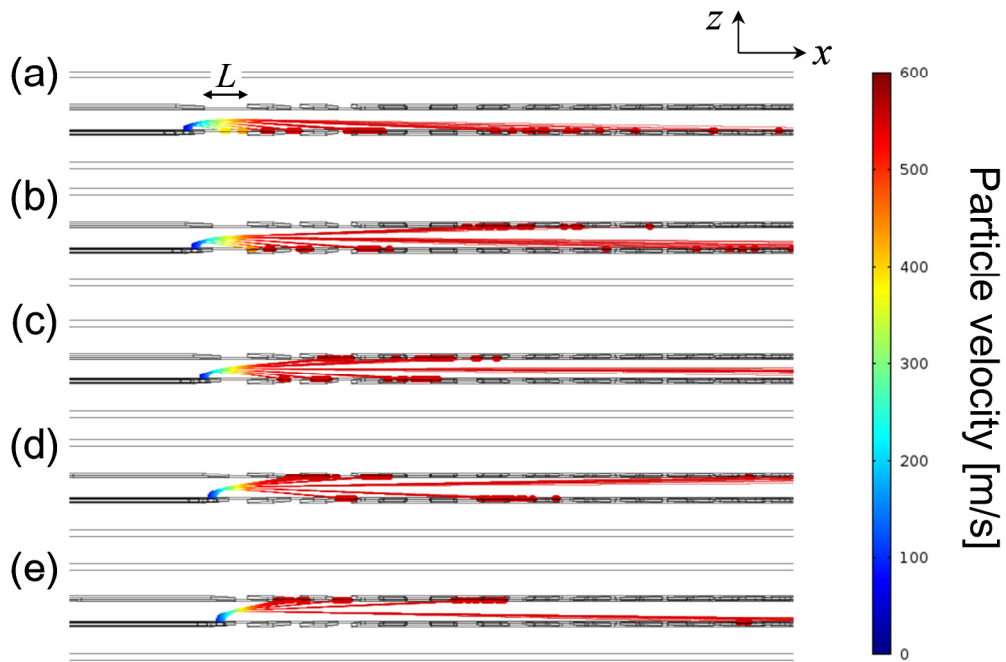


Figure 5.2 Ion trajectory in a micro channel. The distance between the ionization source and the extraction electrode was varied as $L =$ (a) $400\mu\text{m}$, (b) $350\mu\text{m}$, (c) $300\mu\text{m}$, (d) $250\mu\text{m}$, and (e) $200\mu\text{m}$.

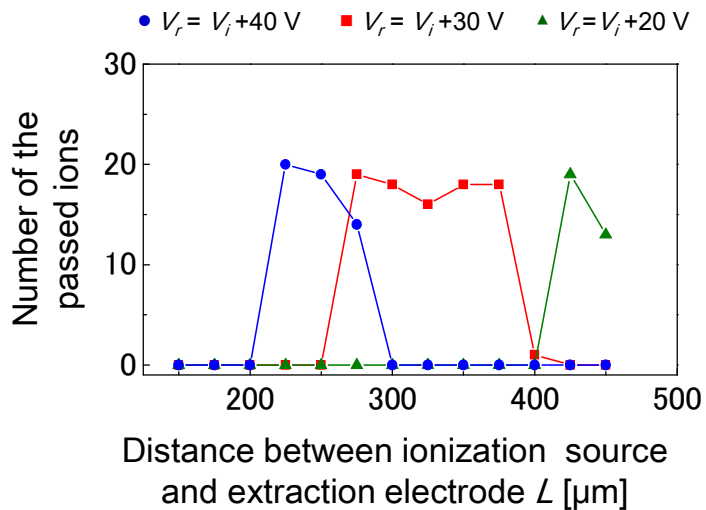


Figure 5.3 Summarization of ion convergence rate with different conditions.

Next, the effect of the shape of the micro electrodes on the ion convergence was studied. It was expected that the electrode shape affects the electric field distribution in a micro channel. Different shape of the electrodes, straight, circular, landscape oval, or portrait oval electrodes were used in the simulation. The applied voltage was as follows; $V_i = 30\text{V}$, $V_r=43.75\text{V}$, $V_l=0$, $V_2=15\text{V}$, and $V_3=-70\text{V}$. Similarly to the previous simulation, it was assumed that 100 particles were uniformly distributed on the $20 \times 95 \mu\text{m}$ area of the ionization source. Figure 5.4 shows the horizontal images of the ion trajectory. In every case, the simulation shows that some ions initially located on the ionization source are passed through the micro channel. In the case of straight electrode, ions are linearly extracted due to the homogenous electric field on y-axis between the ionization source and the straight electrode. In contrast to this, ions are horizontally converged inward the center of the micro channel except straight electrode. After that, the ions are additionally accelerated by the potential difference of V_2 and V_3 . In the case of circular electrode, the ions focus in the narrowest region. However, the ions horizontally spread toward the end of the micro channel. Figure 5.5 shows the vertical images of the ion trajectory. In every case, the ions are vertically converged inward the center of the micro channel due to the inhomogeneous electric field by applying different voltage in micro electrodes. Circular- or oval-shaped electrode shows the better ion focusing than the straight electrode. The landscape oval-shaped electrode shows the best ion focusing at the center between the third and the fourth electrodes. From above

results, it is expected that circular- or oval-shaped micro electrode forms inhomogeneous electric field on z-axis which contributes effective ion focusing.

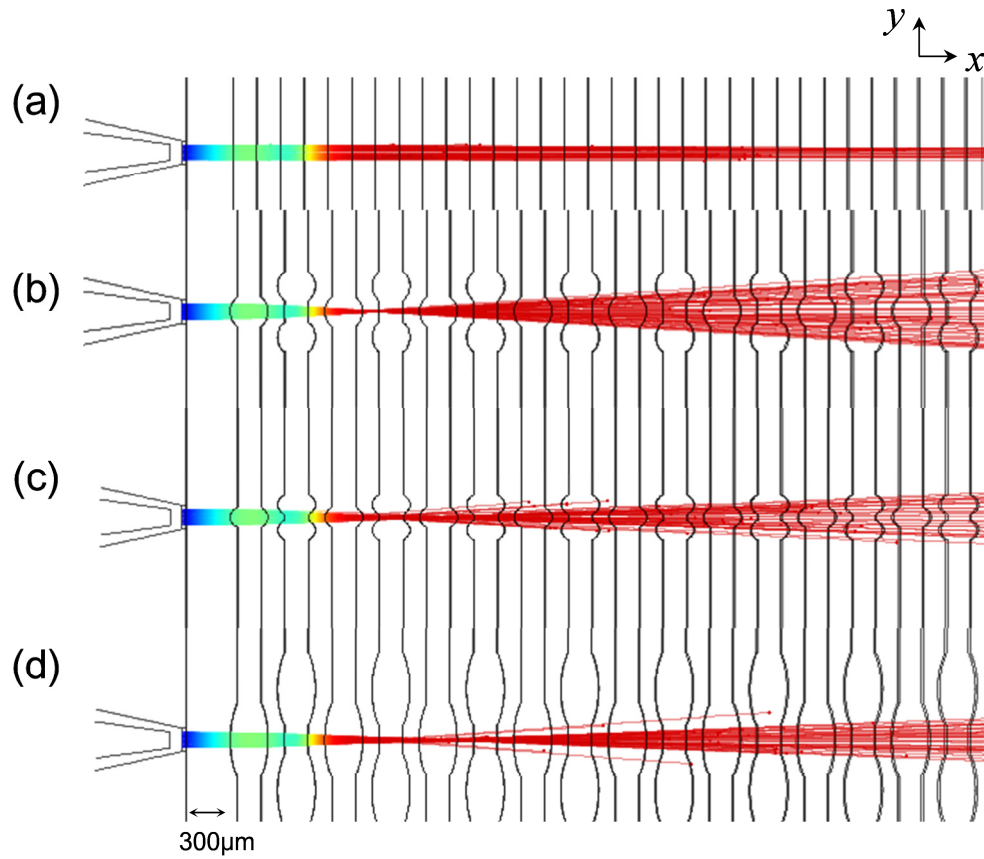


Figure 5.4 Shape dependence of the micro electrodes on the horizontal ion convergence. Numerical simulation is shown in case of (a) straight electrode, (b) circular electrode, (c) landscape oval electrode, and (d) portrait oval electrode.

Applied voltage was adjusted to $V_i = 30V$, $V_r = 43.75V$, $V_1 = 0$, $V_2 = 15V$, and $V_3 = -70V$.

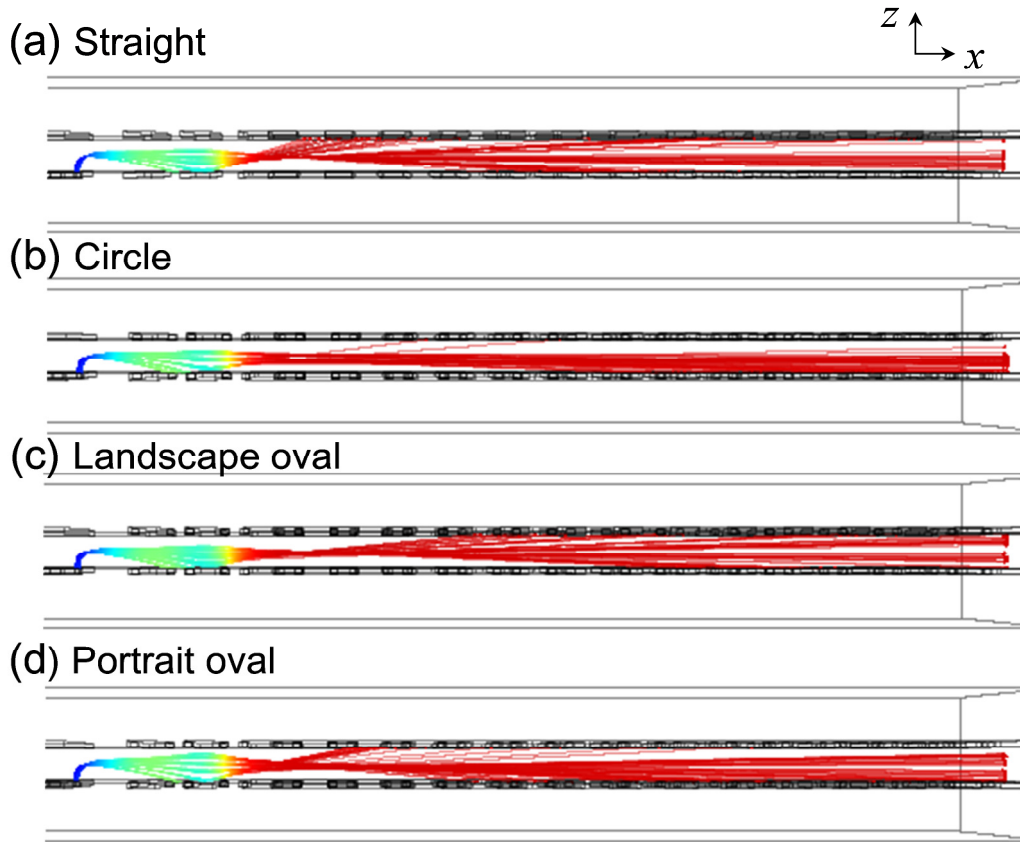


Figure 5.5 *Shape dependence of the micro electrodes on the vertical ion convergence. Numerical simulation is shown in case of (a) straight electrode, (b) circular electrode, (c) landscape oval electrode, and (d) portrait oval electrode.*

Applied voltage was adjusted to $V_i = 30V$, $V_r = 43.75V$, $V_1 = 0$, $V_2 = 15V$, and

$$V_3 = -70V.$$

Figure 5.6 shows the total number of the passed ions in a micro channel with different shaped micro electrodes. In the case of the straight micro electrode, maximum ion convergence rate is less than 20 % as discussed in the Fig. 5.3. In contrast to this, the ion convergence rate increases with circular- or oval-shaped micro electrode. The maximum convergence rate is 42 % in the case of circular

electrode, indicating two times higher than straight electrode. As shown in the Fig. 5.4 (b), horizontal spreading of ions causes the variability of TOF which lead the low selectivity of the TOF-MS. Therefore, portrait oval-shaped micro electrode was adapted to the on-chip ion lens due to high ion convergence and relatively low ion spreading.

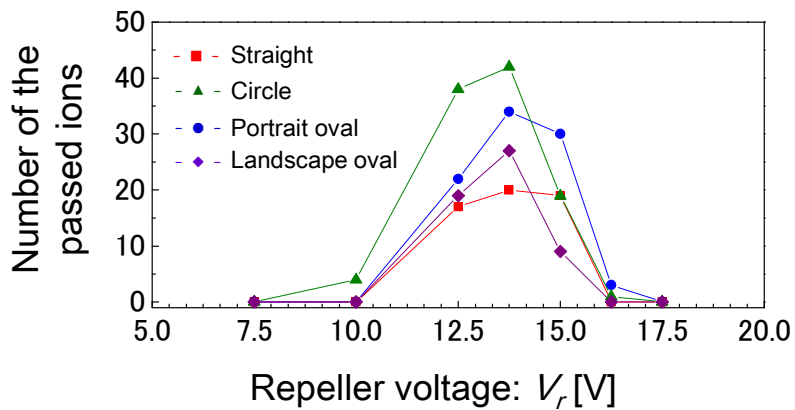


Figure 5.6 Numerically calculated ion convergence rate in 5 mm length of the micro channel with different shaped micro electrode. 100 particles were uniformly distributed on the ionization source at the starting of the simulation.

5.5 Experiment

5.5.1 Chip fabrication

The chip integrated with the ionization source and the ion lens was fabricated in a similar manner to the fabrication of the ionization chip described in the chapter 3. Figure 5.7 shows the fabrication process of the chip. The quartz substrates as a higher insulation material than silicon were used to prevent the

current leakage in the substrate because the voltage was applied on the whole micro electrodes on a chip. Micro patterns of Pt/Cr were fabricated on quartz substrates ($20 \times 20 \text{ mm}^2$ or $30 \times 30 \text{ mm}^2$) using photolithography and lift-off process. Figure 5.8 shows the microscopic images of the fabricated micro structures on the substrate. Mirror reversed micro structures were patterned on each substrate to realize vertically symmetric micro electrodes on a chip. Finally, two substrates were bonded with electrically conductive double-sided tapes to make a small gap of $190 \mu\text{m}$ for the ion travelling. Figure 5.9 shows the photograph of the fabricated chip. The chip connected with electrical wires was vertically placed in a vacuum chamber for the TOF mass spectrometry

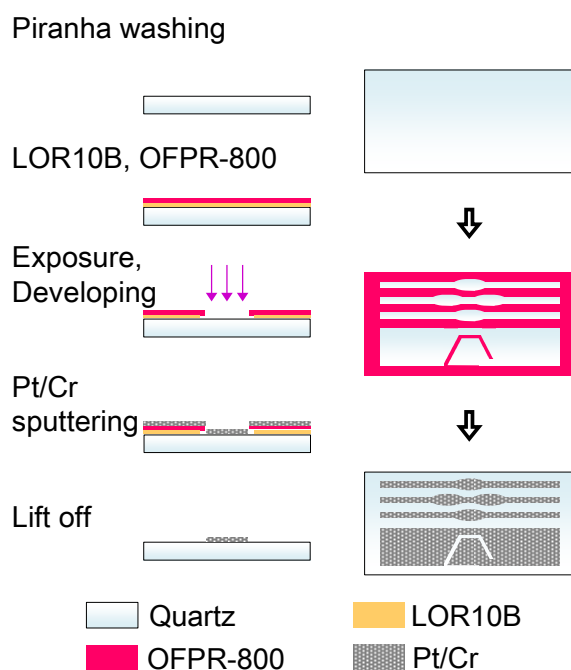


Figure 5.7 Schematic of the fabrication process of the chip.

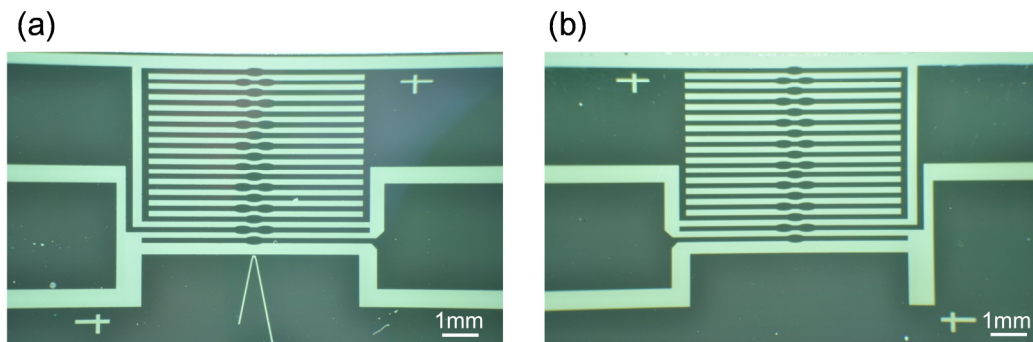


Figure 5.8 *Microscopic images of the fabricated substrates. White part shows the quartz substrate and dark part shows metal layer. (a) Bottom substrate with ionization source. (b) Upper substrate with the ion repeller.*

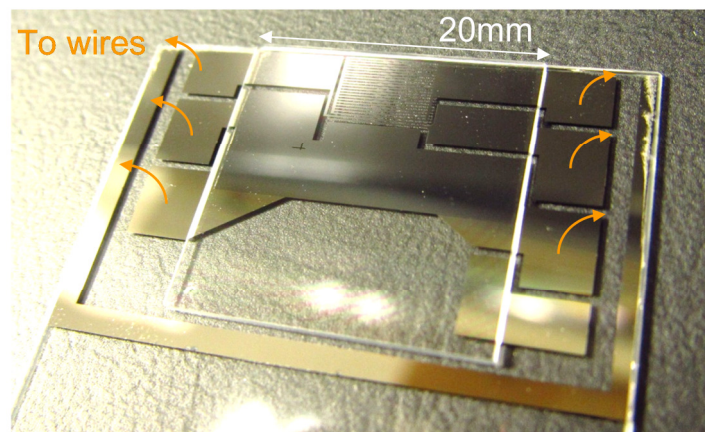


Figure 5.9 *Photograph of the fabricated chip.*

5.5.2 Experimental setup

Figure 5.10 shows the experimental setup for on-chip TOF mass spectrometry. Similar equipment setup explained in the chapters 3 and 4 was used. Currently, an ion detector has not been miniaturized thus the chip was vertically

placed for a channeltron electron multiplier in a vacuum chamber connected to a turbo-molecular pump. The vacuum in the chamber was adjusted to approximately 10^{-3} Pa in the experiments.

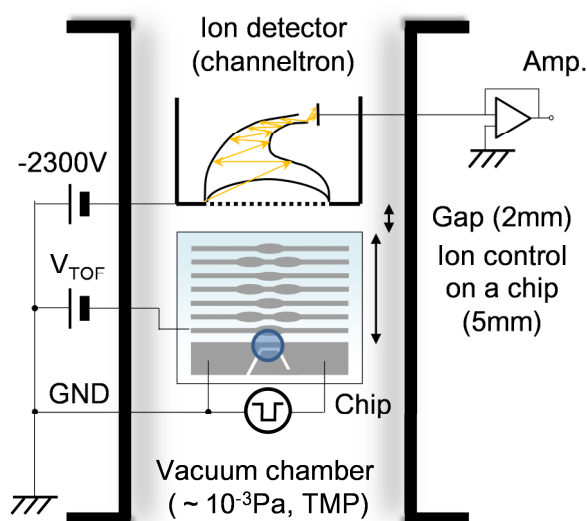


Figure 5.10 *Schematic of experimental setup for on-chip TOF mass spectrometry.*

5.5.3 Sample preparation

0.1 mg/ml of BSA as a protein sample dissolved in DI water and 10 mg/ml of DHAP as a matrix dissolve in acetone were prepared in a similar manner to the chapter 4. Thin-layer method was used to obtain the film like layer of the matrix/protein on the ionization source. Initially, 250 nl of matrix solution was dropped and then 250 nl of matrix/protein solution was applied. After sample applying, both upper and bottom substrates were aligned and bonded.

5.6 Results and discussion

5.6.1 Ionization in a micro channel

Before the mass spectrometry on a chip, ionization in a micro channel is studied without the ion lens and the free flight region for TOF mass analysis. The ionization chip (2.5 mm × 20 mm) fabricated on silicon substrate was used. BSA analyte mixed with DHAP matrix was applied onto the ionization source using thin-layer method. After that, the chip was covered by a piece of silicon substrate with the gap of 190 μm to make micro channel between the ionization source and a channeltron electron multiplier. The chip was placed 4 mm apart the channeltron electron multiplier. Figure 5.11 shows the input pulse voltage for the ionization and the detected TOF signal. The TOF signal indicates broad peak in the range of 0 to 40 μs of TOF. This result means that the generated positive ions are reflected from the ionization source due to its positive potential and then are continuously detected. In the previous chapters 3 and 4, the ions were generated on the ionization source where relatively high voltage of -500 V was exposed by TOF analyzer. In contrast to this, this result shows that ions are produced by only the pulse-heating without direct exposure of high voltage. It means that thermal energy and matrix assistance are requirements for the pulse-heating ionization.

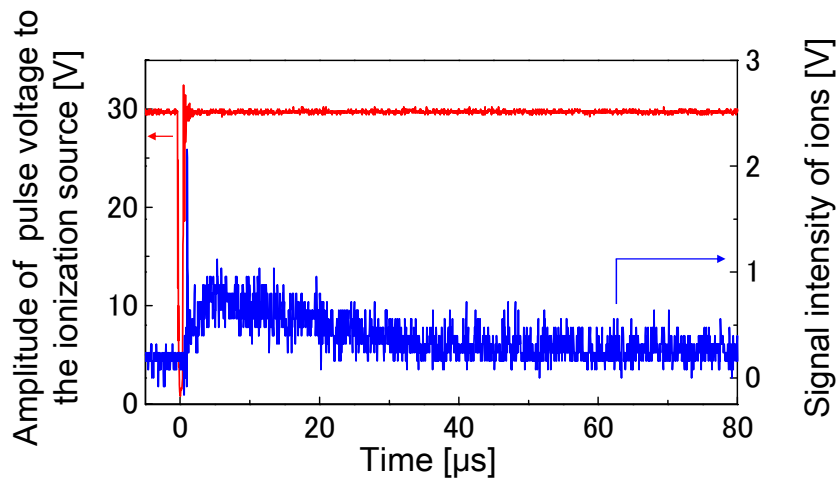


Figure 5.11 Result of the ionization in a micro channel without the ion lens and the TOF mass analyzer. The input voltage ($0.93 \times 10^{-2} \mu\text{J}/\mu\text{m}^2$) and the detected signal by a channeltron electron multiplier are shown.

5.6.2 On-chip TOF mass spectrometry

At first, the relation between the mass of the charged molecules and TOF in a micro channel was estimated by the numerical simulation. Figure 5.12 (a) shows the simulated results of the trajectory of ions having different mass of 66,000, 33,000, 11,000, 1,000, and 150. Second-order approximation shows the following equation of the *mass* [Da] and *TOF* [μs] from the ionization to arrival to the channeltron .

$$mass = 543.96(TOF)^2 + 9.66(TOF) + 11.37 \quad (5.1)$$

From the Fig. 5.12 (b), TOF of the singly-charged BSA ion (m/z of 66,000) is approximately $11.0 \mu\text{s}$ which is twenty times longer than the pulse-heating time of 500 ns.

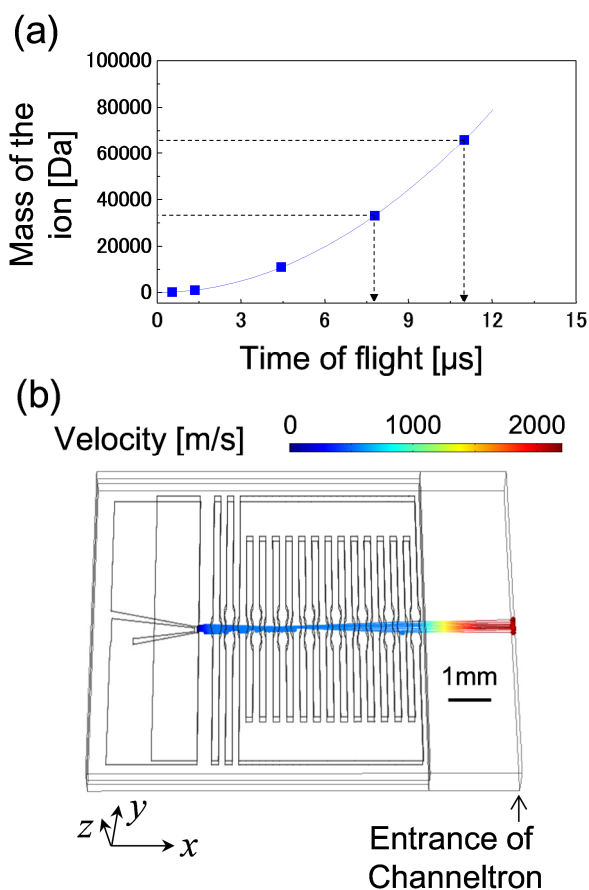


Figure 5.12 (a) The relation between mass and TOF on TOF mass analyzer on a chip. (b) Simulated result of the ion with the mass of 66,000 at $11.0 \mu\text{s}$.

Figure 5.13 shows the results of on-chip mass spectrometry of DHAP matrix with no protein analyte. Dropped matrix solution formed thin-film layer on the ionization source by thin-layer method as shown in the Fig. 5.13 (a). Three times averaged TOF signals are shown. The signal derived from the ions of the

applied matrix is not obtained while desorption of the sample on the micro heater is observed as shown in the Fig. 5.13 (b). The possible cause is expected that the generated ions do not pass through the micro channel due to its fast initial velocity by the pulse-heating.

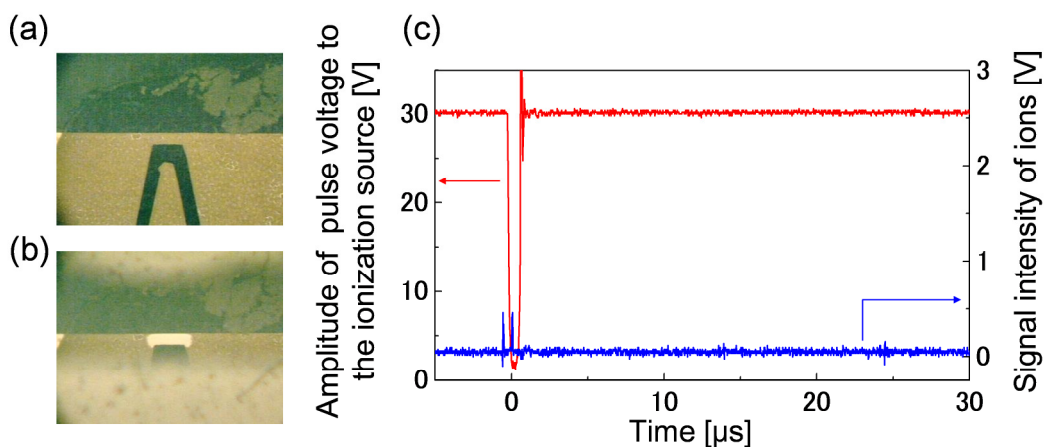


Figure 5.13 *On-chip TOF mass spectrometry of DHAP matrix only with applying pulse-heating of $0.96 \times 10^{-2} \mu\text{J}/\mu\text{m}^2$. Microscopic images of the ionization source (a) before pulse-heating and (b) after pulse-heating. (c) Input pulse voltage and TOF signal.*

Figure 5.14 shows the results of the on-chip mass spectrometry of BSA protein mixed with DHAP matrix using thin-layer method. Making of thin-film layer of the sample as well as sample desorption is observed. Figure 5.14 (c) shows clearly separated peaks at around 1.1, 2.0, 7.8, and 10.5 μs after dropping input voltage to near zero. In contrast to the Fig. 5.11, continuous broad peaks are not observed. Moreover TOF signals at 7.8, and 10.5 μs which approximately

correspond to the singly-charged and the doubly-charged protein ions as discussed in the Fig. 5.12. Currently, pulse-heating time is fixed at 500 ns due to the limitation of property of the handmade FET circuit. Moreover, velocity variation of ions attributed by both initial kinetic energy at the ionization and low acceleration voltage at -100 V may cause lower selectivity than TOF-MS analysis explained in the chapters 3 and 4. To realize more highly selective mass analysis, pulse-heating during a few tens of ns and minimizing the initial kinetic energy by the fabrication of TOF mass analyzer as a reflector mode should be considered in the future. On-chip mass spectrometry of protein analyte with more than 10 kDa of molecular weight was firstly developed using the miniaturized pulse-heating ionization source and the electrostatic ion lens.

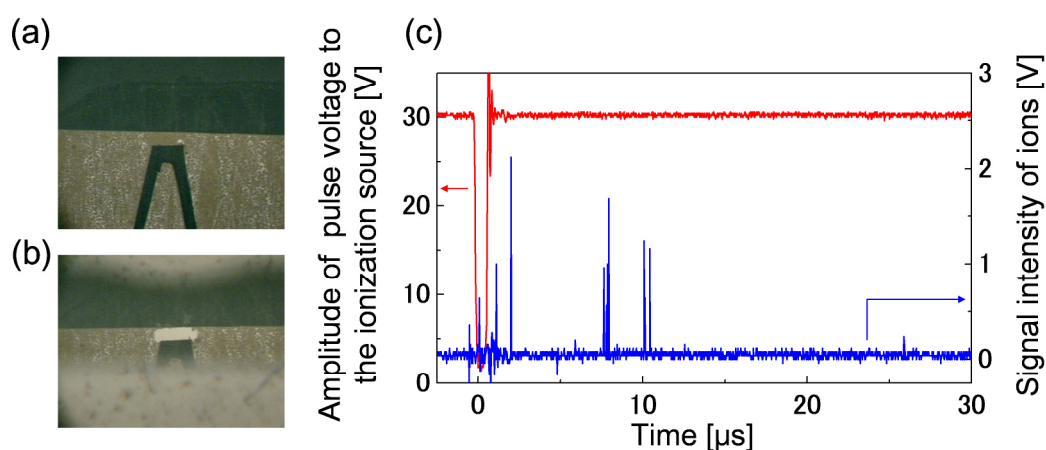


Figure 5.14 *On-chip TOF mass spectrometry of BSA mixed with DHAP matrix with applying of $1.04 \times 10^{-2} \mu\text{J}/\mu\text{m}^2$. Microscopic images of ionization source (a) before pulse-heating and (b) after pulse-heating. (c) Input pulse voltage and TOF signal.*

5.7 Summary

In this chapter, the miniaturized ion lens and the TOF path were developed and integrated with the pulse-heating ionization source for on-chip protein MS. Numerical simulation of the electrostatic ion lens showed that ions can be controlled by a series of fabricated oval-shaped micro electrodes in a micro channel. Finally, on-chip TOF mass spectrometry of BSA as a protein analyte was firstly reported. The signals showed the separated peaks at around 7.8 and 10.5 μ s of TOF which approximately correspond to the singly-charged ion and doubly-charged ion of BSA protein.

References

- [1] Siebert, Peter, et al. "Surface microstructure/miniature mass spectrometer: processing and applications." *Applied Physics A: Materials Science & Processing* 67.2 (1998): 155-160.
- [2] Doms, M., and J. Muller. "A micromachined vapor-jet vacuum pump." *Solid-State Sensors, Actuators and Microsystems Conference, 2007. TRANSDUCERS 2007. International*. IEEE, 2007.
- [3] Wapelhorst, Eric, Jan-Peter Hauschild, and Jörg Müller. "Complex MEMS: a fully integrated TOF micro mass spectrometer." *Sensors and Actuators A: Physical* 138.1 (2007): 22-27.
- [4] Wright, Steven, et al. "Microfabricated quadrupole mass spectrometer with a Brubaker prefilter." *Microelectromechanical Systems, Journal of* 19.2 (2010): 325-337.
- [5] Wright, Steven, et al. "MEMS-based nanospray-ionization mass spectrometer." *Microelectromechanical Systems, Journal of* 19.6 (2010): 1430-1443.
- [6] Chaudhary, Ashish, F. Van Amerom, and R. Timothy Short. "Development of microfabricated cylindrical ion trap mass spectrometer arrays." *Microelectromechanical Systems, Journal of* 18.2 (2009): 442-448.
- [7] Amster, I. Jonathan. "Fourier transform mass spectrometry." *Journal of mass spectrometry* 31.12 (1996): 1325-1337.

CHAPTER 6

CONCLUSIONS

In this thesis, to realize on-chip mass spectrometry (MS) toward the extra sensitive detection of biological samples on-site, the main key elements of on-chip vacuum generation, on-chip ionization source, on-chip electrostatic ion lens, and on-chip time-of-flight (TOF) path were successfully developed. Based on these results, on-chip mass spectrometry device was demonstrated employing the two key outcomes: the miniaturized pulse-heating ionization source and the patterned electrostatic ion lens. Clearly separated peaks of bovine serum albumin as a protein analyte was successfully obtained using the developed on-chip device with 5 mm length of TOF path settled in a vacuum chamber with an ion detector. The on-chip mass spectrometer has potential to operate in a low vacuum due to its significantly shorter flight distance of the target ions than conventional mass spectrometry.

On-chip vacuum generation method was developed using gas-liquid phase transition. Vacuum tight quartz chip with a micro chamber and the diaphragm vacuum sensor was fabricated. Theoretically, it was expected that evacuation of water vapor in high temperature and adsorption and freezing onto the micro chamber in low temperature as -40°C realize a low vacuum around 10 Pa which is required vacuum for the miniaturized mass spectrometry. Currently,

the maximum vacuum of 8.5 kPa was attained on a chip without complex mechanical moving parts and an external vacuum pump.

Next, the miniaturized pulse-heating ionization source was developed. Ionization of a peptide and a protein from solid phase is realized by applying Joule heating without laser, high voltage, or heated ambient gases. Only the assistance of the proper matrix such as 2,5-dihydroxybenzoic acid and 2,5-dihydroxyacetophenone is required for the ionization. Preparation of the thin-film layer of matrix/analyte consisting of micro crystals is effective to obtain the mass spectrum with little fragment peaks. Singly-charged ion of BSA is obtained using thin-layer method with highly volatile solvent like acetone. It is expected that the ionization source shows the sensitivity of 750 attomole as low as a conventional MALDI-MS

Finally, on-chip mass spectrometry of protein analyte was performed. Developed pulse-heating ionization source was integrated with the 5 mm length of TOF mass analyzer composed of oval shaped micro electrodes. Broad peak of the produced ions by the pulse-heating ionization in a micro channel is obtained without the electrostatic ion lens and the TOF path. To use the ion lens and the TOF path, separated ion peaks are detected, corresponding to the numerically simulated TOF of the singly-charged and the doubly-charged BSA ions.

ACKNOWLEDGEMENTS

Firstly, I wish to gratefully acknowledge to my advisor, Professor Yuzuru TAKAMURA, for his supervision, suggestions, kind encouragement and giving me great opportunity to pursue this study throughout my Ph.D study. I also would like to express the deepest appreciation to Assistant Professor Yoshiaki UKITA in University of Yamanashi for his suggestions, kind encouragement, and all of supporting of my Ph.D study. I also would like to thank Professor Tatsuya Shimoda for supporting of the experimental equipment which was critical to achieve all of the experiment. I am also particularly grateful for the assistance given by Lecturer Issey Osaka for the kind supporting of MALDI-MS analysis.

Additionally, I would also like to express the deepest appreciation to my thesis examination committee, Professor Kenzo FUJIMOTO, Professor Takahiro HOHSAKA, Professor Hiroshi MIZUTA, and Associate Professor Takanori ICHIKI who gave helpful comments and suggestions in this thesis.

My sincere gratitude goes to the Japan Advanced Institute of Science and Technology (JAIST) and Japan Society for the Promotion of Science (JSPS) for the financial supports that made it possible to complete this study.

I would also like to thank Dr. Miyuki CHIKAE, Mr. Ryuzo IKEDA, Ms. Kiyomi KOSUGI, and Ms. Keiko KAWAI who kindly supported me for five years in the laboratory. My sincere appreciation is also extended to all members of the

TAKAMURA Laboratory at JAIST. I am also particularly grateful for the assistance given by Mr. Hiroki Harako to support for developing the miniaturized ionization source. I am also grateful for the assistance given by Mr. Gotou, Mr. Maruyama and Ms. Yang for helping the experiment.

Lastly, I would like to express deeply appreciation to my parents for many years of their understanding and grateful supports.

ACHIEVEMENTS

Article with peer review

1. **K. Sugiyama**, Y. Ukita, and Y. Takamura, “Development of on-chip vacuum generation by gas-liquid phase transition”, *Sens. Actuators, A*, 176, pp.138-142, 2012
2. **K. Sugiyama**, H. Harako, Y. Ukita, T. Shimoda, Y. Takamura, “Pulse-heating ionization for protein on-chip mass spectrometry”, *Anal. Chem.*, 86(15), 2014, 7593-7597.

Article without peer review

3. **杉山清隆**、原子洋樹、浮田芳昭、高村禪、「オンチップイオン源を用いた高分子試料の質量分析」、*化学とマイクロ・ナノシステム*第 13 巻第 1 号、pp.37-38、2014.

Patent

4. 北陸先端科学技術大学院大学, 瞬間加熱によるイオン化装置、質量分析計、質量分析システム及びイオン化方法, 特願 2015- 39745, 2015-3-2.

International conference

5. **K. Sugiyama**, Y. Ukita and Y. Takamura, “On-chip vacuum generation by phase transition in micro chamber “, MNE2011, O-LIFE-30, Berlin, (Sep. 2011)

6. **K. Sugiyama**, Hiroki Harako, Y. Ukita and Y. Takamura, “Development of miniaturized ionization source for protein sample coupled with time of flight mass spectrometry “, MNE2013, O-LIFE-18, London, (Sep. 2013)
7. **K. Sugiyama**, Y. Ukita and Y. Takamura, “Development of On-Chip Micro Vacuum System with Gas-Liquid Phase Transition “, EIPBN2011, P10-2, Las Vegas, (June 2011)
8. **K. Sugiyama**, H. Harako, Y. Ukita and Y. Takamura, “STUDY ON ON-CHIP MASS SPECTROMETRY IN A LOW VACUUM OPERATION”, MicroTAS2012, T.7.169, Okinawa, (Oct. 2012)
9. **K. Sugiyama**, Hiroki Harako, Y. Ukita and Y. Takamura, “On-chip ionization source for protein coupled with time of flight mass spectrometry”, MNC2013, 7P-7-114, Sapporo, (Nov. 2013)
10. **K. Sugiyama**, Hiroki Harako, Y. Ukita and Y. Takamura, ” DEVELOPMENT OF MINIATURIZED IONIZATION SOURCE FOR PROTEIN MASS SPECTROMETRY ON A CHIP” , MicroTAS2014, (Oct. 2014), T.614g.

Domestic conference

11. 杉山清隆, 浮田芳昭, 高村禅, 「チップ内微小真空機器のための真空計測法の検討」, 第22回化学とマイクロ・ナノシステム研究会, p.87, 名古屋大学医学部, 2010年11月

12. **杉山清隆**, 浮田芳昭, 高村禪, 「相転移を用いた真空作成チップの研究」, 平成 23 年度応用物理学会北陸・信越支部学術講演会, 金沢歌劇座, 2011 年 11 月
13. **杉山清隆**, 原子洋樹, 浮田芳昭, 高村禪, 「相転移を用いたオンチップ真空作成法の検討」, 18a-GP5-6, 2012 年春季 第 59 回応用物理学関係連合講演会, 早稲田大学, 2012 年 3 月
14. シャルマ ビニート, **杉山清隆**, 浮田芳昭, 高村 禪, “Study on trapping of particle by vortex for washing of single cell” , 17a-C4-6, 2013 年第 74 回応用物理学会秋季関係連合講演会, 同志社大学, 2013 年 9 月
15. **杉山清隆**, 原子洋樹, 浮田芳昭, 高村禪, 「オンチップイオン源を用いた高分子試料の質量分析」, 第 28 回化学とマイクロ・ナノシステム研究会, 3P21, イーグレ姫路, 2013 年 12 月
16. **杉山清隆**, 原子洋樹, 浮田芳昭, 高村禪, 「タンパク質の質量分析に向けたオンチップイオン源の開発」, 2014 年第 61 回応用物理学会春季学術講演会, 19p-E15-6, 青山学院大学相模原キャンパス, 2014 年 3 月
17. **杉山清隆**, 高村禪, 「生体試料の高感度分析を目指した質量分析チップの開発に向けた微小イオン源」, 第 8 回バイオ関連化学シンポジウム, 2P-097, 岡山大学 津島キャンパス, 2014 年 9 月
18. **杉山清隆**, 高村禪, 「オンチップ質量分析に向けた熱パルスイオン源とマトリックスの効果」, 2014 年第 75 回応用物理学会秋季学術講演会, 19p-A2-19 北海道大学, 2014 年 9 月

19. 杉山清隆, 高村禪, 「オンチップ質量分析に向けた熱パルスイオン化法と試料膜形成法」, 2015 年第 62 回応用物理学会春季学術講演会, 13p-D6-5, 東海大学, 2015 年 3 月

Award

20. 第 28 回化学とマイクロ・ナノシステム研究会 優秀ポスター賞